Carrier capture in III-V semiconductor quantum wells

Citation for published version (APA):
Blom, P. W. M. (1992). *Carrier capture in III-V semiconductor quantum wells*. [Phd Thesis 1 (Research TU/e / Graduation TU/e), Applied Physics and Science Education]. Technische Universiteit Eindhoven. https://doi.org/10.6100/IR384664

DOI:
10.6100/IR384664

Document status and date:
Published: 01/01/1992

Document Version:
Publisher’s PDF, also known as Version of Record (includes final page, issue and volume numbers)

Please check the document version of this publication:

• A submitted manuscript is the version of the article upon submission and before peer-review. There can be important differences between the submitted version and the official published version of record. People interested in the research are advised to contact the author for the final version of the publication, or visit the DOI to the publisher's website.
• The final author version and the galley proof are versions of the publication after peer review.
• The final published version features the final layout of the paper including the volume, issue and page numbers.

Link to publication

General rights
Copyright and moral rights for the publications made accessible in the public portal are retained by the authors and/or other copyright owners and it is a condition of accessing publications that users recognise and abide by the legal requirements associated with these rights.

- Users may download and print one copy of any publication from the public portal for the purpose of private study or research.
- You may not further distribute the material or use it for any profit-making activity or commercial gain
- You may freely distribute the URL identifying the publication in the public portal.

If the publication is distributed under the terms of Article 25fa of the Dutch Copyright Act, indicated by the “Taverne” license above, please follow below link for the End User Agreement:

www.tue.nl/taverne

Take down policy
If you believe that this document breaches copyright please contact us at:

openaccess@tue.nl

providing details and we will investigate your claim.

Download date: 17. Nov. 2023

Carrier Capture in III-V Semiconductor Quantum Wells

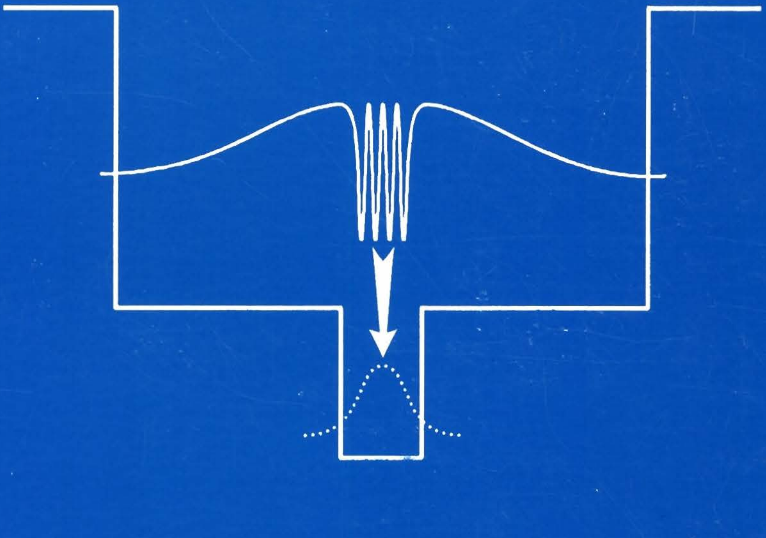

Paul W.M. Blom

Carrier Capture in III-V Semiconductor Quantum Wells

PROEFSCHRIFT

ter verkrijging van de graad van doctor aan de Technische
Universiteit Eindhoven, op gezag van de Rector Magnificus,
prof. dr. J.H. van Lint, voor een commissie aangewezen
door het College van Dekanen in het openbaar te verdedigen
op maandag 9 november 1992 te 16.00 uur

door

Paulus Wilhelmus Maria Blom

geboren te Maastricht

Dit proefschrift is goedgekeurd door de promotor
prof. dr. J.H. Wolter
en de copromotor
dr. J.E.M. Haverkort

The work described in this thesis was carried out at the Department of Physics of the Eindhoven University of Technology and was part of the research program of the Dutch Foundation for Fundamental Research on Matter (FOM), which is financially supported by the Dutch Organization for the Advancement of Research (NWO).

aan mijn ouders
aan Desiree

Contents

4. Relevance of the Carrier Capture Efficiency for Quantum Well Lasers

Chapter 1

General Introduction

The advent of crystal growth techniques in the past decade offers the possibility to deposit atomic layer upon atomic layer of a specific semiconductor in a controlled manner. These ultrathin semiconductor layer structures, so-called heterostructures, exhibit new basic physical phenomena as for example the Quantum Hall Effect[1]. A widely used type of heterostructure is the quantum well, which is schematically plotted in Fig. 1.1. A quantum well structure consists of a thin layer of semiconductor W, the quantum well, embedded between two thick layers of a semiconductor B with a larger band gap, the barrier layers. When the thickness of the quantum well is comparable

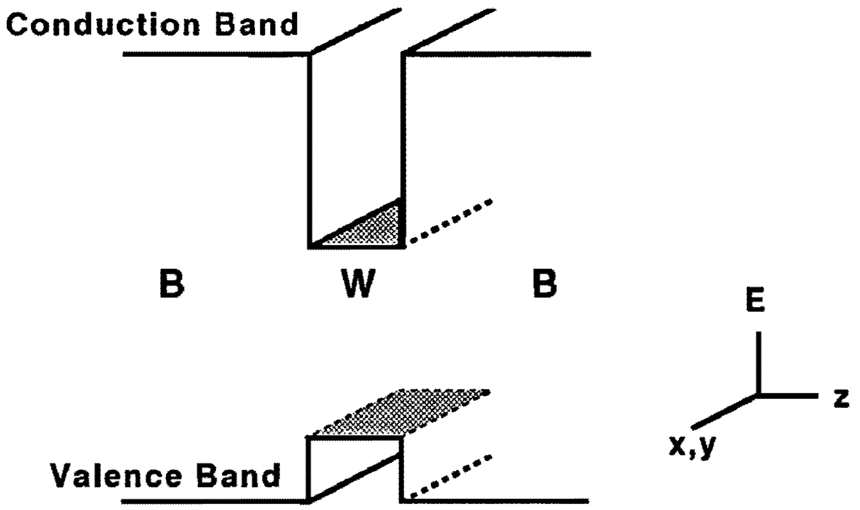

Fig. 1.1. The macroscopic potential seen by the electrons in the conduction band and the holes in the valence band of a semiconductor quantum well structure. The carriers are confined in the energetically favourable layers with the smallest band gap.

to the de Broglie wavelength of the carriers, the motion of the carriers perpendicular to the layer structure (z-direction) is quantized. In this case a discrete spectrum of energy levels is created for the potential in the well. If excess carriers are injected or photogenerated in the barrier layers, the carriers will diffuse to the energetically favourable quantum well where they are captured. However, there seems to be a fundamental problem in the understanding of the carrier capture process by a quantum well according to the large differences between observed and predicted capture times in literature[2-11]. Furthermore, the performance of quantum well lasers is often suggested to be related to the injection efficiency of carriers into the quantum well[12], but a detailed analysis is lacking.

In this thesis we present the results of both experimental and theoretical studies of the carrier capture process in GaAs/$Al_xGa_{1-x}As$ separate confinement heterostructure quantum well (SCHQW) structures. We have observed an oscillating carrier capture time between 3 and 20 ps as a function of quantum well thickness, which is for the first time in agreement with a state-of-the-art ambipolar capture model based on quantum mechanical calculations of Brum and Bastard[3]. As a result the carrier capture efficiency in QW laser structures can be improved by more than one order of magnitude by optimizing the dimensions and composition of the active layers. Furthermore we have strong indications that a low capture efficiency can degrade laser performance through excess carrier heating, non-uniform pumping of the individual quantum wells, and carrier accumulation in the barrier layers. By maximizing the carrier capture efficiency in laser structures we for the first time are able to predict the active layer architecture for an optimum laser performance.

Quantum well lasers were expected to exhibit a lower threshold current than bulk double heterostructure (DH) lasers[13], due to the modification of the density of states. The absence of this performance improvement in the first quantum well lasers[14] appeared to be related to the injection efficiency of the carriers in the laser structure[12], a problem which is not present in bulk lasers. After the application of cladding layers, which improve the collection of carriers by the quantum well and the optical confinement, the quantum well lasers have demonstrated a superior laser performance with regard to bulk DH lasers, such as low threshold current density[12,15], low temperature dependence of threshold current[16-18], extended lasing wavelength tunability by varying structure parameters, and excellent dynamic properties[19-20]. In this thesis we consider a quantum well laser structure as shown in Fig. 1.2. This SCHQW structure consists of a GaAs quantum well, surrounded by $Al_xGa_{1-x}As$ barrier layers and by AlAs cladding layers. The electrons and holes are injected into the barrier

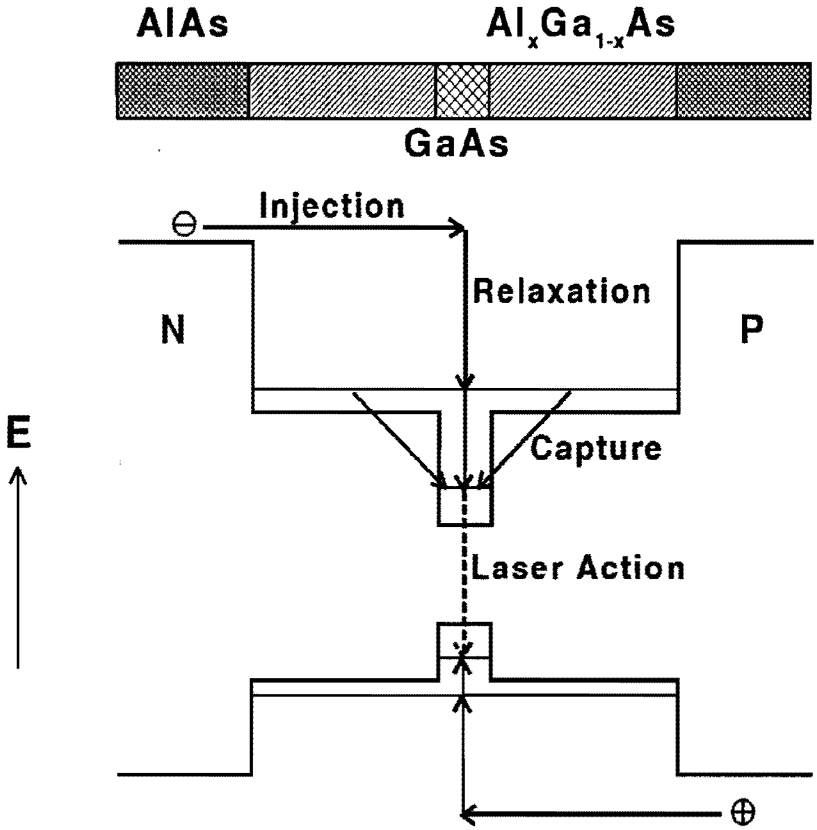

Fig. 1.2. Representation of a GaAs/$Al_xGa_{1-x}As$ SCHQW laser structure with AlAs cladding layers. The electrons and holes are injected from the n- and p-doped AlAs cladding layers respectively into the $Al_xGa_{1-x}As$ barrier layers. After injection the carriers are captured by the quantum well and subsequently participate in the laser action.

layers from the n- and p-doped cladding layers respectively. After a fast relaxation process to the lowest energy states in the barrier layers, the carriers are captured by the quantum well where they can participate in the lasing action. The capture process is expected to be relevant for the design of low-threshold semiconductor quantum well lasers as well as for the development of gain-switched quantum well lasers with improved modulation frequency[21-24].

In early theoretical studies[25,26] the carrier capture was regarded as a classical process in which the carrier capture time defined a longitudinal optical (LO) phonon-scattering-limited mean free path in bulk GaAs. In these calculations, the bulk GaAs LO phonon scattering time of 0.1 ps leads to a mean free path length of about 60 Å. As a result, carrier capture was expected to be efficient for quantum wells with a thickness larger than 60 Å. In more recent studies[2-5] the quantum mechanical character of the capture process was taken into account. In this approach the capture time is expected to show resonances as a function of the quantum well thickness. The capture process, which is governed by the emission of LO phonons, is enhanced whenever a barrier state couples into the quantum well giving rise to efficient capture at distinctly different QW thicknesses as in the classical model mentioned above. For a GaAs/$Al_xGa_{1-x}As$ single quantum well (SQW) structure capture times oscillating between 30 ps-1 ns were predicted by Brum and Bastard[3]. Babiker and Ridley[4] reported capture times oscillating between 1-10 ps for a GaAs/$Al_xGa_{1-x}As$ superlattice, in which the formation of minibands and the folded spectrum of polar optical phonons were taken into account. Furthermore, they predicted[27] additional resonances in the carrier capture process in a superlattice due to the two dimensional properties of the phonon states in the quantum wells of the superlattice. With respect to the carrier capture time, it is a major question whether the predicted oscillations in the carrier capture time do exist or not. Or in other words, is the quantum mechanical approach, which predicts these oscillations, correct or is the classical approach adequate?

Experimentally, most observed capture times seemed to contradict the theoretical predictions or at least did not show the predicted oscillations of the carrier capture time. Capture times of <20 ps[6], 4 ps[7] and 2-3 ps[8] were obtained from time-resolved studies on SQW structures. From CW photoluminescence experiments on a GaAs/Al$_x$Ga$_{1-x}$As MQW structure[9] a capture time of 0.1 ps was derived. Electron capture times of <1 ps were reported[10,11] for In$_y$Ga$_{1-y}$As/InP multiple quantum well (MQW) structures from time-resolved luminescence experiments and no well width dependence was observed. It was deduced that for thick barrier layers (>500 Å) the carrier capture process is dominated by drift and diffusion, while thin barrier layers (<200 Å) give rise to a quantum mechanical process. It was reported by Tsang[14] that the active layer thickness for MQW laser structures which gives rise to an optimum laser performance is in the order of 1000-1500 Å. The question whether the capture process in these laser structures is dominated by classical diffusion and drift (no oscillations expected) or by quantum mechanical capture (oscillations expected) is relevant for the optimization of the capture efficiency in quantum well laser structures.

In this thesis we focus on the carrier capture process in GaAs/Al$_x$Ga$_{1-x}$As SCH single quantum wells. As a model structure we choose a quantum well with thickness L_w, located in the middle of a wide well with thickness $2\times L_b+L_w$ (Fig. 1.3a). The energy states in the quantum well are indicated as 'bound states' whereas the energy states in the wide well are labelled as 'barrier states'. For simplicity the AlAs cladding layers are assumed to be of infinite height. Furthermore, we adopt a constant effective mass m^* for the carriers throughout the whole structure and its dispersion relations are taken as parabolic and isotropic with respect to the wave vector **k**. The energy zero is taken at the onset of the QW continuum. As a result the potential energy is zero in the barrier layers and $-V_0$ inside the quantum well. After injection, the carriers relax very fast ($<$ 1 ps) by LO phonon emission until they are within one LO phonon energy of the lowest barrier state. Then the carriers are scattered from the lower barrier states into the quantum well. The dominant scattering mechanism for carrier capture was calculated to be the scattering of carriers by polar optical phonons[28,29]. The capture process in which a carrier in an initial barrier state emits a LO phonon and is captured by the well is depicted in Fig. 1.3b. Using Fermi's Golden Rule the

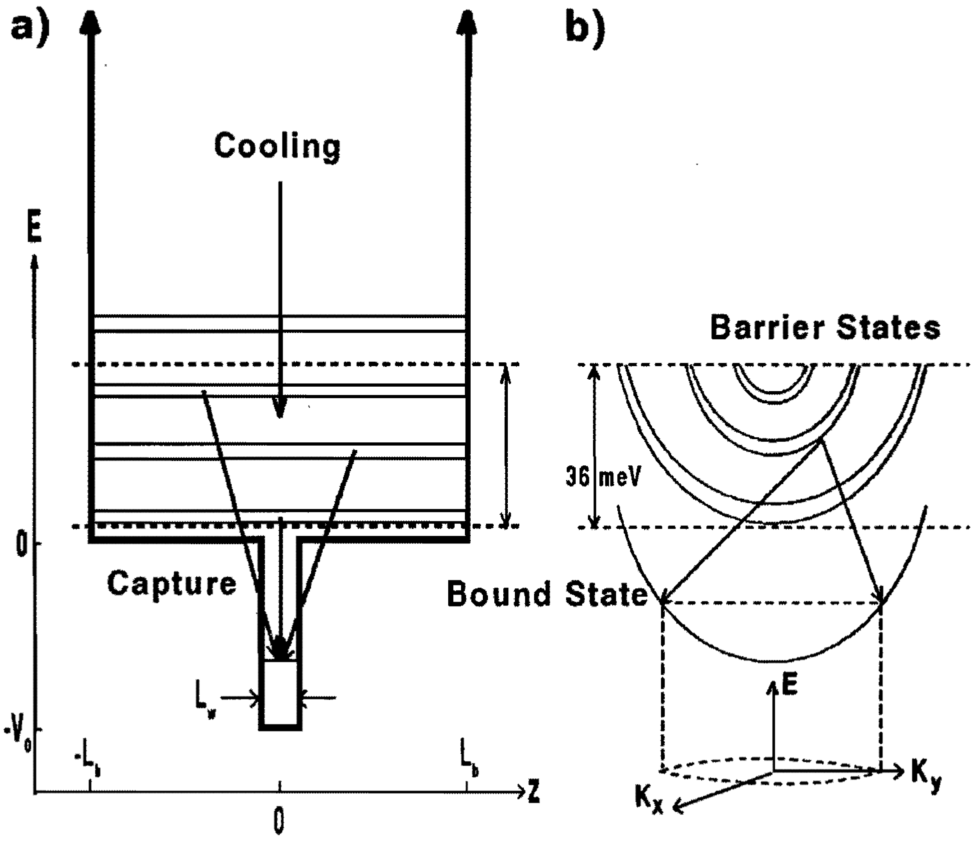

Fig. 1.3. A schematic of the electron capture process in the GaAs/Al$_x$Ga$_{1-x}$As SCH single QW structure. The energy levels (Fig. 1.3a) in the barrier appear in pairs with wave functions of even and odd symmetry with regard to the quantum well. The allowed final states in momentum space for a capture process from an initial barrier state to a final bound state are indicated by the dashed circle in Fig. 1.3b.

total scattering rate is determined by the matrix element for LO phonon emission as well as the sum over those final states which are compatible with energy conservation. By emitting a LO phonon the carriers lower their energy by 36.8 meV, which defines the allowed final states in momentum space as indicated by the dashed circle in Fig. 1.3b. The length of the phonon wave vector involved in the capture process is thus dependent on the energy position of the bound states in the quantum well. As a result a change of the quantum well width affects not only the carrier wave functions, but also the length of the phonon wave vectors involved in the capture process.

In chapter 2 we present a quantum mechanical model for carrier capture in single and multiple quantum well structures, which predicts the dependence of the carrier capture time on quantum well thickness and laser energy. Furthermore, it is demonstrated that for multiple quantum wells (MQW) the capture times oscillate not only as a function of well width but also as a function of barrier width, due to oscillations in the wave function overlap with the barrier states. The predicted capture times for large MQW structures are very short (< 1 ps), which is in agreement with the reported experimental results. We showed that the large discrepancy in literature between predicted capture times[3] (SQW) and experimental capture times[9-11] (MQW) is mainly due to the often neglected strong dependence of the capture times on structure parameters such as well width, barrier width and number of wells.

In chapter 3 we present the experimental capture times obtained from two different techniques with picosecond resolution. We make use of the upconversion technique and the time-resolved pump and probe technique. The carrier capture times are experimentally studied by both QW luminescence rise times and barrier luminescence decay measurements. In the first technique we compare the QW rise times after direct (below the barrier band gap) and indirect (above the barrier band gap) excitation, in order to eliminate the effect of relaxation of the carriers in the quantum well. For a correct elimination of this relaxation process, we first investigated the dependence of the QW exciton luminescence rise time after direct excitation on laser energy. In previous studies[30-38] exciton luminescence rise times of several hundreds of picoseconds were obtained and no dependence on the laser energy was observed when the laser excess energy exceeded the exciton binding energy. From time-resolved luminescence experiments it was deduced[30,35,37,38] that the exciton relaxation process is responsible for the long rise times of several hundreds of picoseconds of the exciton luminescence after excitation with a laser pulse. Various mechanisms were proposed for the reduced energy loss rate of excitons in quantum wells, such as the migration of excitons towards the lower energy positions in an inhomogeneous quantum well by emission of acoustic phonons[30,32,35], the intrinsic relaxation of excitons [37], and a drift-diffusion motion driven by potential fluctuations in the quantum well plane[38]. In GaAs/AlGaAs quantum well structures with a quantum well thickness of only 26 Å, which enhances the exciton relaxation process as a result of interface roughness[35], we for the first time demonstrate that the exciton luminescence rise times oscillates as a function of laser excess energy because of resonances in the exciton formation process. A minimum in the rise times is observed whenever, after an initial phonon cascade, the sum of the excess electron and hole energies with regard to their subband minima is a discrete number of LO phonon energies larger than the exciton ground state. For thick quantum wells no resonant exciton formation process would be observed, since the variations in our exciton rise time (15 ps) are very small in comparison with the reported luminescence rise times of 400 ps[30,35,37,38].

With regard to the carrier capture process we report the first experimental observation of oscillations in the carrier capture time between 3 and 20 ps as a function of quantum well thickness, obtained from QW luminescence rise time measurements as well as by two-pulse correlation measurements on the luminescence decay of the barrier layers. The observed capture times are for the first time in agreement with theoretical predictions from an ambipolar capture model. In this model, which takes into account the mutual electrostatic interaction between electrons and holes, the net capture process is governed by a quantum mechanical capture process of the electrons and a classical capture process of the holes. The ambipolar character of the capture process was confirmed by experiments on p- and n-doped samples. Furthermore, these experiments reveal the dependence of the carrier capture time on the barrier subband population as well as the dominance of LO phonon emission in the capture process.

Chapter 4 describes the relevance of the carrier capture efficiency for the performance of a quantum well laser. Under lasing conditions the carrier capture process is not only governed by LO phonon emission but also by carrier-carrier scattering induced capture, which both give rise to oscillations in the capture time as a function of quantum well thickness. In single quantum well lasers a small phonon induced capture rate is expected to lead to excess carrier heating due to a high carrier-carrier induced capture rate. In multiple quantum well lasers a low capture efficiency tends to pile up all injected carriers on the p-doped side, resulting in an unequal pumping of the quantum wells. Furthermore, an efficient capture process reduces the accumulation of carriers in the barrier layers, which improves the dynamic behaviour of a quantum well laser.

References

1 K. v. Klitzing, G.Dorda, and M. Pepper, Phys. Rev. Lett. **48**, 494 (1979).

2 S.V. Kozyrev, and A.Ya. Shik, Sov. Phys. Semicond. **19**, 1024 (1985).

3 J.A. Brum, and G. Bastard, Phys. Rev. B **33**, 1420 (1986).

4 M. Babiker, and B.K. Ridley, Superlatt. and Microstruct. **2**, 287 (1986).

5 Y. Murayama, Phys. Rev. B **34**, 2500 (1986).

6 J. Feldmann, G. Peter, E.O. Göbel, K. Leo, H.-J. Polland, K. Ploog, K. Fujiwara, and T. Nakayama, Appl. Phys. Lett. **51**, 226 (1987).

7 D.J. Westland, D. Mihailovic, J.F. Ryan, and M.D. Scott, Appl. Phys. Lett. **51**, 590 (1987).

8 B. Deveaud, F. Clerot, A. Regreny, K. Fujiwara, K. Mitsunaga and J. Ohta, Appl. Phys. Lett. **55**, 2646 (1989).

9 D. Bimberg, J. Christen, A. Steckenborn, G. Weimann, and W. Schlapp, J. Luminesc. **30**, 562 (1985).

10 B. Deveaud, J. Shah, T.C. Damen, and W.T. Tsang, Appl. Phys. Lett. **52**, 1886 (1988).

11 R. Kersting, X.Q. Zhou, K. Wolter, D. Grützmacher, and H. Kurz, Superlatt. Microstruct. **7**, 345 (1990).

12 W.T. Tsang, Appl. Phys. Lett. **39**, 786 (1981)

13 N. Holonyak, Jr., R.M. Kolbas, R.D. Dupuis, and P.D. Dapkus, IEEE J. Quantum Electron. QE-**16**, 170 (1980)

14 W.T. Tsang, Appl. Phys. Lett. **38**, 204 (1980).

15 T. Fuji, S. Yamakoshi, K. Nanbu, O. Wada, and S. Hiyamizu, J. Vac. Sci. Technol. **2**, 259 (1984).

16 R. Chin, N. Holonyak, Jr., B.A. Bojak, K. Hess, R.D. Dupuis, and P.D. Dapkus, Appl. Phys. Lett. **36**, 19 (1979).

17 K. Hess, B.A. Bojak, N. Holonyak, Jr., R. Chin, and P.D. Dapkus, Solid-State Electron. **23**, 585 (1980).

18 Y. Arakawa, and H. Sakaki, Appl. Phys. Lett. **40**, 939 (1982).

19 Y. Arakawa, K. Vahala, and A. Yariv, Appl. Phys. Lett. **45**, 950 (1984).

20 Y. Arakawa, and A. Yariv, IEEE J. Quantum Electron. QE-**21**, 1666 (1985).

21 W. Rideout, W.F. Sharfin, E.S. Koteles, M.O. Vassell, and B. Elman, IEEE Photon. Technol. Lett. **3**, 784 (1991).

22 R. Nagarajan, T. Fukushima, S.W. Corzine, and J.E. Bowers, Appl. Phys. Lett. **59**, 1835 (1991).

23 W.F. Sharfin, J. Schlafer, W. Rideout, B. Elman, R.B. Lauer, J. LaCourse, and F.D. Crawford, IEEE Photon. Technol. Lett. **3**, 193 (1991).

24 R. Nagarajan, T. Fukushima, M. Ishikawa, J.E. Bowers, R.S. Geels, and L.A. Coldren, IEEE Photon. Lett. **4**, 121 (1992).

25 H. Shichijo, R.M. Kolbas, N. Holonyak, Jr., J.J. Coleman, and P.D. Dapkus, Solid State Commun. **27**, 1029 (1978).

26 J.Y. Tang, K. Hess, N. Holonyak, Jr., J.J. Coleman, and P.D. Dapkus, J. Appl. Phys. **53**, 6043 (1982).

27 M. Babiker, M.P. Chamberlain, A. Ghosal, and B.K. Ridley, Surf. Science **196**, 422 (1988).

28 P.J. Price, Ann. of Physics **133**, 217 (1981).

29 B.K. Ridley, J. Phys. C: Solid State Phys. **15**, 5899 (1982)

30 Y. Masumoto, S. Shionoya, and H. Kawaguchi, Phys. Rev. B **29**, 2324, (1984).

31 D.A.B. Miller, D.S. Chemla, T.C. Damen, T.H. Wood, C.A. Burrus, A.C. Gossard, and W. Wiegmann, IEEE J. Quantum Electronics QE-**21**, 1462 (1985).

32 T. Takagahara, Phys. Rev. B **31**, 6552 (1985).

33 T. Takagahara, Phys. Rev. B **32**, 7013 (1985).

34 J. Feldmann, G. Peter, E.O. Göbel, P. Dawson, K. Moore, C. Foxon, and R.J. Elliot, Phys. Rev. Lett. **59**, 2337 (1987).

35 J. Kusano, Y. Segawa, Y. Aoyagi, S. Namba, and H. Okamoto, Phys. Rev. B **40**, 1685 (1989).

36 A. Honold, L. Schultheis, J. Kuhl, and C.W. Tu, Phys. Rev. B **40**, 6442 (1989).

37 T.C. Damen, J. Shah, D.Y. Oberli, D.S. Chemla, J.E. Cunningham, and J.M. Kuo, Phys. Rev. B **42**, 7434 (1990).

38 M. Zachau, J.A. Kash, and W.T. Masselink, Phys. Rev. B **44**, 8403 (1991).

Chapter 2

Calculation of the LO Phonon Induced Carrier Capture Time

2.1. Introduction

The carrier capture efficiency is expected to influence both the quantum efficiency[1] and the dynamical performance[2-4] of quantum well lasers. The problem of the capture of carriers in quantum well structures was first studied by Shichijo et al.[5] and Tang et al.[6], who performed a classical calculation of the mean free path length for LO phonon scattering. In such a classical description (section 2.2) the capture process is described by a local capture time, which solely characterizes the scattering process between 3-dimensional barrier states and 2-dimensional subbands for carriers which are spatially located in the well. In more recent studies[7-10] the quantum mechanical aspect of the carrier capture process was taken into account. Strong resonances (30 ps -1 ns) of the capture times were predicted by Brum and Bastard[8]. In recent experiments[11-16], however, the observed capture times ranged from 0.3-3 ps and no well width dependence was observed. Thus there seems to be a fundamental problem in the understanding of the carrier capture process by a quantum well.

Since the carrier capture times are expected to depend strongly on structure parameters such as well width, barrier width and number of wells, a direct comparison between predicted capture times of a *single* quantum well[8] and experimental results on *multiple* quantum wells[14-16] is not correct. The dependency of the capture times of our GaAs/AlGaAs SCH-SQW structures on structure parameters and experimental conditions are calculated in section 2.3 by applying and extending the capture model of Brum and Bastard[8]. In section 2.4 we applied this model to multiple quantum wells, which enables us to compare the reported experimental results on MQW structures with our theoretical predictions. Finally, in section 2.5 we propose an ambipolar capture model, in which the different capture times of electrons and holes and the carrier distribution in the barrier subbands after excitation are taken into account.

2.2. Classical Model of the Carrier Capture Process

The validity of a quantum mechanical description of the carrier capture process depends on the coherence length of the carriers, which is limited by inelastic scattering processes. For a coherence length which is small in comparison with the width of the barrier layers, the carriers are not able to establish coherent wave functions and the carriers should be regarded as a classical fluid. Such a situation might occur at high temperature or at a high carrier density where carrier-phonon and carrier-carrier scattering processes limit the coherence length severely. The classical capture process is then governed by diffusive transport in the barrier layers in combination with a local capture time. This local capture time contains the scattering process between the 3-dimensional barrier states, which are spatially located in the well, but energetically above the well, and the 2-dimensional subbands for carriers which are spatially and energetically located in the quantum well.

We consider a large GaAs/Al$_x$Ga$_{1-x}$As SCH-SQW with 2000 Å barrier layers and a well width of 70 Å as schematically indicated in Fig. 2.1. The temporal development of the carrier density in a separate confinement laser structure can be described in a one-dimensional rate equation[17]

$$\frac{\delta n(z,t)}{\delta t} = D \cdot \frac{\delta^2 n(z,t)}{\delta z^2} - B \cdot \frac{n(z,t)}{\tau_b} - W \cdot \frac{n(z,t)}{\tau_{loc}} \,, \qquad (1)$$

where z is the direction perpendicular to the quantum well layer. In this equation D

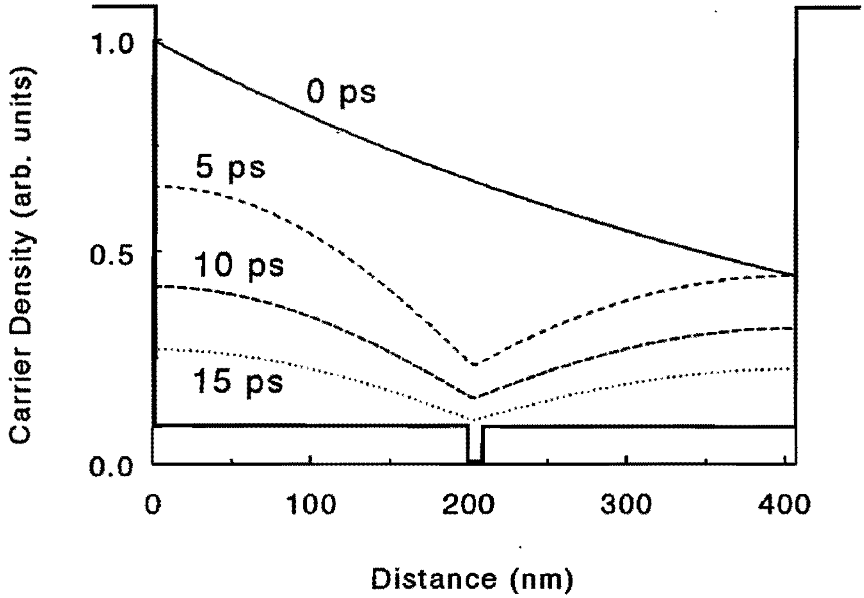

Fig. 2.1. Temporal dependence of the carrier distribution after excitation with a short laser pulse (t=0) in a SCH-SQW structure with a barrier width of 2000 Å and a well width of 70 Å. In the calculation we used a diffusion constant D=25 cm²/s and a local capture time τ_{loc}=0.1 ps.

is the ambipolar diffusion constant, B and W are unity in the barrier and well, respectively, and zero elsewhere. The recombination losses in the barrier are given by τ_b^{-1} and the scattering rate of the carriers into the well is determined by the local capture time τ_{loc}^{-1}. The initial carrier distribution at t=0 is instantaneously excited by a short laser pulse and is determined by the absorption coefficient α for laser photons, which results in

$$n(z,0) = n_0 \, e^{-\alpha z} \, . \qquad (2)$$

The flow of carriers across the AlAs confinement layers is prevented by assuming periodic boundary conditions. In Fig. 2.1 the temporal evolution of the carrier concentration in the barrier layers of the GaAs/AlGaAs SQW is plotted for a diffusion coefficient D=25 cm^2/s and a local capture time τ_{loc}=0.1 ps. The photogenerated carriers tend to form a constant distribution in the barrier layers within a few picoseconds, with a dip at the position of the quantum well. It is important to note that the calculations are performed under ambipolar conditions, where the strong interactions between electrons and holes maintain an equal density of electrons and holes at each position in the structure.

After capture into the well, the carriers relax to the lowest energy states by emission of LO phonons and then recombine radiatively. The relaxation process and the radiative recombination, characterized by the time constants τ_{rel} and τ_{qw} respectively, are easily described by a two-level model, resulting in simple rate equations

$$\frac{\delta N_2(t)}{\delta t} = \frac{N_b(t)}{\tau_{loc}} - \frac{N_2(t)}{\tau_{rel}} , \tag{3}$$

$$\frac{\delta N_1(t)}{\delta t} = \frac{N_2(t)}{\tau_{rel}} - \frac{N_1(t)}{\tau_{qw}} . \tag{4}$$

In these equations N_2 and N_1 represent the occupation of the upper and lower level in the quantum well respectively, and N_b is the total carrier concentration above the quantum well, which is found from Eq. (1). The relaxation time constant within the well and the radiative lifetime can be determined from the time-evolution of the quantum well luminescence (N_1/τ_{qw}) after direct excitation (below the barrier band gap). For direct excitation the first term of the RHS of Eq. (3) is no longer applicable and the temporal dependence of N_2 is given by $N_2(t)=N_2(0)\exp(-t/\tau_{rel})$. The diffusion constant and the local capture time are then provided by indirect excitation (above the barrier band gap). The time-evolution of the quantum well luminescence of the structure of Fig. 2.1 is shown in Fig. 2.2 after direct and indirect excitation with a short laser pulse. In the calculation we used a diffusion constant D=25 cm^2/s,

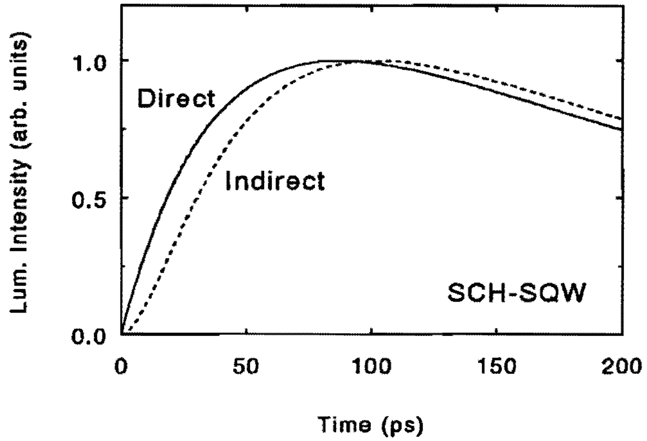

Fig. 2.2. Calculated temporal evolution of the quantum well luminescence after direct (below the barrier band gap) and indirect (above the barrier band gap) excitation with a laser pulse. The parameters used are a diffusion constant $D=25\ cm^2/s$, a local capture time $\tau_{loc}=0.1\ ps$, a relaxation time constant $\tau_{rel}=40\ ps$ and a radiative lifetime $\tau_{qw}=250\ ps$.

a local capture time $\tau_{loc}=0.1$ ps, a relaxation time constant $\tau_{rel}=40$ ps and a radiative lifetime $\tau_{qw}=250$ ps. As a result by comparing the experimental rise times of the quantum well luminescence after direct and indirect excitation (section 3.4) with the theoretical predictions as shown in Fig. 2.2, we are able to obtain the local capture time as a function of quantum well thickness (section 4.4).

2.3. Quantum Mechanical Calculation of the Carrier Capture Times in Single Quantum Wells

For small quantum well structures, in which the barrier width is of the same order of magnitude as the coherence length of the carriers, the capture process is expected to be dominated by quantum mechanical effects. We consider a GaAs/$Al_xGa_{1-x}As$ SCHQW as shown in Fig. 2.3. The transition probability $W_{k,k'}$ for a carrier in an

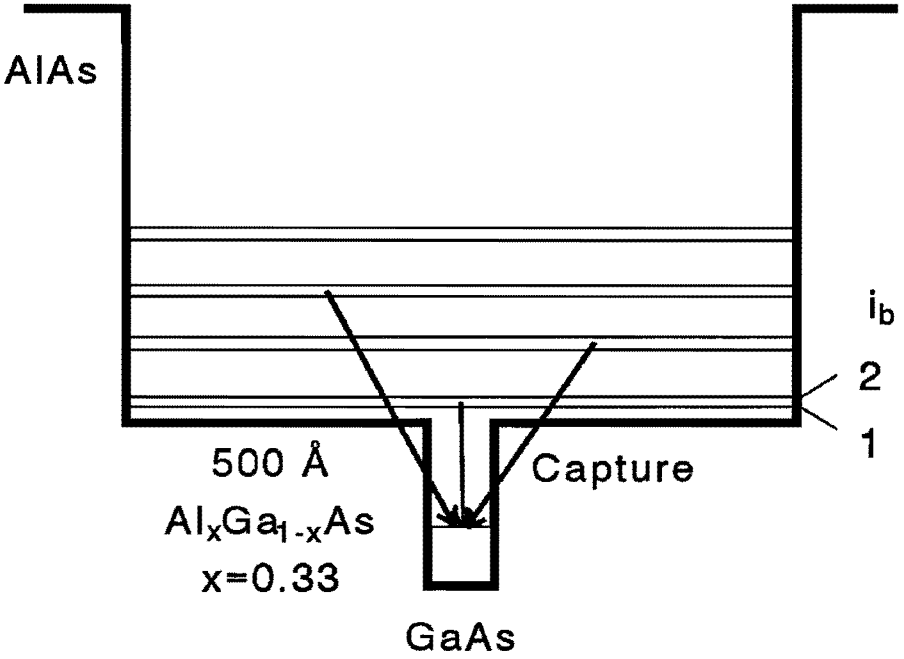

Fig. 2.3. A schematic of the carrier capture process in the $GaAs/Al_xGa_{1-x}As$ SCH single QW structure considered in this study. The energy levels in the barrier (labelled $i_b=1,2..$) appear in pairs with wave functions of even and odd symmetry with regard to the quantum well.

initial barrier state with wave vector **k** to emit a LO phonon and to become captured into a bound state in the quantum well with wave vector **k'** is given by[18]

$$W_{k,k'}=\frac{2\pi}{\hbar}\,\frac{1}{(2\pi)^3}\int dq_z\,|I(q_z)|^2\;|c|^2\delta(\boldsymbol{k}-\boldsymbol{k}'-\boldsymbol{q})|_{xy}\,\delta(E_i(k)-E_f(k')-\hbar\omega)\ , \qquad (5)$$

with q_z the phonon wave vector parallel to the growth axis, $I(q_z)$ the overlap integral between the quantum well and the barrier envelope functions which determines momentum conservation in the z-direction, given by

$$I(q_z)\ =\ \int dz\ \exp(-iq_z z)\psi_f^*(k')\psi_i(k)\ , \qquad (6)$$

and $|c|$ the Fröhlich coupling constant for LO phonons

$$|c|^2 = \frac{1}{4\pi\epsilon_0} \frac{2\pi e^2 \hbar\omega}{q^2} \left(\frac{1}{\epsilon_{r0}} - \frac{1}{\epsilon_{r\infty}}\right) . \tag{7}$$

The total scattering rate for a transition from an initial state to the allowed final states is given by

$$\tau(k)^{-1} = \int W_{k,k'} \, dk' . \tag{8}$$

It is assumed that no LO phonons are present, so there is no thermally activated escape from the quantum well. The capture time τ is now valid for carriers in the whole structure and is therefore called the overall capture time.

First we consider the envelope functions of the initial barrier states. The probability that an electron in a barrier state is located in the GaAs layer ('above' the well) is shown in Fig. 2.4 as a function of well width for the two lowest barrier states. It is shown that this probability is strongly enhanced for certain resonant well widths. In Fig. 2.5 the barrier wave function is plotted for a resonant quantum well width of 46 Å. We demonstrate that for the resonant well widths the wavelength of the barrier wave function above the quantum well exactly matches with the quantum well thickness. As a result the wave function reaches its maximum value at the edge of the quantum well, which gives rise to a large probability of the electron being in the GaAs layer. These resonant wave functions appear at those quantum well widths where a barrier energy level is decreasing in energy and just starts to become a bound state of the quantum well, as is shown in the inset of Fig. 2.4. They correspond to the so-called virtual bound levels[8] and give rise to maxima in the overlap integral and thus to large capture rates for these well widths, since the final bound states are also localized in the GaAs layer.

The overlap integral (Eq. 6), which depends on the quantum well design parameters

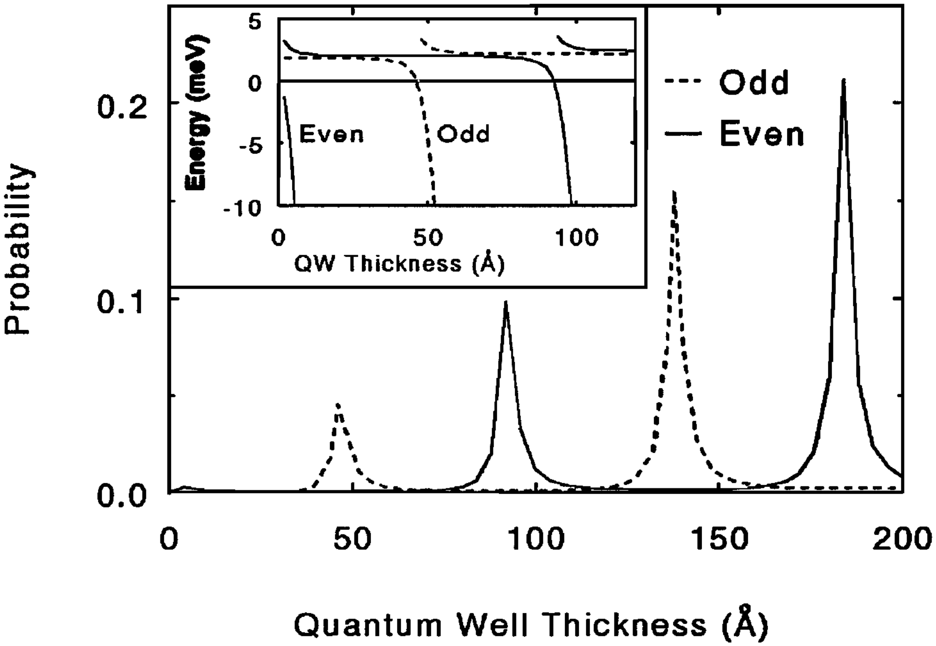

Fig. 2.4. The probability that an electron, which is energetically located in the lowest barrier state of the $Al_xGa_{1-x}As$ barriers, is spatially localized inside the GaAs quantum well layer as a function of the quantum well width for the structure shown in Fig. 2.3. The inset shows the position of the lowest two electron energy levels in the barrier with regard to the barrier bandgap (0 meV). The probability peaks at those QW thicknesses where a new energy level is bound into the quantum well.

by means of the wave functions, provides information about the relative strength of the LO phonon induced transitions between the different energy levels. In Fig. 2.6 the overlap integral is shown as a function of q_z for a transition of an electron in the lowest barrier state to the bound state of a 30 Å quantum well. The overlap integral vanishes at $q_z=0$ due to the orthogonality of the wave functions involved in the capture process. Furthermore the overlap integral can be separated into a contribution

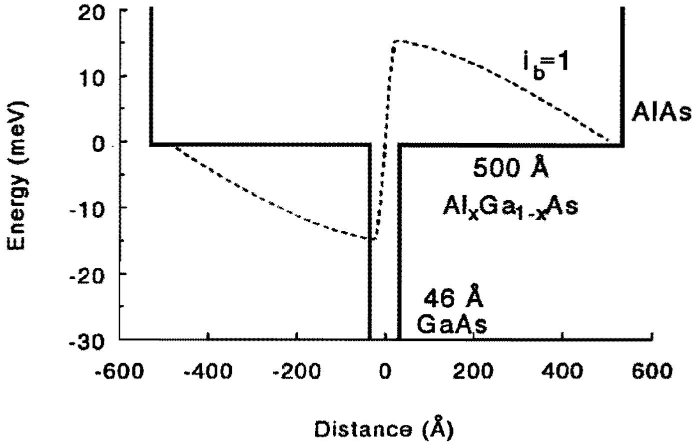

Fig. 2.5. The wave function (dashed line) of the lowest $Al_xGa_{1-x}As$ barrier state at a resonant quantum well width of 46 Å (see Fig. 2.4) as a function of the position parallel to the growth axis.

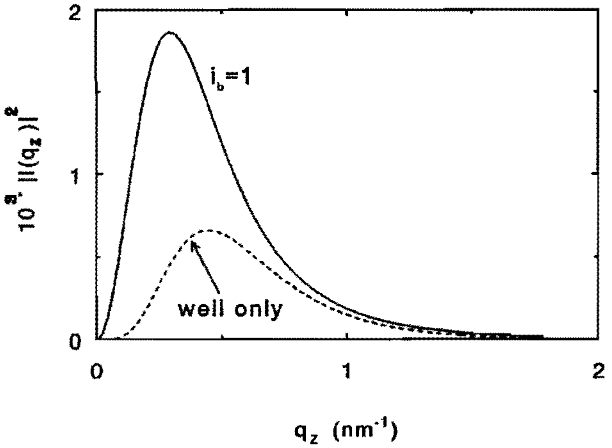

Fig. 2.6. The overlap integral $I(q_z)^2$ as a function of the phonon wave vector q_z (solid line) for a quantum well width of 30 Å. The relative contribution of the GaAs quantum well layer to the total overlap integral is shown as a dashed line.

of the overlap integral in the GaAs quantum well layer and a contribution due to transitions in the $Al_xGa_{1-x}As$ barrier layers. The relative contribution of the transition in the GaAs layer is also plotted in Fig. 2.6. We demonstrate that the relative contribution of transitions in the barrier layers to the overlap integral is twice as strong as the contribution of the quantum well layer in the overlap integral. This unexpected result is due to the fact that the wave function of the electron barrier state is located 96% in the barrier layers and only 4% in the quantum well layer, whereas the wave function of the bound state is located 90% in the quantum well and 10% in the barrier layers. Therefore, the overlap of the wave functions involved in the capture process is larger in the barrier layers than that in the quantum well layer. As a result of the large contribution of the bulk-like barrier layers to the capture process we expect that the carrier capture process is well described by assuming bulk phonons. The incorporation of 2D phonons[19] would only affect the contribution of the quantum well layers, which only dominates the capture process in structures with thin barrier layers such as for example superlattices. In Fig. 2.7 the overlap integral is plotted for capture processes from several different barrier states into the same bound state of the 30 Å quantum well. We observe that the carrier capture probability increases with increasing barrier subband number due to an improved overlap of the corresponding wave functions. As a result the carrier capture time depends strongly on the population of the barrier subbands. Thus the observed capture times in time-resolved luminescence studies depend on experimental conditions such as laser excess energy and excitation density, which determine the position of the Fermi-level of the carriers in the barrier layers as well as the carrier temperature.

By calculating the carrier capture time we assume that there are no LO phonons present before excitation, eliminating thermally activated escape from the well. Calculations of the carrier capture times were first presented by Brum and Bastard[8]. They found strong oscillations as a function of well width. They assumed a constant carrier distribution in the barrier states up to 36 meV above the barrier band gap for both electrons and the holes. This distribution corresponds to the situation where

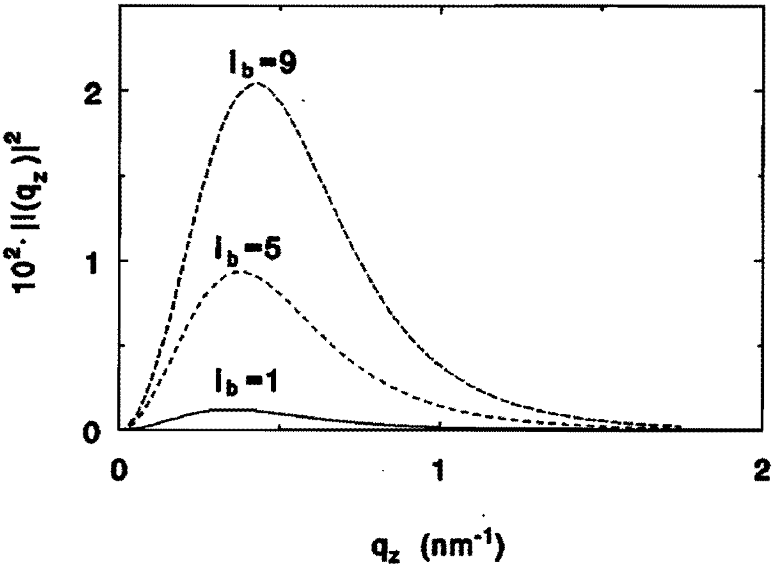

Fig. 2.7. The overlap integral $I(q_z)^2$ *as a function of the phonon wave vector* q_z *for transitions from three barrier states to the bound state of a 30 Å quantum well. The overlap integral increases one order of magnitude between the lowest barrier state* ($i_b=1$)*, which corresponds to the overlap integral of Fig. 2.6, and the ninth barrier state.*

carriers are injected at very high excess energies and cool down to below 36 meV by emitting LO phonons. Assuming this constant carrier distribution we calculated the well width dependence of the electron and hole capture time for the SCHQW structure as shown in Figs. 2.8 and 2.9. A minimum in the capture time is observed whenever a new bound state is coupled into the quantum well. Furthermore, we find that the hole capture rate is one order of magnitude larger than the electron rate, because of the larger effective mass; thus the total capture rate is limited by the relative slow capture process of the electrons. The oscillation period of the heavy-holes is short in comparison with the electrons due to their large effective mass, which gives rise to a large number of energy levels. The electron capture times in our calculation range from 5 to 80 ps, which is one order of magnitude smaller than the electron capture

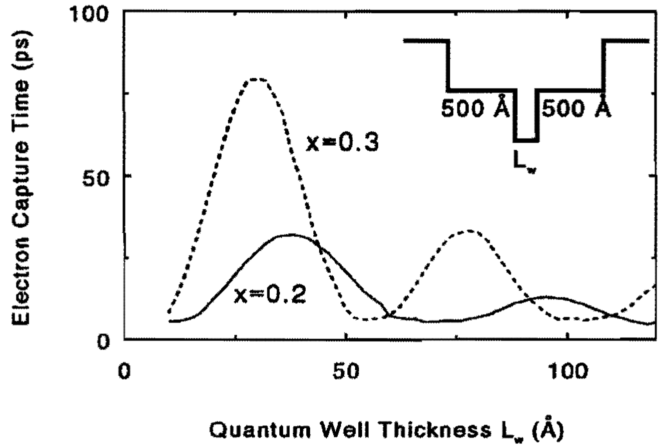

Fig. 2.8. Electron capture time vs quantum well width L_w for a GaAs/Al$_{0.3}$Ga$_{0.7}$As SCH-SQW structure. The thickness of the barrier layers amounts to 500 Å. The carrier distribution in the barrier layers is assumed to be constant up to 36 meV above the barrier band gap. A minimum in the capture time occurs whenever a new state is coupled by the quantum well.

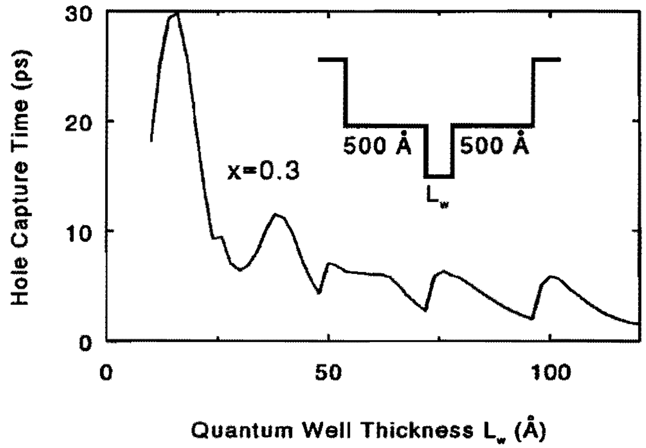

Fig. 2.9. Heavy-hole capture time vs quantum well width L_w for the SCH-SQW structure of Fig. 2.3.

times (50 ps-1 ns) obtained by Brum and Bastard[8]. This decrease of the capture time is due to the fact that the barrier width of our sample is about ten times smaller, which enhances the overlap of the barrier states and the bound states and thus the capture rate. As a result the calculated capture times are linearly proportional to the total structure width. It should be noted that we assumed parabolic bands in our calculations, which is valid for electrons but not for holes. Therefore, the calculated hole capture times only indicate the order of magnitude of the capture time but not the exact structural dependence. In the next section we will extend the quantum mechanical capture model to multiple QW structures in order to explain the fast capture times which were reported[14-16] for these structures.

2.4. Optimization of the Carrier Capture Efficiency in Multiple Quantum Well Structures

There is a fundamental difference in the capture process of a SCH-MQW structure compared to a SCH-SQW structure. The capture time in a SCH-SQW is proportional to the SCH barrier width[20], since a larger barrier reduces the overlap of the barrier wave functions with the bound states in the well. In a SCH-MQW this overlap also depends on the barrier width between the wells[21]. Since the carrier capture process is limited by the relatively slow capture of the electrons, we therefore focus on the electron capture time. In Fig. 2.10 we show the barrier width dependence of the electron capture time for a GaAs/$Al_{0.3}Ga_{0.7}As$ laser structure with three 50 Å thick quantum wells. We observe two minima in the capture time at barrier widths D_b of 155 and 280 Å. In Fig. 2.11 the wave function of the barrier state located 27 meV above the barrier band gap is shown for barrier widths of 155 Å (2.11a, minimum capture time) and 90 Å (2.11b, maximum capture time). For the barrier width of 155 Å the barrier wave functions have a large overlap with the wells, which enhances the capture process. For the barrier widths at which the capture time is at a maximum,

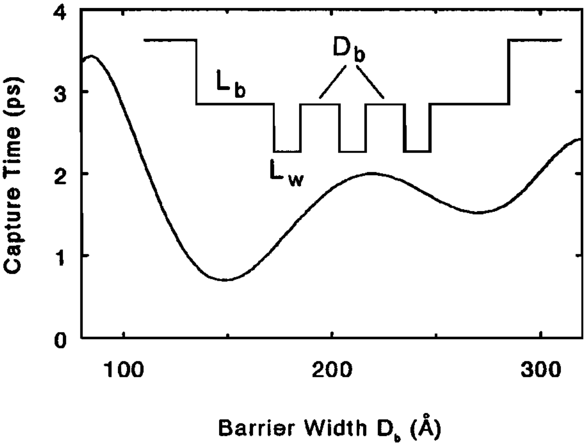

Fig. 2.10. Electron capture time vs barrier width D_b for a GaAs/Al$_x$Ga$_{1-x}$As SCH-MQW structure. The inset shows the conduction band of the structure with three 50 Å wells, a barrier width L_b of 500 Å, and an aluminum fraction of 0.3.

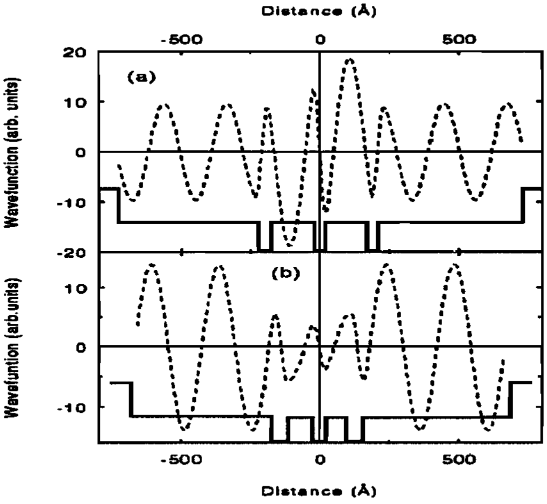

Fig. 2.11. The wave function (dashed line) of the barrier level located 27 meV above the barrier band gap for a) a barrier width of 155 Å, which corresponds to a minimum capture time, and b) a barrier width of 90 Å, corresponding to a maximum capture time.

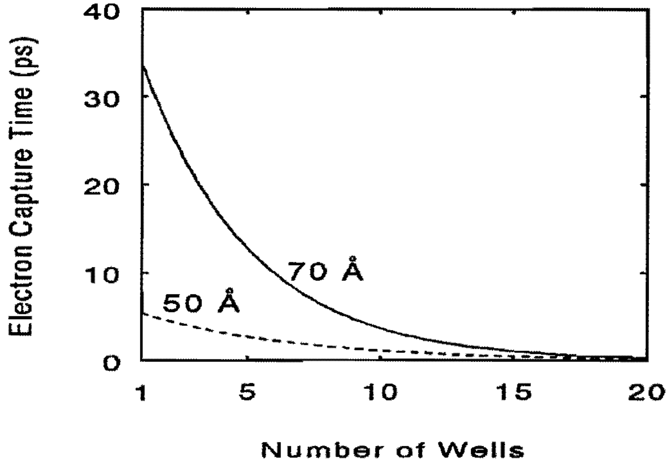

Fig. 2.12. Electron capture time as a function of the number of wells in a GaAs/Al$_x$Ga$_{1-x}$As SCH-MQW structure for quantum well thicknesses of 50 (dashed line) and 70 Å (solid line), respectively. The barrier width L_b is assumed to be 500 Å, the width of the barriers between the wells D_b amounts to 100 Å, and the aluminum fraction is 0.3. For large MQW structures (number of wells > 20) the electron capture times are all < 1 ps, independent of well width.

the barrier wave functions are mainly localized in the confinement layers (L_b) of the MQW, so they have a poor overlap with the bound states in the well.

An increase of the number of wells in the laser structure results in an increase of the total number of final bound states. It also gives rise to a decrease in the capture time. Fig. 2.12 demonstrates that the capture time is nearly inversely proportional to the number of wells for all the other structure parameters fixed. For example, a change from 1 to 10 wells in a SCH-MQW structure with 70 Å well width gives rise to a decrease of the capture time from 34 to 2 ps. If the number of wells exceeds about 20, it appears that the capture times are below 1 ps for all well widths, which is in agreement with the experimental results on the carrier capture time in MQW structures[14-16].

For the optimization of laser structures it is important to know how structure parameters like well width L_w, barrier width D_b and aluminum fraction x in the active layer determine the capture process. For example, a change in the aluminum fraction from 0.2 to 0.3 increases the capture efficiency for a structure with a 50 Å well width by a factor 4. A change of the barrier width from 100 to 155 Å gives rise to an increase of the capture rate by a factor of 5. Thus the capture rate can be enhanced by more than an order of magnitude by choosing the optimum combination of the structure parameters. The coupling of a new bound state in the quantum wells, which gives rise to an optimum capture efficiency, is determined by both the well width and the aluminum fraction in the barrier layers. In Fig. 2.13 we plot as a function of well width the optimum aluminum fraction for the carrier capture process. Also shown is the wavelength of the corresponding electron-heavy hole transitions for these combinations. The capture process in a GaAs/$Al_xGa_{1-x}As$ quantum well laser structure, with the electron-heavy hole transition at for example 840 nm, is optimized for a quantum well width of 70 Å and an aluminum fraction of 0.2 in the barrier layers. In

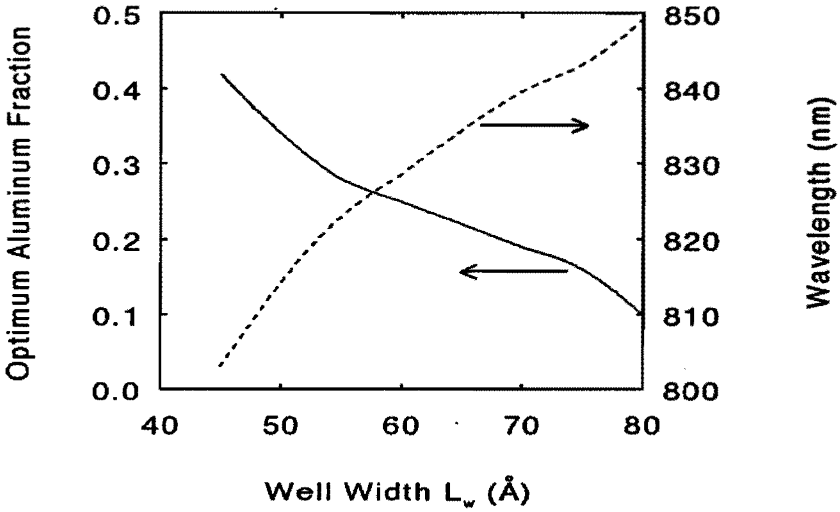

Fig. 2.13. Aluminum fraction for optimum capture (solid line) vs well width and the corresponding wavelength of the electron-heavy hole transition (dashed line).

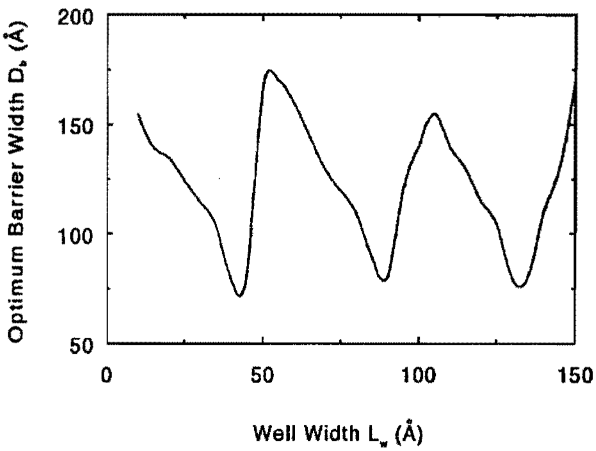

Fig. 2.14. Barrier width D_b for optimum capture in a GaAs/Al$_x$Ga$_{1-x}$As SCH-MQW structure vs well width at an aluminum fraction of 0.3.

Fig. 2.14 the optimum barrier width is shown. This width is small (< 100 Å) just before a new bound state is coupled into the well. After the coupling of a new bound state the optimum barrier width jumps to widths of 150-170 Å. For other aluminum fractions or different compounds, such as InGaAsP or InAlGaP, the bound states are coupled at different well widths, so the curve in Fig. 2.14 shifts along the x-axis.

The carrier capture efficiency in GRINSCH-MQW lasers can also be optimized using our model when we approximate the GRINSCH by a staircase-like barrier with step heights of 36 meV. By choosing the width of the individual steps, the index profile of the staircase-like barrier can be made nearly identical to a true graded-index barrier. As a consequence of the fast carrier cooling due to optical phonons, the carriers relax very efficiently in the staircase-like structure until they are within 36 meV of the barrier band gap. As a result of this cooling, the carriers are approximately confined in a SCHQW type of structure, which is the lowest step in the staircase-like barrier. As an example we calculated the capture time as a function of the barrier width D_b in a SCH-MQW with L_b=100 Å, which corresponds to a GRINSCH structure with a slope of 0.18 meV/Å, as is shown in Fig. 2.15. As

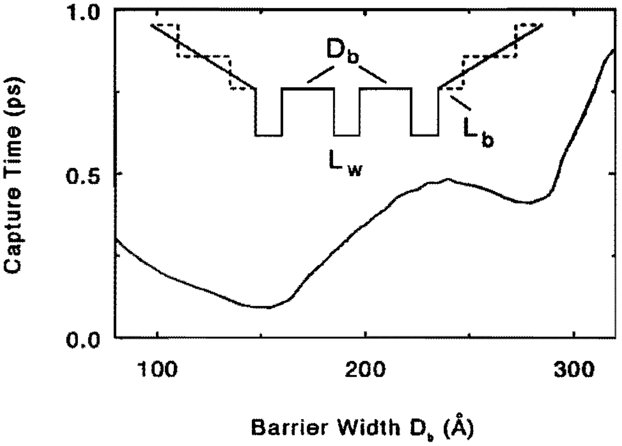

Fig. 2.15. Electron capture time vs barrier width D_b for a GaAs/Al$_x$Ga$_{1-x}$As SCH-MQW structure with a well width of 50 Å, a barrier width L_b of 100 Å, and an aluminum fraction of 0.3. The inset shows the graded-index barrier with a slope of 0.18 Å/meV approximated by a staircase-like barrier with step heigths of 36 meV.

already stated above the capture time is proportional to the width L_b of the barrier. Therefore, in a GRINSCH structure the decrease of the barrier thickness gives rise to a very efficient carrier capture. In comparison with the data for the SCH-MQW in Fig. 2.10 with L_b=500 Å we now find that the oscillations in the capture time reduce from (0.8-3.5 ps) to (0.1-0.6 ps). On the other hand, our step-like approximation of a GRINSCH does not influence the resonances in well width and barrier width between the wells. The minima in the capture time are still located at barrier widths D_b=155 and 280 Å, independent of L_b. As a result the calculated structure parameters for optimum carrier capture are valid for SCH-MQW structures as well as GRINSCH-MQW structures.

In conclusion, we have demonstrated that the carrier capture efficiency in SCH-MQW and GRINSCH-MQW laser structures can be improved by more than an order of magnitude by optimizing the dimensions and composition of the layers in the active region. The predicted capture time for large MQW structures is very short (< 1ps), in agreement with reported experimental results. In the next section we discuss how the quantum mechanical capture model applies to experimental conditions.

2.5. Dependence of the Carrier Capture Time on the Barrier Subband Population

In sections 2.3 and 2.4 the carrier capture times were calculated by assuming a constant carrier distribution up to 36 meV above the barrier band gap for the initial barrier states of both electrons and holes. Our experiments, however, are carried out at low excess energies for which such a constant hole distribution is unrealistic. We approximate the initial carrier distribution function in the barrier subbands by calculating the overlap of the envelope functions of the hole and electron barrier states, which determines the absorption strength. From this approximation, we obtain the result that the *number* of barrier subbands which are occupied after absorption of a laser pulse is equal for both electrons and holes. So in our model the initial barrier states of the capture process are determined by the number of allowed transitions after absorption of a laser pulse. After excitation the relaxation of the carriers in the barrier subbands is governed by carrier-carrier scattering and not by LO phonon emission, since the separation of the barrier subbands (4-8 meV) is less than the LO phonon energy (36.8 meV). The carrier-carrier scattering induced inter-subband transitions between the barrier states are relatively slow processes at carrier densities below 5.10^{17} cm^{-3}. The inter-subband scattering is several orders of magnitude slower than the intra-subband scattering as a result of the orthogonality of the barrier wave functions involved in the scattering process[22]. Experimentally, a carrier-carrier induced inter-subband scattering time of 20 ps was observed[23] at a carrier density of 3.10^{17} cm^{-3}, which equals the density in our correlation experiments. Therefore, most of the carriers will only relax within a few hundred femtoseconds to their barrier subband minimum (intra-band) during the capture process, resulting in an equal population of the barrier subbands. Our calculations show that the capture probability in a barrier subband is only slightly dependent on the exact position of the carriers in the subband. A difference in the carrier wave vector parallel to the quantum well plane only changes the length of the phonon vector in the capture process, not the overlap integral. Therefore, an increase of the excitation density from 2.10^{15} cm^{-3} to 2.10^{17} cm^{-3} only affects the distribution of the carriers within each barrier subband and not the relative population of the different subbands. As a result at these low excitation densities no large dependence of the carrier capture times on the excitation density is expected.

We demonstrate in Fig. 2.16 for a 50 Å single quantum well that the capture times of electrons and holes decrease whenever a new pair of barrier states is excited. The sharp decrease at an excess energy of 36 meV, which was also experimentally observed[24], originates from the presence of a quantum well bound state located only 4 meV below the barrier band gap. Only electrons with an excess energy larger than 32 meV, which corresponds to a laser excess energy of 36 meV, are able to make a LO phonon induced transition to this bound state. The overlap of the wave function of this bound state with the wave functions of the barrier states is large and thus the capture rate is large, since the wave function of a bound state close to the continuum is only weakly confined in the quantum well layer. The electrons which have an excess energy of less than 32 meV with regard to the barrier band gap are only able to make a transition to the lowest bound subband. Such a transition results in a small capture rate due to the small overlap of the wave functions. The large phonon wave vectors involved in such a capture process also lead to a small capture rate, since the LO phonon matrix element is inversely proportional to the square of the length of the phonon wave vector. We finally note that the carrier capture rate is limited by the relatively slow capture rate of the electrons for small excess energies (<36 meV), whereas for high excess energies the capture rate is limited by the holes.

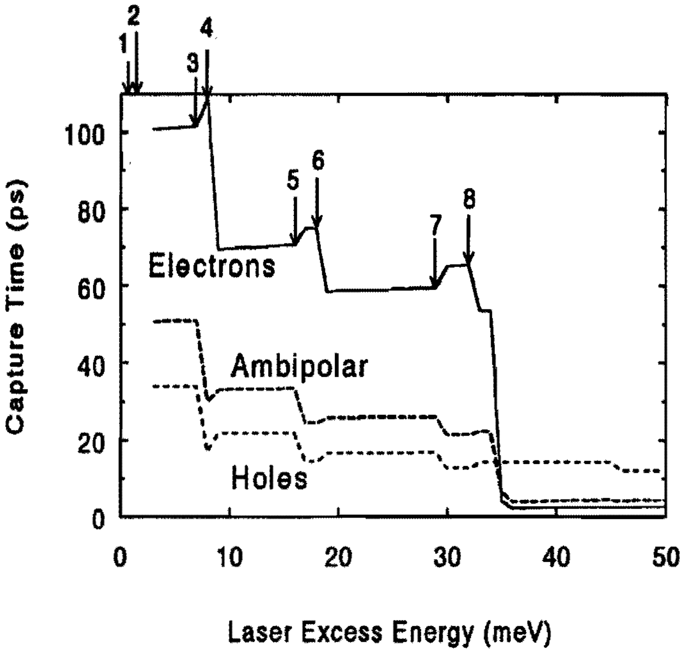

Fig. 2.16. Calculated electron, heavy hole and ambipolar capture times as a function of the laser excess energy with respect to the barrier bandgap, in a SCHQW structure with a well width of 50 Å. The positions of the energy levels in the barrier are indicated by the arrows. For excess energies larger than 36 meV the electrons are captured by the bound state which is only 4 meV below the continuum resulting in a sharp decrease of the capture time.

2.6. Ambipolar Carrier Capture

At low excess energies, as relevant for our experiments, holes will be captured by the well first. After capture, they will electrostatically attract electrons towards the quantum well, resulting in an increase of the electron capture rate. The remaining holes in the barrier layers will be electrostatically repelled by the well, which gives rise to a decrease of the hole capture rate. The net result is an ambipolar capture process with a capture rate which is in between the electron and hole capture rates.

This ambipolar capture rate can be derived by inserting the electron and hole capture rates in a rate equation model. The solution of such a model reads

$$\frac{dn_b}{dt} = -\frac{n_b}{\tau_e} - \frac{1}{2}\left(\frac{p_b}{\tau_h} - \frac{n_b}{\tau_e}\right) = -\frac{(\tau_e + \tau_h)}{2\tau_e\tau_h} n_b = -\frac{n_b}{\tau_a} \tag{9}$$

$$\frac{dp_b}{dt} = -\frac{p_b}{\tau_h} + \frac{1}{2}\left(\frac{p_b}{\tau_h} - \frac{n_b}{\tau_e}\right) = -\frac{(\tau_e + \tau_h)}{2\tau_e\tau_h} p_b = -\frac{p_b}{\tau_a} , \tag{10}$$

with τ_e and τ_h the electron and hole capture times and τ_a the ambipolar capture time. The term $0.5*(p_b/\tau_h-n_b/\tau_e)$ represents the increase and decrease of the electron and hole capture rate, respectively, as a result of their mutual electrostatic interaction.

The validity of the quantum mechanical capture model for both electrons and holes is dependent on the coherence length of the carriers, which is limited by inelastic scattering processes. For a coherence length which is small in comparison with the width of the barrier layers, the carriers are not able to establish coherent wave functions and the carriers should be regarded as a classical fluid. Quantization of the barrier states was observed[25] by photoluminescence excitation spectroscopy in GaAs/$Al_xGa_{1-x}As$ SCH-SQW for structure widths up to 750 Å. Furthermore, from a time-resolved luminescence study[26] on single quantum well structures with and without confinement layers an effective trapping area of about 800 Å was obtained. As a result we expect that the carrier capture process in our structures, with a width of 1000 Å, is governed by the quantum mechanical oscillations. It should be noted that the coherence length of the heavy holes is one order of magnitude smaller than the electron coherence length, due to the large effective mass which enhances the inelastic scattering processes. As a result the capture of the heavy holes should be described in terms of a classical diffusion process. Therefore, we expect that the ambipolar capture process in our structure is governed by a quantum mechanical capture process of the electrons and a classical capture process of the holes. From steady-state photoluminescence experiments in GaAs/$Al_xGa_{1-x}As$ single quantum well structures,

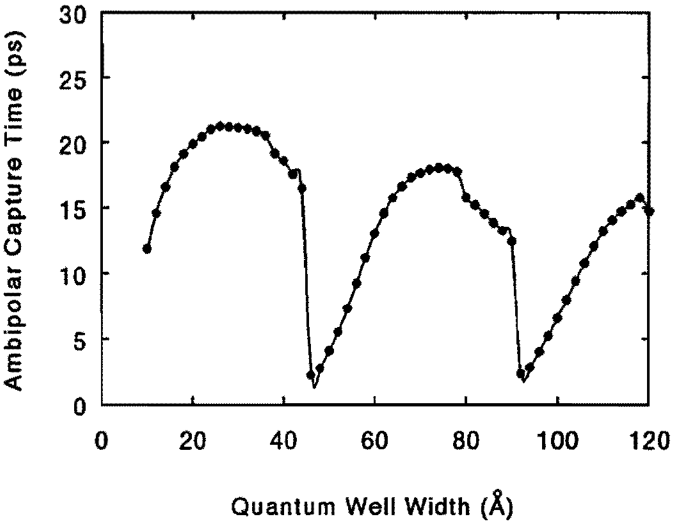

Fig. 2.17. Ambipolar capture time as a function of quantum well thickness for the GaAs/Al$_x$Ga$_{1-x}$As SCH-SQW structure of Fig. 2.3. The ambipolar capture time consists of a quantum mechanical electron capture time, which oscillates as a function of well width, and a classical hole capture time of 12.5 ps.

with a width of 1500 Å, resonances in the carrier capture were already observed as a function of well width[27]. Furthermore, it was demonstrated that the resonances were due to the quantum mechanical character of the electron capture process, which supports our capture model. From the mobility of our n-doped bulk Al$_x$Ga$_{1-x}$As samples we obtain a diffusion time of 12.5 ps for the holes in our structures. This classical diffusion time is also roughly equal to the quantum mechanical hole capture time for a laser excess energy of 36 meV, as shown in Fig 2.16. As a result we calculated our ambipolar capture time with a classical hole diffusion time, which is independent of well width, and a quantum mechanical electron capture time, which shows oscillations as a function of well width. The well width dependence of our ambipolar capture time is plotted in Fig. 2.17. The predicted variations of the carrier capture time originate from the quantum mechanical character of the electron capture process. In the next chapter the dependence on structure of the ambipolar capture time as well its dependence on laser energy, which determines the barrier subband population, will be experimentally investigated by subpicosecond time-resolved luminescence spectroscopy.

References

1 P.W.M. Blom, P.J. van Hall, J.E.M. Haverkort, and J.H. Wolter, SPIE Proceedings Vol. **1677**: Ultrafast Laser Probe Phenomena in Semiconductors and Superconductors, edited by R.R. Alfano, to be published.

2 R. Nagarajan, T. Fukushima, S.W. Corzine, and J.E. Bowers, Appl. Phys. Lett. **59**, 1835 (1991).

3 W. Rideout, W.F. Sharfin, E.S. Koteles, M.O. Vassell, and B. Elman, IEEE Photon. Technol. Lett. **3**, 784 (1991).

4 S.D. Offsey, L.F. Lester, W.J. Schaff, and L.F. Eastman, Appl. Phys. Lett. **58**, 2336 (1991).

5 H. Shichijo, R.M. Kolbas, N. Holonyak, Jr., J.J. Coleman, and P.D. Dapkus, Solid State Commun. **27**, 1029 (1978).

6 J.Y. Tang, K. Hess, N. Holonyak, Jr., J.J. Coleman, and P.D. Dapkus, J. Appl. Phys. **53**, 6043 (1982).

7 S.V. Kozyrev, and A.Ya. Shik, Sov. Phys. Semicond. **19**, 1024 (1985).

8 J.A. Brum, and G. Bastard, Phys. Rev. B **33**, 1420 (1986).

9 M. Babiker, and B.K. Ridley, Superlatt. and Microstruct. **2**, 287 (1986).

10 Y. Murayama, Phys. Rev. B **34**, 2500 (1986).

11 J. Feldmann, G. Peter, E.O. Göbel, K. Leo, H.-J. Polland, K. Ploog, K. Fujiwara, and T. Nakayama, Appl. Phys. Lett. **51**, 226 (1987).

12 D.J. Westland, D. Mihailovic, J.F. Ryan, and M.D. Scott, Appl. Phys. Lett. **51**, 590 (1987).

13 B. Deveaud, F. Clerot, A. Regreny, K. Fujiwara, K. Mitsunaga and J. Ohta, Appl. Phys. Lett. **55**, 2646 (1989).

14 D. Bimberg, J. Christen, A. Steckenborn, G. Weimann, and W. Schlapp, J. Luminesc. **30**, 562 (1985).

15 B. Deveaud, J. Shah, T.C. Damen, and W.T. Tsang, Appl. Phys. Lett. **52**, 1886 (1988).

16 R. Kersting, X.Q. Zhou, K. Wolter, D. Grützmacher, and H. Kurz, Superlatt. Microstruct. **7**, 345 (1990).

17 A. Weller, P. Thomas, J. Feldmann, G. Peter, and E.O. Göbel, Appl. Physics **A48**, 509 (1989).

18 P.J. Price, Ann. of Physics **133**, 217 (1981).

19 M. Babiker, M.P. Chamberlain, A. Ghosal, and B.K. Ridley, Surf. Science 196, **422**, (1988).

20 P.W.M. Blom, R.F. Mols, J.E.M. Haverkort, M.R. Leys, and J.H. Wolter, Proceedings of the 16th European Conference on Optical Communications, Amsterdam 1990, Vol. **1**, p. 59, ISBN 90-5199-037-5.

21 P.W.M. Blom, J.E.M. Haverkort, and J.H. Wolter, Appl. Phys. Lett. **58**, 2767 (1991).

22 S.M. Goodnick, and P. Lugli, Phys. Rev. B. **37**, 2578 (1989).

23 J.A. Levenson, G. Dolique, J.L. Oudar and I. Abram, Phys. Rev. B **41**, 3688 (1990).

24 P.W.M. Blom, C. Smit, J.E.M. Haverkort, and J.H. Wolter, accepted for publication in Phys. Rev.B.

25 M.H. Meynadier, C. Delalande, G. Bastard, M. Voos, F. Alexandre, and J.L. Liévin, Phys. Rev. B **31**, 5539 (1985).

26 H.-J. Polland, K. Leo, K. Rother, K. Ploog, J. Feldmann, G. Peter, E.O. Göbel, K. Fujiwara, T. Nakayama, and Y. Ohta, Phys. Rev. B **38**, 7635 (1988).

27 A. Fujiwara, S. Fukatsu, Y. Shiraki, and R. Ito, Surf. Science **263**, 642 (1992).

Chapter 3

Carrier Capture Time Measurements in GaAs/Al$_x$Ga$_{1-x}$As Separate Confinement Single Quantum Wells

3.1. Introduction

In chapter 2 we have presented both a classical diffusion model and a quantum mechanical model for the carrier capture process in a SCHQW laser structure. The question whether the capture process in these laser structures is dominated by classical diffusion and drift (no oscillations expected) or by quantum mechanical capture (oscillations expected) is relevant for the optimization of the capture efficiency in quantum well laser structures. In order to investigate the capture mechanism we measured the carrier capture times of four separate confinement heterostructure single quantum well structures (SCH-SQW) with well widths corresponding to maxima and minima in the capture times of the quantum mechanical model (section 3.2.A). In order to study the carrier capture dynamics in our GaAs/Al$_x$Ga$_{1-x}$As quantum well structures we have at our disposal a subpicosecond (0.6 ps) laser system. Time-resolved luminescence experiments are performed using the upconversion technique (section 3.2.B) and the pump and probe technique (section 3.2.C). For both experimental techniques the time-resolution is only limited by the duration of the laser pulse.

In section 3.3 we discuss the dependence of the QW luminescence rise times after direct excitation on laser energy, which is relevant for the determination of the carrier capture time from the QW luminescence rise times (section 3.4). Furthermore, the carrier capture times are also obtained from barrier luminescence decay measurements (section 3.5). The dependence of the capture time on quantum well thickness (section 3.6) and laser excess energy (section 3.7) are reported and compared with theoretical predictions. Furthermore, we tracked the Fermi-level in the barrier during capture, which will be reported in section 3.8.

3.2. Experimental Techniques for Subpicosecond Luminescence Spectroscopy

The scattering mechanisms of charged carriers in low dimensional semiconductor systems have been extensively studied in the past decades[1-3]. Information about the various scattering mechanisms can be obtained by investigating the time-resolved behaviour of the carrier distribution function. The time domains of the dominant scattering mechanisms, i.e. carrier-phonon and carrier-carrier collisions, are in the picosecond and femtosecond regime. The investigations of these scattering processes therefore require an experimental technique with high spectral as well as high temporal resolution. As a result of the availability of ultrashort laser pulses optical spectroscopy has proven to be very suitable[4]. In this section our GaAs/Al$_x$Ga$_{1-x}$As quantum well structures as well as the utilized time-resolved luminescence techniques will be discussed.

A. Quantum Well Samples

The experiments presented in this thesis are performed on GaAs/Al$_x$Ga$_{1-x}$As QW structures grown by Molecular Beam Epitaxy (MBE)[5,6]. The carrier capture process is studied in GaAs/Al$_x$Ga$_{1-x}$As single QW structures as shown in Fig. 3.1. These structures consist of ten separate single quantum wells with equal width. The quantum wells are surrounded by 500 Å Al$_{1-x}$Ga$_x$As barrier layers and 100 Å AlAs cladding layers. An advantage of using ten quantum wells rather than one single QW is the

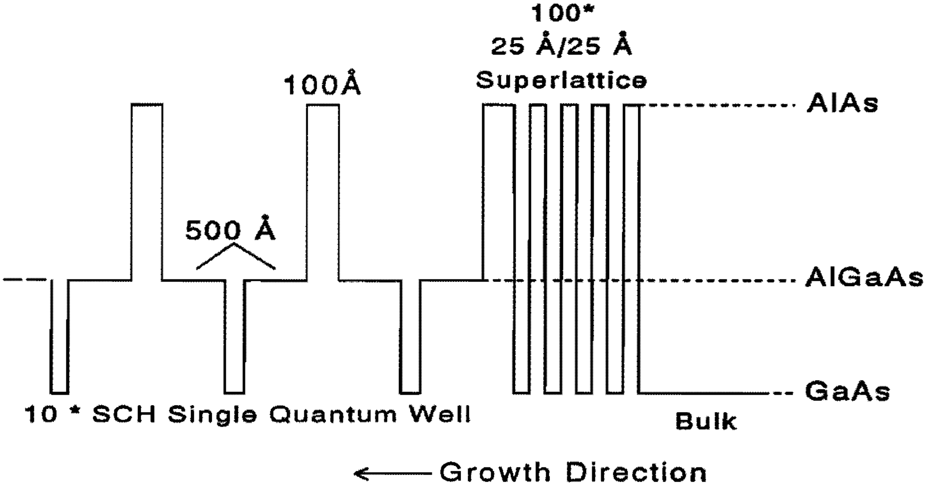

Fig. 3.1. A schematic of the conduction band structure of the multiple SCH-SQW sample used in the experiments. The structures consists of 10 single quantum wells with equal well width which are separated by 100 Å AlAs confinement layers. The Al fraction in the $Al_xGa_{1-x}As$ *barrier layers ranges in the various samples from 0.3 to 0.4 and the quantum well widths were chosen to be 30, 50, 70, and 90 Å, which correspond alternately to maxima and minima in the LO-phonon induced capture times.*

increased luminescence intensity, allowing to measure at a reduced excitation density where carrier-carrier scattering can be neglected as a capture mechanism. As demonstrated in section 2.4, for large multiple quantum well structures the capture time reduces to < 1 ps, independent of well width, which can not be measured with our experimental resolution. By applying the AlAs barriers between the wells, we combine the advantage of large signals from MQW samples with the slow capture process of SQW structures. However, the number of SQW structures in a sample is limited, due to variations of the excitation density in the various wells. The excitation density induced in the single wells close to the surface of the sample is higher than the density induced in the quantum wells close to the superlattice, due to absorption of the laser pulse. Large differences in excitation density, i.e. more than one order of magnitude, are inconvenient in studies of the dependence of the carrier capture and relaxation processes on excitation density. By limiting the number of SQW structures to 10, the difference in excitation density between the first and last QW amounts to a factor of 3 for indirect excitation and is negligible for direct excitation.

In our time-resolved experiments we measure the carrier capture times in quantum wells with well widths L_w=30, 50, 70, and 90 Å. In the quantum mechanical model, which has been discussed in chapter 2 (Fig. 2.17), the well widths L_w=30 and 70 Å correspond to a maximum in the capture time and L_w=50 and 90 Å to a minimum. In the classical point of view the quantum wells of 70 and 90 Å, which exceed the mean scattering length of 60 Å, are expected to collect the carriers more efficiently than the 30 and 50 Å quantum wells. The quantum well structures are grown on top of a 100 period GaAs/AlAs superlattice, which improves the quality of the quantum well interfaces. We also performed experiments on structures with n-doped and p-doped 30 Å quantum wells, in order to study the ambipolar character of the capture process. The structures of the samples used are summarized in Table I. The aluminum

TABLE I. Structure parameters of the samples used in the experiments

Sample	L_w (Å)	x	FWHM exciton (meV)	life time (ps)
W231	26	0.30	10.1	290
W234	90	0.30	4.0	290
W235	48	0.35	7.8	150
W240	70	0.36	5.5	82
W253 (i)	26	0.40	10.0	206
W272 (p)	26	0.39	10.0	180
W273 (n)	26	0.39	10.0	280

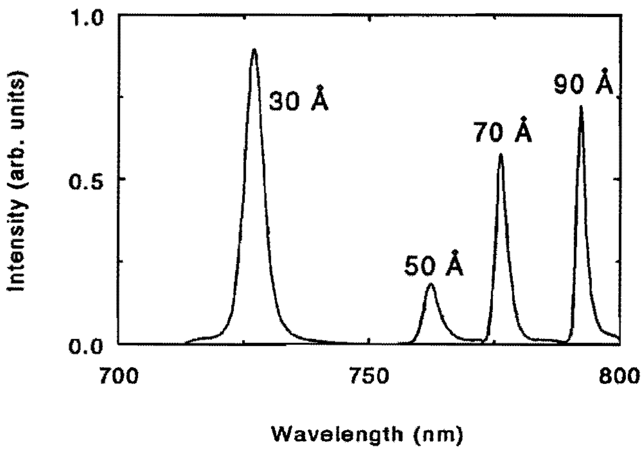

Fig. 3.2. Time-integrated photoluminescence spectrum which contains the QW exciton peaks of the four samples with various well widths. The spectra were obtained at T=4.2 K by CW excitation with a He/Ne laser and the excitation density amounted to 110 mW/cm^2. The FWHM of the exciton peaks were 10.1, 7.8, 5.5, and 4.0 meV for the well widths of 30, 50, 70, and 90 Å respectively.

fraction of the barrier layers was determined from the spectral position of the barrier luminescence peak as well as from photoluminescence excitation (PLE) measurements. The quantum well thickness has been calculated from the spectral position of the QW exciton peak. The FWHM of the QW exciton luminescence peak was determined from the spectra as shown in Fig. 3.2, which were obtained for the various structures at a CW excitation density of 110 mW/cm^2. We observe that a decreasing well width gives rise to an increasing FWHM of the exciton luminescence, since the shift of the energy levels in the well due to a variation in the quantum well thickness of one monolayer increases with decreasing well width. The lifetimes of the photoexcited carriers were determined from the decrease of the QW luminescence after excitation with a short laser pulse, which was measured by using the upconversion technique (section 3.2.B)

B. The Upconversion Technique

As a result of the availability of ultrashort laser pulses luminescence techniques were developed in which the time resolution is limited by the width of the laser pulse. The upconversion technique makes use of the nonlinearity induced by the laser pulse as a "lightgate" for the luminescence. It is based on a frequency mixing technique, which was first used by Mahr and Hirsch[7]. In this upconversion technique the luminescence excited by an ultrashort laser pulse is mixed with the laser itself in a nonlinear crystal to generate the sum or difference frequency radiation. Since the mixing process takes place only during the presence of the laser pulse, this provides time resolution comparable to the laser pulse width, provided certain conditions are satisfied.

Our laser system consists of a modelocked Coherent Antares Nd:YAG laser and a Coherent 702 double jet dye laser. After frequency doubling the YAG laser output consists of a pulse train at 532 nm with a pulse width of 80 ps, a repetition rate of 76 MHz and a maximum power of 3 W. The synchronously pumped double jet dye laser makes use of the dye DCM as a gain medium and of DTDCI as a saturable absorber. Due to the saturable absorber the pulse width is reduced to 0.6 ps at a typical output power of 200 mW in the wavelength range of 610-670 nm.

The experimental setup for the upconversion technique is shown in Fig. 3.3. The laser beam is divided by a beamsplitter (BS) into two parts. One part of the laser beam (10%) is used for the excitation of the sample. By means of three mirrors (M1..M3) the laser pulses are focused on the sample by a positive lens L1 (f=60 mm) to an excitation spot of 40 μm. The sample is mounted on a cold finger which is connected to a liquid nitrogen or helium bath. After collection through lens L1 (f/3) the luminescence of the sample is focused on the nonlinear $LiIO_3$ crystal by lens L2 (f=100 mm). The spot size of the luminescence on the nonlinear crystal is determined by the lens combination L1 and L2 and amounts to 70 μm. The other part of the laser beam (90%) is deflected to a delay line and is used for the sum frequency generation.

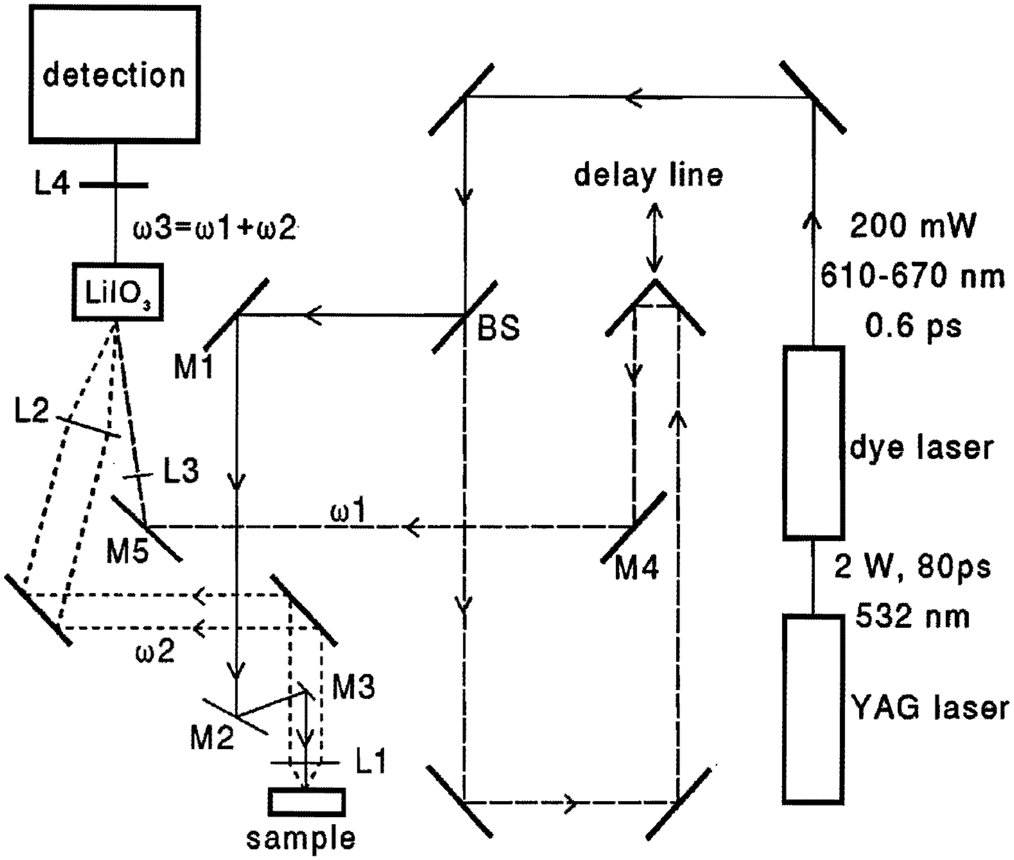

Fig. 3.3. Schematic of the luminescence upconversion setup. The dye laser beam, with a typical power of 200 mW and a pulse width of 0.6 ps, is split into two beams by a beamsplitter BS. The sample is excited via the mirrors M1..M3 and lens L1 with a typical power of 2 mW, which gives rise to an excitation density of 2.10^{16} cm^{-3} in a GaAs/AlGaAs MQW structure. The spot sizes of the luminescence and laser on the nonlinear crystal are determined by the lens combination L1..L3 and amount to 70 μm. After sum frequency generation the upconverted signal of several hundred counts per second is focused into the spectrometer by a quartz lens L4.

The delay line consists of a retro-reflector attached to a translator, which is controlled by a stepper motor drive. A single step equals a displacement of 12.5 μm which corresponds to a time delay of 83.3 fs. The maximum time delay of the system is limited by the length of the translator and amounts to 2 ns. From the delay line the

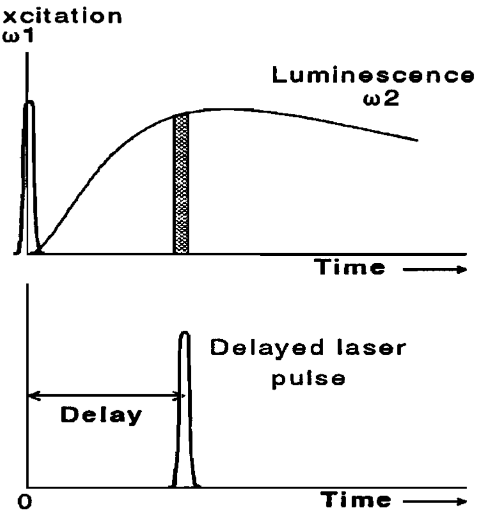

Fig. 3.4. In a nonlinear crystal sum frequency radiation can be generated only with that part of the luminescence which coincides with the delayed laser pulse.

laser beam is guided (M4,M5) to and focused into (L3, f=200 mm, spot size=70 μm) the nonlinear crystal.

Sum-frequency generation between the laser pulses (ω_1) and the luminescence (ω_2) is obtained at a frequency $\omega_3=\omega_1+\omega_2$ whenever both pulses overlap in time as well as position. At a fixed delay sum frequency radiation is only generated between the laser pulses and that part of the luminescence which arrives exactly at the same time at the crystal as the laser pulse, as is illustrated in Fig. 3.4. As a result the dependence of the sum frequency radiation as a function of the delay directly reflects the change of the luminescence intensity as a function of time. The whole design of the setup is optimized for a maximum sensitivity which requires an optimal upconversion efficiency. A maximum spatial overlap can be obtained by optimizing the lens combination L1..L3 to realize equal spot sizes of the laser and luminescence light on the nonlinear crystal. The intensity of the sum frequency radiation is dependent on the product of the luminescence intensity and the laser intensity. Apart from energy conservation ($\omega_3=\omega_1+\omega_2$), sum frequency generation requires phase-matching[8], i.e. $\mathbf{k}_3=\mathbf{k}_1+\mathbf{k}_2$, where $\mathbf{k}_1$, $\mathbf{k}_2$, and $\mathbf{k}_3$ are the wave vectors of the laser pulse, the luminescence and the sum frequency radiation, respectively. In an anisotropic crystal such as $LiIO_3$, with different indices of refraction for the ordinary and extraordinary rays, phase-matching can be obtained by adjusting the angle between the k-vectors of the light and the optical axis. However, since the luminescence is emitted in all directions from the excitation spot, the spread in the direction of the luminescence wave vectors in the nonlinear crystal is determined by the relative aperture of lens L2. For collinear phase matching, the acceptance angle for the luminescence upconversion is quite limited. Fortunately, the angle of acceptance of the luminescence by the nonlinear crystal can be somewhat enhanced by using a non-collinear geometry[9] (Fig. 3.5.) A maximum experimental quantum efficiency of 1.10^{-5} was obtained at an

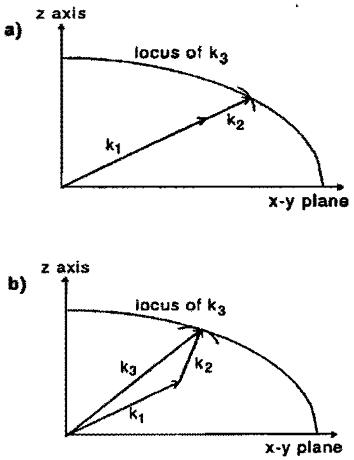

Fig. 3.5. Locus of the sum frequency wave vector k_3 in the plane of the optic axis (z-axis) whose location is determined by phase-matching conditions for

*a:) collinear phase-matching by which **k** conservation is only valid for one particular direction of **k** and*

b:) non-collinear phase-matching, which enlarges the angle of acceptance of the luminescence allowing an increase in the upconversion efficiency.

external angle of 18° between the luminescence (k_2, 700-800 nm) and the laser pulse (k_1, 610-670 nm) for a typical laser power on the non-linear crystal of 30 mW.

The temporal resolution of the sum frequency (330-370 nm) generation is limited not only by the width of the laser pulse, but also by the group velocity dispersion in the nonlinear crystal between the laser pulse (610-670 nm) and the luminescence (720-800 nm)[10]. For a laser pulse of 620 nm and luminescence of 800 nm the group velocity dispersion in our $LiIO_3$ crystal with a thickness of 3 mm amounts to 0.6 ps, which is equal to the laser pulse width. By using non-collinear phase matching this dispersion is reduced by more than a factor of three due to the reduction of the effective length of the upconversion region. For broad luminescence spectra the spectral resolution of the upconversion technique is determined by the spectral bandwidth of the nonlinear crystal, which is governed by the phase-matching condition. By adjusting the angle of the nonlinear crystal the time-resolved spectral distribution of the luminescence can be obtained. The spectral resolution can further be enhanced by dispersing the upconverted signal in a spectrometer. Due to the small signal of the upconverted photons, typically 100 counts/sec, photon counting techniques are used to discriminate against noise. Furthermore, a cooled photomultiplier (EMI 9659 QA) is used to reduce the dark noise. In this thesis the upconversion technique is used to study the carrier capture process as well as the dynamics of excitons in $GaAs/Al_xGa_{1-x}As$ quantum well structures.

C. The Pump and Probe Technique.

A direct method to study the carrier dynamics in semiconductors is the optical pump and probe technique[3,11,12], in which the amount of probe induced photoluminescence is measured as a function of the pump-probe delay. After photoexcitation with the pump pulse, the optically created nonthermal carrier distribution relaxes by carrier-carrier and carrier-phonon collisions. Within a very short time (< 1 ps) the carriers thermalize to a Fermi-Dirac distribution characterized by an effective temperature T_{eff} which is higher than the lattice temperature[4,13,14]. The hot carrier plasma then relaxes to the lattice temperature within several tens of picoseconds. The pump pulse is of sufficient intensity to partly saturate the absorption of the probe pulse as a result of Pauli's exclusion principle. By measuring the reflection, absorption or transmission of the probe pulse as a function of the time delay between the pump and probe pulse, time-resolved information on the occupation of the energy levels located at the laser energy can be obtained. In our experimental setup we determine the absorption of the probe pulse by measuring the intensity of the time-integrated luminescence induced by the probe pulse as a function of the laser wavelength and of the pump-probe delay, yielding both the energy dependence and the temporal dependence of the carrier occupation. A schematic of the experimental setup is shown in Fig. 3.6. The laser and detection systems are equivalent to the systems described in section 3.2.B. We use two laser pulses, which are separated by beamsplitter BS1, with equal energy and temporal width of 0.6 ps. The first strong laser (pump) pulse is used for the excitation of the sample. The second weaker laser (probe) pulse, which excites the sample with a variable delay with regard to the pump pulse, is used for detection. A single step of the delay line of 2 μm gives rise to a time delay of 13.3 fs, the total temporal range amounts to 300 ps. By using linear polarizers (POL) in front of our detection system, which block the reflections of the linear polarized pump or probe beam, we are able to use detection energies as little as 10 meV from the laser energy.

At zero time delay between the pump and probe beam we observe undesirable interference effects, which effectively limit our method to time delays larger than 2 ps. In our carrier capture experiments on the SCHQW samples, as discussed in section 3.2.A, the excitation density of the pump pulse (20 mW) is 3.10^{17} cm^{-3} and of the probe pulse (8 mW) $1.3.10^{17}$ cm^{-3} for an excess energy of the laser of 36 meV with regard to the barrier band gap. For these excitation densities a typical change in the absorption of the probe pulse of 15% is obtained, depending on the time delay. The experimental error in this technique is mainly due to the noise of the laser system of

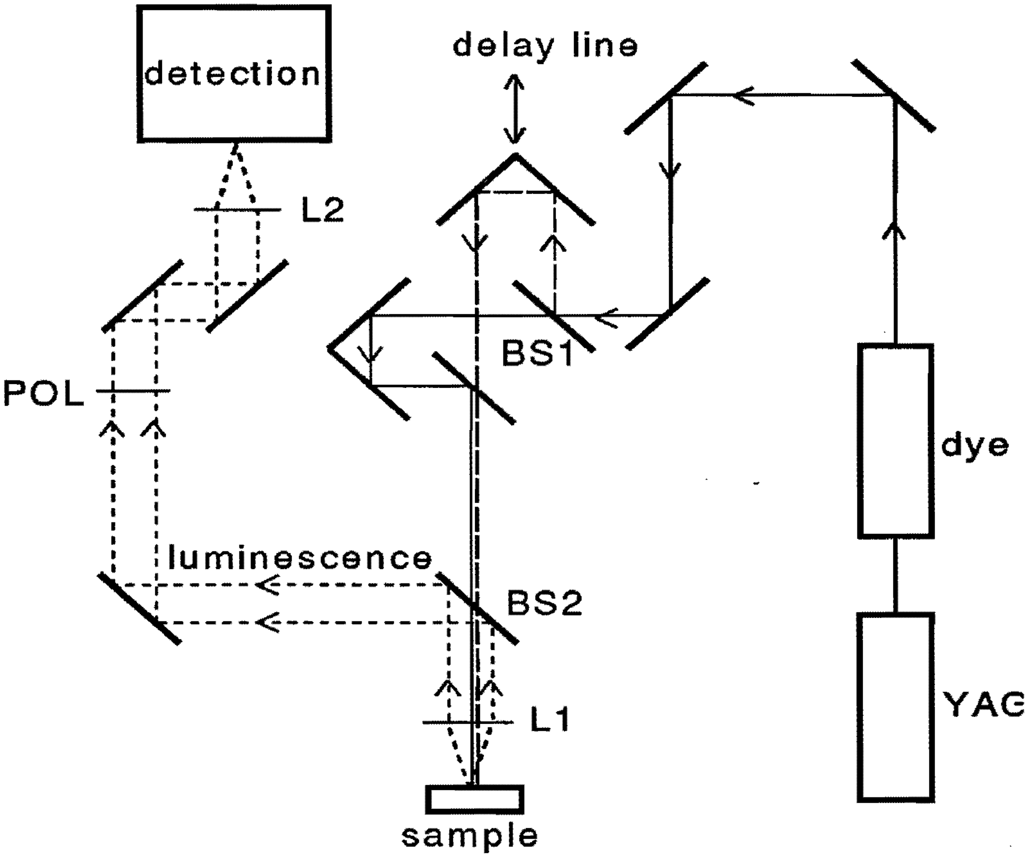

Fig. 3.6. Schematic of the experimental setup of the excitation and probe technique. The sample is excited by two laser pulses, which are separated by a beamsplitter (BS1). After excitation of the sample by the pump pulse (20 mW), the probe pulse (8 mW) excites the sample with an adjustable delay with regard to the pump pulse. A measurement of the time-integrated luminescence, which is induced by the probe pulse, as a function of time delay between the pump and probe pulse, then provides the time-resolved occupation of the energy levels at the laser energy. For laser energies close to the luminescence energy, the reflections of the linear polarized laser spots on the sample are blocked by linear polarizers (POL).

about 4%, which is almost one third of the total variation of the luminescence of the probe pulse due to saturation effects. This noise, however, can be reduced by a factor of 4 by continuously monitoring the laser intensity with a photodiode for normalizing the detected luminescence and by using long integration times of 10 s. Under these conditions the relative uncertainty in the absorption change of the probe pulse is approximately 0.07.

In comparison with the upconversion technique, which has a larger dynamic range, the pump and probe technique has a larger sensitivity and is experimentally less complicated. We use the pump and probe technique for the measurements of the decrease of the carrier concentration in the barrier states after excitation with a laser pulse, which is directly related to the carrier capture dynamics.

3.3. Resonant Exciton Formation in GaAs/Al$_x$Ga$_{1-x}$As Quantum Wells

As discussed in section 2.2 information about the carrier capture process can be obtained from the differences in the rise time of the quantum well exciton luminescence after direct (below the barrier band gap) and indirect (above the barrier band gap) excitation with a subpicosecond laser pulse (0.6 ps). By comparing the QW luminescence rise times after direct and indirect excitation, we eliminate the effect of relaxation of the carriers to the lowest level, where the luminescence is detected. However, a dependence of the QW rise time on laser energy after direct excitation is relevant for the interpretation of the experimental results. In that case, the relaxation of the carriers in the quantum well after indirect excitation will depend on the energy at which the carriers enter the quantum well after the capture process. As a result the laser energy for direct excitation has to be chosen in such a way that the carriers will start their relaxation process from the same energy position in the quantum well after direct and indirect excitation.

The exciton luminescence rise time after direct excitation is governed by carrier cooling, exciton formation and exciton relaxation. In previous studies[15-23] exciton luminescence rise times of several hundreds of picoseconds were obtained and no dependence on the laser energy was observed. This relatively slow rise time was attributed to the slow exciton relaxation process[15,20,22,23]. An expected dependence of the exciton formation process on laser energy was not observed since variations in the exciton formation time, which is expected to be < 20 ps, are very small in comparison with the luminescence rise times. However, in thin quantum wells the slow exciton relaxation process is enhanced due to an increase of the scattering rates of the excitons as a result of the interface roughness[20]. Then the exciton luminescence rise times become comparable with the exciton formation time, which enables us to investigate the dependence of the exciton formation process on laser energy.

We investigated the exciton luminescence rise times of GaAs/AlGaAs multiple quantum well structures as discussed in section 3.2.A, which consist of 10 wells with a thickness of 26 Å. The aluminum fraction in the AlGaAs layers is 0.3 (sample A) and 0.4 (sample B). For both aluminum fractions the quantum wells contain only one electron bound state. The spectral peak of the exciton luminescence had a FWHM of 10 meV for both samples. Our spectral window is determined by the phase-matching conditions in the non-linear crystal and amounts to 2 meV. As a result we only monitor the time-resolved behaviour of the central part of the exciton luminescence peak. In Fig. 3.7 the time evolution of the exciton luminescence of sample A after excitation with a subpicosecond laser pulse is shown for laser energies of 1.892 eV and 1.877 eV, which are both beneath the barrier band gap of sample A. For the different laser energies rise times of 27 and 32 ± 1 ps were obtained respectively. The

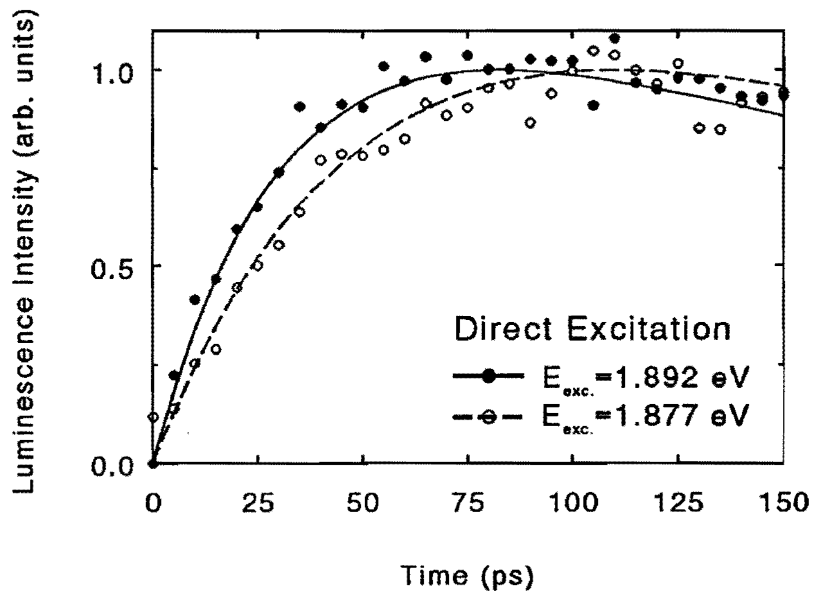

Fig. 3.7. Time-evolution of the exciton luminescence of sample A at the spectral peak (1.705 eV) for two different excitation photon energies. The experiments were carried out at T=8 K with an excitation density of 5.10^{10} cm^{-2} in the quantum wells. The fitted curves, which are plotted as solid and dashed lines, provide luminescence rise times of 27 ps and 32 ps for the laser energies of 1.892 eV and 1.877 eV respectively.

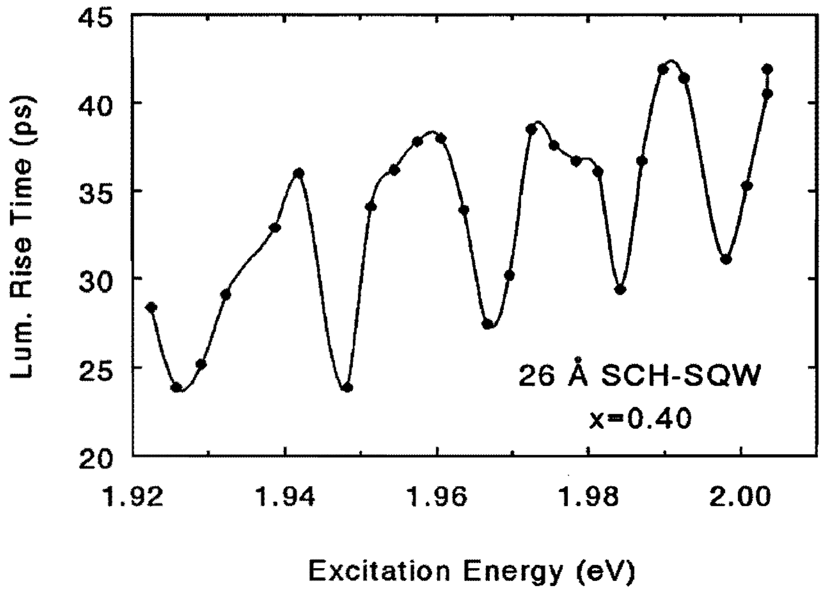

Fig. 3.8. Exciton luminescence rise times (●) at T=8 K as a function of excitation energy of sample B (x=0.4). The excitation density amounts to 5.10^{10} cm^{-2}. Oscillations between 25 and 40 ps in the exciton luminescence rise times are observed with a periodicity of 20 meV. The solid line is a guide to the eye.

time-resolved experiments were carried out at T=8 K using the upconversion technique at an excitation density of 5.10^{10} cm^{-2}. Fig. 3.8 shows the dependence of the exciton luminescence rise times on laser energy in the interval 1.92-2.00 eV for sample B. We observe an oscillating rise time of the exciton luminescence with a period of nearly 20 meV and a difference in amplitude of about 15 ps. This oscillating rise time was also observed in sample A with the same periodicity.

The rise time of the exciton luminescence is determined sequentially by the relaxation of the photoexcited electrons and holes, the formation of excitons and the exciton relaxation. An electron and hole can form an exciton by means of acoustic and optical phonon emission as well as carrier-carrier scattering. In order to explain the

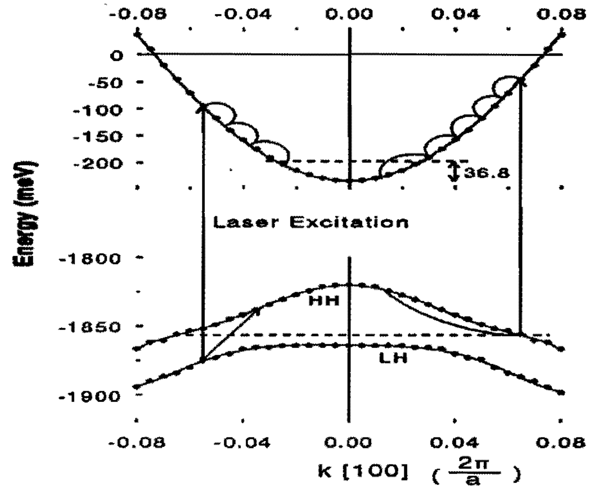

Fig. 3.9. The calculated band structure of a 26 Å $GaAs/Al_{0.4}Ga_{0.6}As$ *quantum well, which consists of one electron subband, one light-hole subband and two heavy-hole subbands. The dispersion of the electron and hole subbands is calculated using empirical pseudo-potentials*[24]*. After photoexcitation the electrons and holes emit LO phonons until they are within one LO phonon energy (36.8 meV) of their subband minima.*

oscillations in the rise time we consider the positions of the electrons and holes in their subbands after photoexcitation and during exciton formation. In Fig. 3.9 the band structure of the bound states in a quantum well with a well width of 26 Å is plotted. The quantum well contains one electron bound state, one light-hole bound state and two heavy-hole bound states. The dispersion relations of the various subbands in momentum space are calculated by means of an empirical pseudo-potential method described by Cuypers and van Haeringen[24]. After absorption of laser photons, electrons are excited from the first heavy- and light hole subbands to the electron subband. Initially, the spread of the electrons in energy and momentum space is small, since it is only determined by the laser linewidth (0.5 meV). Thus the electrons are created at two specific energies in their subband and the holes at a certain energy in the heavy- and light-hole subbands. After excitation both the electrons and holes will relax by means of a LO phonon cascade until they are within one LO phonon energy of their subband minima, as shown in Fig. 3.9. The light holes will first relax within their own subband and subsequently scatter to the heavy-hole subband. During and after the LO phonon cascade the carriers spread out in momentum and energy space due to carrier-carrier scattering. As a result of the larger effective mass the carrier-carrier scattering and thus the diffusion in momentum space of the heavy-holes are almost one order of magnitude larger than the scattering rate and diffusion of the electrons. From Monte-Carlo calculations[25] we obtained that for a carrier density of 5.10^{10} cm^{-2} the distribution of the electrons in momentum space only broadens from 0.5 meV to a few meV during the LO phonon cascade. In Fig. 3.10 the energy positions after the phonon cascade of the electrons (3.10a), which were excited from the heavy- (e_{hh}) and light-hole bands (e_{lh}), and of the heavy- (hh) and light holes (lh) (3.10b), relative to their subband minima, are plotted as a function of laser energy.

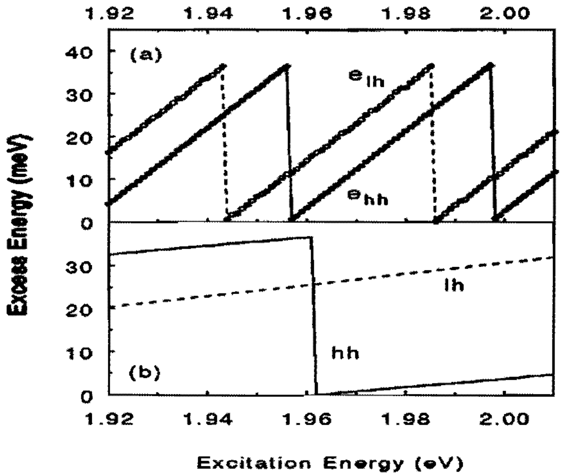

Fig. 3.10. The excess energy of the electrons (3.10a), which are excited from the heavy-hole (e-hh) and light-hole (e-lh) subbands, and holes (3.10b) after the LO phonon cascade as a function of the excitation energy. The electron excess energies continuously vary between 0 and 36.8 meV with a period of 42 meV. The excess energy of the light holes gradually decreases from 32 meV to 20 meV as the excitation energy decreases from 2010 meV to 1920 meV. The heavy-hole excess energy first decreases from 5 meV to 0 meV as the excitation energy decreases from 2010 meV to 1962 meV and then jumps to the LO phonon energy.

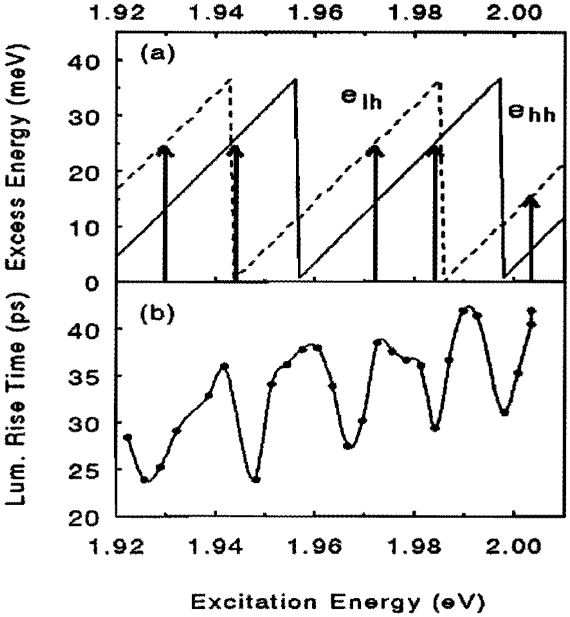

Fig. 3.11. Comparison between electron excess energies (3.11a) and exciton luminescence rise times (3.11b) as a function of excitation energy. A minimum in the exciton rise times is observed whenever free electrons and holes are able to form excitons by LO phonon emission. The minima correspond to electron excess energies of about 25 meV, since holes are available at the subband maximum for all laser energies.

In order to understand the origin of the oscillating behaviour of the exciton rise time we compare in Fig. 3.11 the position of the photoexcited electrons after their LO phonon cascade (3.11a) with the observed rise times (3.11b) as a function of laser energy. We find that the minima in the experimental rise times correspond to the situation that electrons and holes can form an exciton by the emission of a LO phonon, a process which is expected[26] to take place within 100 fs. For example at a laser energy of 1.985 eV the excess energy of the electrons excited from the heavy-hole subband (e_{hh}) amounts to 25 meV, whereas the excess energy of the heavy-hole is about 2 meV. By emitting a LO phonon of 36.8 meV, the electron-hole pair lowers its total energy by 10 meV, which is nearly equal to the exciton binding energy for a thin quantum well[27]. With decreasing laser energy the next minimum occurs at 1.970 eV where the excess energy of the electrons excited from the light-hole subband amounts to 25 meV after the phonon cascade. The energy positions of the LO phonon assisted exciton formation, which are indicated by the arrows in Fig. 3.11a, correspond within a few meV to the observed minima of the exciton luminescence rise times. It should be noted that the inaccuracy in the exact position of the exciton ground state also amounts to a few meV, due to the large FWHM of 10 meV of the exciton peak. For laser energies smaller than 1.960 eV the excess energy of the heavy-holes is close to the LO phonon threshold. By means of carrier-carrier scattering, which is a fast process for the heavy holes as a result of their large effective mass, a part of the heavy-hole population exceeds the LO phonon threshold and is immediately transferred to the subband minimum by LO phonon emission. It should be noted that the electrons have to emit 4 to 6 LO phonons to reach the subband minimum, which gives rise to a scattering time of about 1 ps for the total phonon cascade. Our Monte-Carlo simulation reveals that for all laser energies a large part of the heavy holes, which have to emit only one or no LO phonon, is already transferred to their subband minimum before the electrons have completed their LO phonon cascade. Therefore, we also observe minima in the rise times at laser energies of 1.948 and 1.927 eV, where the electron excess energies are close to 25 meV. According to our model, we should also expect a minimum at a laser energy of 1.957 eV, where the electron excess energy e_{hh} equals zero and the light-hole excess energy (lh) amounts to 25 meV. However, since the holes are already spread out in energy before the electrons have completed their LO phonon cascade, no minimum is observed at this laser energy.

In a sample with n-doped quantum wells, however, this minimum should appear, since electrons are already available at the subband minima at the moment that the light holes have completed their cascade and start to diffuse in momentum space. The experimental exciton rise times for a n-doped (2.10^{11} cm^{-2}) GaAs/Al$_x$Ga$_{1-x}$As multiple quantum well with a well width of 26 Å and an aluminum fraction of 0.4 is plotted

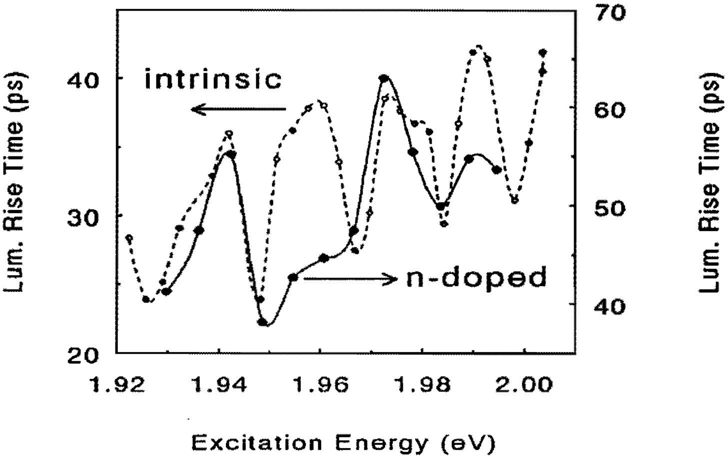

Fig. 3.12. Exciton luminescence rise times (●) as a function of excitation energy for a sample with n-doped quantum wells. The layer structure of the sample is identical to sample B and the dopant density is 2.10^{11} cm^{-2}. Compared to the intrinsic sample B (dashed line) no maximum is observed at a laser energy of 1.957 eV, due to the LO phonon emission induced exciton formation of holes (lh) with an excess energy of 25 meV and electrons at their subband minimum.

in Fig. 3.12 as a function of laser energy. The exciton peak of the n-doped sample was shifted slightly (9 meV) to a higher energy in comparison with the undoped sample, due to a somewhat smaller width. Therefore, in order to compare the rise times of both samples the laser energies of the n-doped sample are shifted 9 meV to lower energy. We observe that for the n-doped sample the maximum in the luminescence rise time at 1.957 eV of the undoped sample has disappeared, which strongly supports our model.

The diffusion of the carriers by means of carrier-carrier scattering in energy and momentum can be enhanced by increasing the excitation density. We find that with increasing excitation density from 5.10^{10} cm^{-2} to 5.10^{11} cm^{-2} the oscillations of the rise times are reduced within our experimental error of ±1 ps. As expected, we find that both the rise time as well as the amplitude of the oscillations decrease since at high carrier densities the electron distribution is already smeared out before the phonon cascade is completed. The decrease of the average rise time with increasing excitation density, which was already observed by Damen et al.[22], was attributed by them to an increase of the exciton-exciton collisions, which enhances the relaxation of the excitons after formation.

For thicker quantum wells with more than one bound electron state no dependence of the exciton luminescence rise time on laser energy was observed. Then the number of energy positions where carriers are created increases, which smears out the resonances. Furthermore, the carriers created in the highest subbands smear out in energy and momentum during the relaxation due to the inter-subband scattering, which is about one order of magnitude slower than intra-band scattering[28]. Thus the choice of the laser energy in order to obtain the same cooling in the quantum well after direct and indirect excitation is only relevant for rise time measurements at low excitation densities on thin quantum wells.

In conclusion we for the first time have observed oscillations in the exciton luminescence rise times as a function of laser energy. The origin of these oscillations arises from the LO phonon assisted exciton formation, a process which is dominant whenever the sum of the excess energies of the electrons and holes amounts to 25 meV. Furthermore, we have demonstrated that our model is consistent with experiments on n-doped samples, which show an additional minimum in the rise time. Finally, the amplitude of the oscillations decreases with increasing excitation density as a result of the enhanced carrier-carrier scattering.

3.4. Rise Time of the Quantum Well Luminescence

The capture times of photoexcited carriers in the SCH-SQW structures reported in section 3.2.A, are experimentally measured by two different techniques with picosecond resolution. In the first technique, we deduce the carrier capture times from subpicosecond time-resolved luminescence experiments using an upconversion lightgate (3.2.B). The capture times are determined from the differences in the rise time of the quantum well luminescence after direct (below the barrier band gap) and indirect (above the barrier band gap) excitation with a subpicosecond laser pulse (0.6 ps), in order to eliminate the effect of relaxation of the carriers in the quantum well. In order to obtain the same cooling inside the quantum well for direct and indirect excitation, the number of carriers inside the wells is kept constant in both experiments and the excitation energy for direct excitation is chosen one LO phonon energy (36.8 meV) times $(1+m^*_e/m^*_h)$ below the excitation energy for indirect excitation. The sample temperature is maintained at a temperature of 8 K in order to avoid phonon absorption induced heating of the carriers. In Fig. 3.13 the time

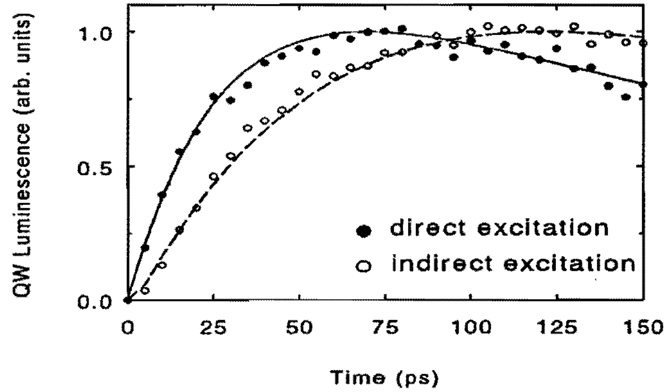

Fig. 3.13. Experimental determination of the carrier capture time using rise time differences of the quantum well luminescence after direct (closed circles) excitation into the quantum well and indirect (open circles) excitation into the $Al_xGa_{1-x}As$ barriers with a laser pulse (0.6 ps). The curves are fitted to the experiments using simple rate equations. From these fits a capture time of 20 ps is derived for this structure. The experiments were carried out at an excitation density of 2.10^{16} cm^{-3} and at a temperature of 8 K on a $GaAs/Al_xGa_{1-x}As$ SCH-SQW structure with a well width of 26 Å.

evolution of the quantum well luminescence is shown for a 26 Å quantum well after direct and indirect excitation. This experiment is carried out at a laser intensity of 2 mW for indirect excitation, corresponding to a low excitation density of 3.10^{16} cm^{-3}. For indirect excitation, the laser excess energy with regard to the barrier band gap is 36 meV. By fitting the experimental rise times to the rate equations, as discussed in section 2.2, we obtain a capture time of 19.1 ± 2 ps for this well width. Furthermore, no dependence of the capture time on the excitation density was found in the range 3.10^{15} cm^{-3} to 2.10^{17}cm^{-3}. For larger excitation densities no capture times could be obtained due to band filling in the quantum well. Finally, we performed upconversion measurements at T=77 K in order to investigate the temperature dependence of the carrier capture time, as shown in Fig. 3.14. An increase of the temperature is expected to decrease the carrier capture efficiency due to an enhanced LO phonon absorption, which gives rise to an increase of the carrier escape from the well. From

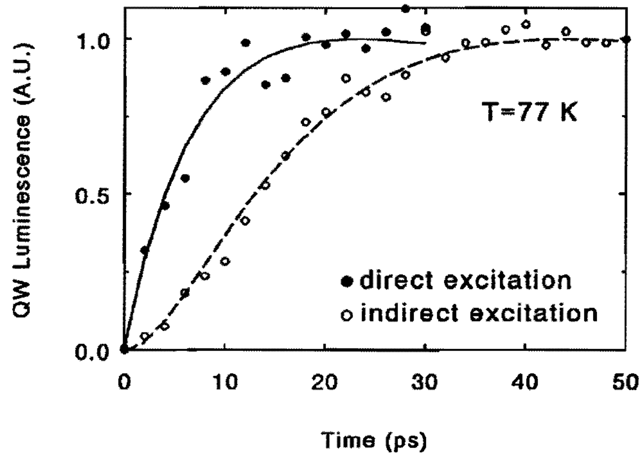

Fig. 3.14. Experimental determination of the carrier capture time at T=77 K using rise time differences of the quantum well luminescence after direct (closed circles) excitation into the quantum well and indirect (open circles) excitation into the $Al_xGa_{1-x}As$ barriers. The other experimental conditions are identical to those in the measurement of Fig. 3.14.

the rise time difference a capture time of 17.7±2 ps was obtained, which equals the capture time of 19.1±2 ps measured at T=8 K within experimental error. At T=77 K, however, the phonon absorption process is still two orders of magnitude smaller than the LO phonon emission process. Furthermore, a large carrier escape is only possible for a large occupation of the energy states located within one LO phonon energy of the barrier states. This large occupation is not obtained as a result of the low excitation density and the large depth (250 meV) of the quantum well. Therefore, no temperature dependence of the carrier capture time is observed up to 77 K.

3.5. Decay of the $Al_xGa_{1-x}As$ Barrier Luminescence

The rise time difference of the quantum well luminescence has been compared with the decrease of the carrier concentration of the barrier states. Therefore, we have performed two-pulse correlation experiments on the luminescence of the barrier states. In a two-pulse correlation experiment, the PL-*decay* of the barrier layers shows up as an *increase* of the correlated PL-signal. This can be understood as follows: A strong excitation pulse (2.10^{17} cm^{-3}) creates electrons and holes in the barrier states and reduces the absorption of a second laser pulse (1.10^{17} cm^{-3}) with the same photon energy. If, however, the delay between the laser pulses exceeds the carrier capture time, then the absorption of the second laser pulse is no longer reduced. As a result the barrier luminescence due to the probe pulse is expected to increase with increasing time delay between the laser pulses until the carriers of the first pulse are captured by the well. In Fig. 3.15a the correlated barrier luminescence is shown for a 70 Å quantum well as a function of the delay between the laser pulses together with a fitted curve, which indicates a capture time of 14.8 ± 2 ps. The temporal width of the laser pulses was 0.6 ps and the excess energy of the pump and probe pulse (2.014 eV) with regard to the barrier band gap (1.981 eV) was 33 meV. The detection energy was set to the maximum of the barrier luminescence (1.987 eV) with a broad detection window of 10 meV. The fact that the increase of the correlated barrier luminescence

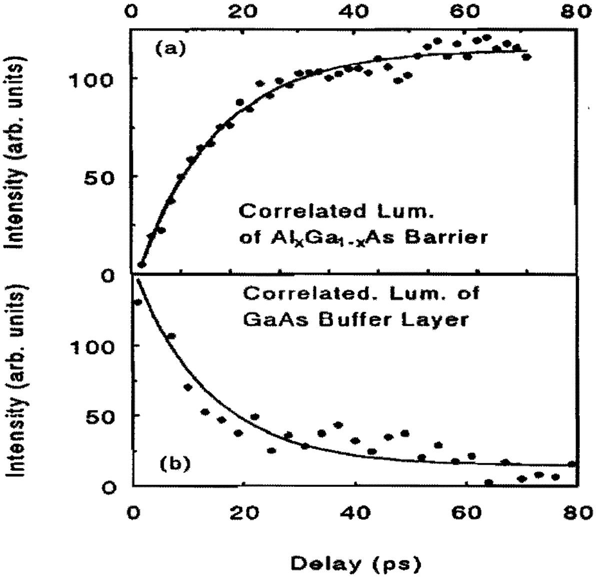

Fig. 3.15. Determination of the capture time from the decay of the barrier population. In the upper part (Fig. 3.15a) the correlated $Al_xGa_{1-x}As$ barrier luminescence is shown as a function of time delay between two laser pulses for a SCHQW with a 70 Å quantum well. The time-increase of the probe induced barrier luminescence results from a time-increase of the absorption of the probe pulse and is directly related to the carrier capture time. In the lower part (Fig. 3.15b) the correlated luminescence of the GaAs buffer layer, which is located underneath the quantum wells, is plotted as function of the delay between the laser pulses. The decrease of the bulk GaAs luminescence arises from the fact that the transmission of the probe pulse through the quantum well structure decreases in time as a result of the carrier capture process.

is actually due to an increase of the probe absorption is confirmed by a "transmission" type of experiment in which we detect on the luminescence energy of the bulk GaAs buffer layer, which is located between the substrate and the quantum wells. The intensity of the bulk GaAs luminescence peak decreases with decreasing probe *transmission* through the SCHQW structure, resulting in a decrease of this GaAs luminescence as a function of the pulse delay, as is shown in Fig. 3.15b. As expected, the time constant of the increase of the $Al_xGa_{1-x}As$ luminescence (Fig. 3.15a) is also found in the decrease of the GaAs luminescence (Fig. 3.15b) as a function of the delay between the laser pulses.

3.6. Well Width Dependence of the Carrier Capture Time

We have measured the capture time for a set of SCHQW samples with different quantum well thickness. The variation of the observed carrier capture times as a function of well width is shown in Fig. 3.16. In all measurements the excess energy of the laser with regard to the barrier band gap was between 30 and 36 meV. We for

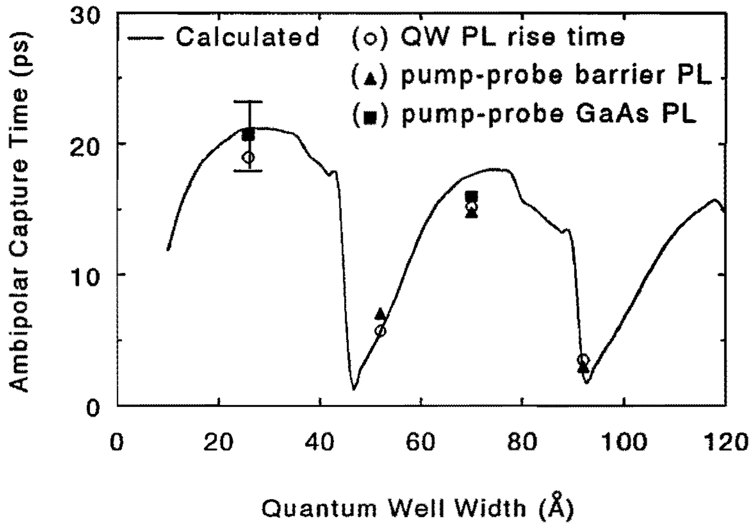

Fig. 3.16. Observation of an oscillating carrier capture time. The figure shows the agreement between the experimentally observed capture times with the theoretical calculated ambipolar capture times. The experimental data have been obtained by (○) upconversion measurement of the difference in QW rise times, by (▲) two-pulse correlation measurements of the population decay in the barrier layers and by (■) "transmission-like" correlation experiments detecting the bulk GaAs PL-signal.

the first time find oscillations in the carrier capture time between 3 and 20 ps as a function of quantum well width. It should be noted that for all samples the capture times obtained from the correlation measurements reproduce within experimental error (±2 ps) with the capture times derived from the quantum well rise times. Also included are the predictions of our ambipolar capture model. In this model, the variations of the capture time are governed by the quantum mechanical electron capture time, as discussed in section 2.6. The observed capture times are in excellent agreement with the theoretically predicted ambipolar capture times.

The large discrepancies between predicted[29,30] (SQW and superlattice) and experimental[31-36] (MQW) capture times reported in literature and especially the lack of observed oscillations in the carrier capture time, were initially attributed[37] to the fact that the quantum mechanical approach of the carrier capture process in quantum well structures would not be valid, because the barrier states are not coherent over the entire barrier width. For structures with thick barrier layers of 2000 Å, as regarded by those authors, the classical approach is expected to provide a more realistic description of the capture process than the quantum mechanical model. However, in a recent theoretical study[38] we showed that the carrier capture efficiency in MQW structures oscillates not only as a function of well width but also as a function of the barrier width between the wells. This strong dependence of the carrier capture time on the quantum well and barrier width appears to be one of the main reasons for the large discrepancies between predicted and experimental capture times reported in literature. The reported experimental results[31-36] for large MQW structures of < 1 ps, which seem to contradict to the quantum mechanical predictions[29] (SQW), are in very good agreement with the recent predictions of the quantum mechanical capture times in precisely these large MQW structures[38].

In order to verify the ambipolar character of the carrier capture, we measured the carrier capture times in samples with p- and n-doped quantum wells and undoped barrier layers. If the holes are captured first by the quantum well, the quantum well luminescence rise time of the n-doped sample should be faster than the rise time of the p-doped sample. In our experiments no dependence of the carrier capture time on the dopant was observed, which confirms the ambipolar character of the carrier capture process. Because of the mutual agreement between the ambipolar capture model and two experimental methods for determining the structure-dependence of the carrier capture time, we are confident that our ambipolar capture model provides a realistic description of the carrier capture process in SCHQW structures.

3.7. Carrier Distribution in the Barrier after Excitation: Relevance for Capture

A. Pump-Probe Measurements

We investigated the dependence of the carrier capture times on the population of the barrier subbands after excitation with a laser pulse. The carrier distribution function is dependent on the laser excess energy with regard to the barrier bandgap. In Fig. 3.17 the observed rise of the correlated barrier luminescence is shown for laser excess energies of 32 and 36 meV in a SCHQW structure with a quantum well width of 50 Å. At a laser excess energy of 36 meV, as plotted in Fig. 3.18, we observe a sharp decrease of the carrier capture time from 20 to 6 ps. The 50 Å quantum well contains two bound states for the electrons, located at 190 meV and 4 meV below the barrier band gap respectively. It should be noted that a laser excess energy of 36 meV with regard to the barrier band gap corresponds to an excess energy of 32 meV for the electrons and to an excess energy of only 4 meV for the heavy holes, due to the differences in the effective masses. Electrons with an excess energy larger than 32 meV are able to emit a 36 meV LO phonon and are captured into the second subband, which is located only 4 meV below the barrier band gap. The electrons which have an excess energy of less than 32 meV with regard to the barrier band gap are only able to make a transition to the lowest bound state. Thus we show that the

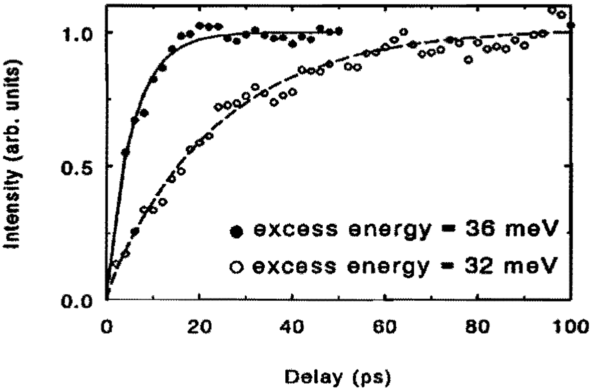

Fig. 3.17. Correlated $Al_xGa_{1-x}As$ barrier luminescence for a 50 Å SCHQW as a function of time delay between two laser pulses at laser excess energies of 32 meV (open circles) and 36 meV (closed circles) relative to the barrier band gap. The fitted curves indicate capture times of 6 and 22 ps for the excess energies of 32 meV (dashed line) and 36 meV (solid line) respectively. The experiments were carried out at an excitation density of 1.10^{17} cm^{-3} and a temperature of 8 K. The detection window was set to 10 meV.

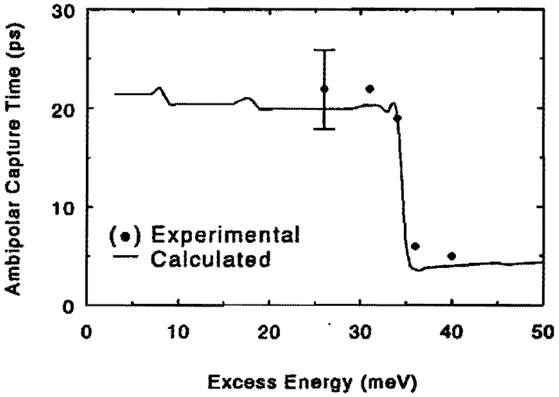

Fig. 3.18. Calculated (solid line) and experimental (closed circles) ambipolar capture time as a function of laser excess energy for a 50 Å quantum well structure. The observed decrease of the capture time at an excess energy of 36 meV originates from the presence of a quantum well bound state close (4 meV) to the continuum and proves that phonon emission is the dominant mechanism for capture.

experimental capture times strongly depend on the population of the energy levels in the barrier.

Furthermore, the sharp decrease of the carrier capture time demonstrates the dominance of the LO phonon emission in the capture process as well as the quantum mechanical character of the electron capture process. For the quantum wells with no bound state close to the continuum only a slight decrease of the carrier capture time as a function of laser energy is observed. We did not measure the capture times for laser excess energies larger than 41 meV, since for these laser energies the electron excess energy exceeds 36 meV. As a result the electrons are able to emit a LO phonon before the capture process which complicates the distribution function.

B. Upconversion Measurements

One can also try to investigate the dependence of the carrier capture times on laser excess energy by the upconversion measurements of the QW luminescence rise times. In Fig. 3.19 the capture times of a 26 Å quantum well are shown as a function of the laser excess energy. We observe that the observed "effective" capture time increases with increasing excess energy, in contradiction with theoretical expectations. However, it should be noted that also for laser energies larger than the barrier band gap a certain part of the carriers is still directly excited in the quantum well, as is schematically indicated in the band diagram of Fig. 3.20a. These carriers are captured by the quantum well by an intraband LO phonon emission with a time constant of 0.1 ps. In Fig. 3.20b the integrated QW luminescence is plotted as a function of laser energy in order to determine the absorption difference after direct and indirect excitation. The part of the carriers that is directly excited in the quantum well is indicated by the shaded area. For laser energies just above the barrier band gap, a large part of the QW luminescence will arise from carriers which are directly excited in the quantum well and no large difference in the rise times after direct and indirect excitation will be observed.

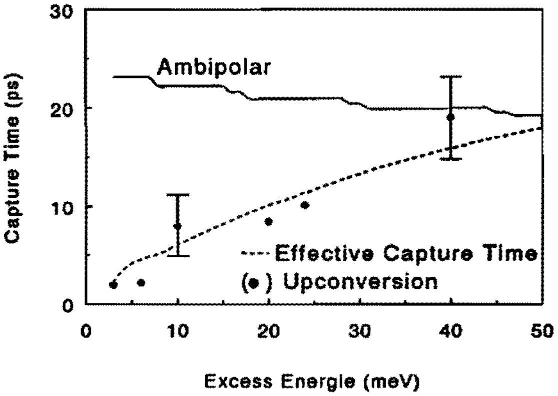

Fig. 3.19. Experimental capture times (•) as function of laser excess energy relative to the barrier band gap obtained from QW rise time measurements. Also included are the calculated ambipolar capture times as well as the effective capture time, which incorporates the contribution of the carriers which are directly excited in the quantum well.

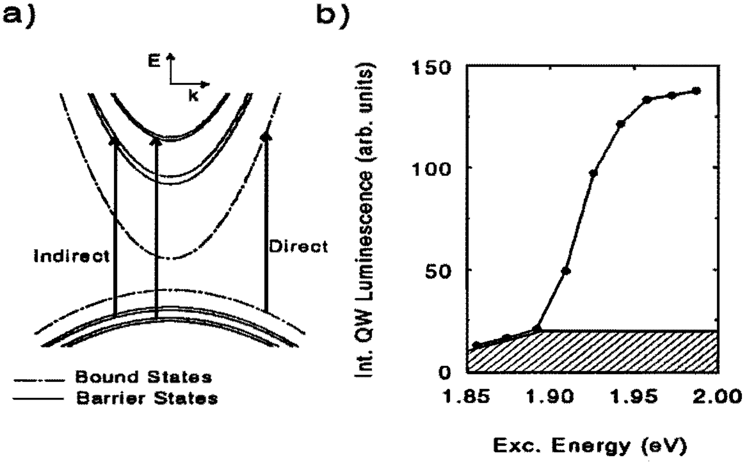

Fig. 3.20. Band structure of a SQW (3.20a) indicating that laser energies larger than the barrier band gap also give rise to direct excitation at large wave vectors. Also shown (3.20b) is the integrated QW luminescence as a function of laser energy in order to determine the absorption after direct and indirect excitation. The contribution of the carriers which are directly excited in the quantum well to the total absorption is indicated by the shaded area.

The observed capture time depends on the ratio between the directly and indirectly excited carriers as well as on both their capture times. From the capture times of the directly (0.1 ps) and indirectly excited carriers (ambipolar capture time) and their ratio, which is provided by the absorption curve of Fig. 3.20b, we are able to calculate an effective capture time. This effective capture time then represents the net capture time, which would actually be expected from the experimental rise time difference. The calculated and the observed effective capture times are also plotted in Fig. 3.19 together with the theoretical ambipolar capture time. The agreement with the experimental capture times confirms the large contribution of the directly excited carriers to the capture process at small laser excess energies. For larger excess energies, where the number of directly excited carriers is small in comparison with the indirectly excited carriers, the effective capture time approaches the theoretical ambipolar capture time.

3.8. Measurement of the Quasi Fermi Level in the Barrier

In the previous experiments we showed that the carrier capture time depends on the population of the barrier states. The carrier capture time was determined by measuring the energy integrated barrier luminescence with a broad detection wavelength window. For low carrier densities ($<2.10^{17}$ cm^{-3}), where carrier-carrier scattering is small in comparison with LO phonon emission, the carrier distribution in the barrier subbands after photoexcitation will be mainly determined by the capture times of the various subbands. At high carrier densities ($>5.10^{17}$ cm^{-3}), however, the photoexcited carriers will form a Fermi-Dirac like distribution immediately after photoexcitation. In such an experiment the number of carriers and thus the quasi Fermi level in the barrier layers will decrease, due to the capture process, as a function of time after excitation with a laser pulse. As a result, the population of the barrier subbands and thus the carrier capture time will be time dependent. Therefore, the carrier capture times, which are determined from the QW luminescence rise times and the barrier luminescence decay, are time-averaged values. We study the dynamical behaviour of the carrier capture process by measuring the position of the quasi Fermi level after excitation with a subpicosecond laser pulse (0.6 ps) as a function of time. This can be achieved by reducing the detection wavelength window to 3 meV and then varying the *detection* energy at a fixed laser excess energy. After excitation with the first laser pulse (3.10^{17} cm^{-3}) the quasi Fermi level of the electrons in the barrier states starts to decrease due to the capture of the carriers. As long as the quasi Fermi level is above the detection energy, the carriers created by the weaker probe pulse (1.10^{17} cm^{-3}) will contribute to the luminescence at the detection energy and thus to the rise of the correlated barrier luminescence. If, however, the quasi Fermi level is below the detection energy, then the carriers of the second pulse will quickly relax down to the quasi Fermi level without contributing to the luminescence at the detection energy. As a result the rise of the correlated barrier luminescence as a function of pulse delay stops at the moment the quasi Fermi level, which is determined by the number of carriers created with the pump pulse, has passed the detection energy. In our experiments the quasi Fermi level is lifted almost 9 meV by the second laser pulse, which means that the quasi Fermi level is 9 meV below our detection energy at the moment that the barrier luminescence reaches its maximum constant value. By measuring the rise time of the correlated barrier luminescence at various detection energies we are able to track the electron quasi Fermi level as a function of time. In Fig. 3.21 the rise of the correlated barrier luminescence is shown for a 50 Å QW for detection energies located at 9 meV and 15 meV above the barrier band gap. The time constants of the correlated rise times are 25.0 ± 2 ps and 15.2 ± 2 ps respectively. The excess energy of the laser with regard to the barrier band gap was 36 meV. By detecting at 15 meV above the barrier band gap we deduce from the rise time of 15.2 ps that the quasi Fermi level was located 6 meV above the barrier bandgap 15 ps after excitation. In Fig. 3.22 the position of the quasi Fermi level with regard to the barrier bandgap, which is determined from measurements at several detection energies, is plotted as a function of time. As stated above, the decrease of the carrier

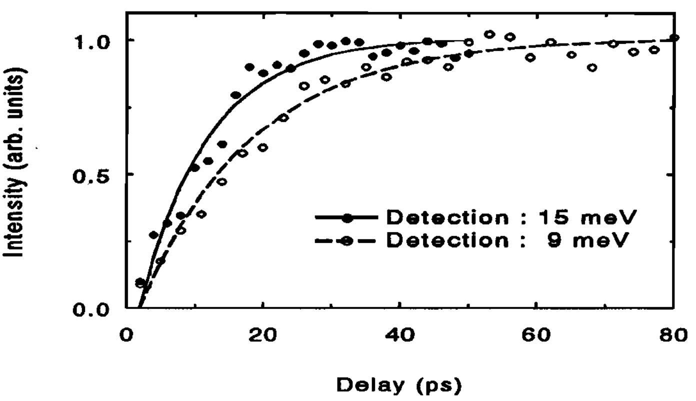

Fig 3.21. Correlated $Al_xGa_{1-x}As$ barrier luminescence for a 50 Å SCHQW as a function of time delay between two laser pulses at detection energies of 9 (open circles) and 15 meV (closed circles) above the barrier bandgap. The fitted curves provide capture times of 15 (solid line, 15 meV) and 25 ps (dashed line, 9 meV) respectively. The experiments were carried out with a laser excess energy of 36 meV at an excitation density of 2.10^{17} cm^{-3} and a temperature of 8 K. The detection window was set to 3 meV, which is the main difference with Fig. 3.15a.

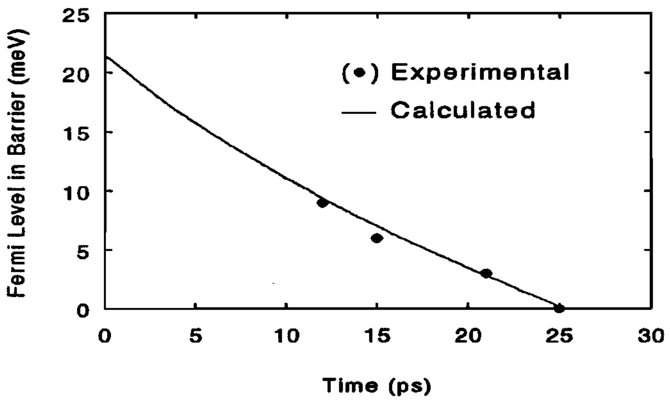

Fig. 3.22. Predicted (solid line) and measured (closed circles) position of the electron Fermi level in the barrier as a function of time after excitation with a laser pulse. The excess energy of the detection energies relative to the barrier band gap was varied between 9-18 meV, whereas the laser excess energy of both the pump and probe pulse was constant at 36 meV.

concentration and thus the quasi Fermi level after photoexcitation will be governed by a time-dependent capture time. The carrier capture process, however, is generally characterized by a time-averaged constant capture time. The calculated decrease of the quasi Fermi level due to the measured time-averaged capture time is also shown in Fig. 3.22 as the solid curve. The agreement between the experimental points and the curve calculated with a time-averaged capture time suggests that the time-averaged capture time provides an adequate approximation of the dynamics of the capture process.

In conclusion, from both subpicosecond QW rise times measurements and pump-probe correlation experiments on the barrier luminescence, oscillations in the capture time between 3 and 20 ps were deduced, dependent on quantum well thickness. The observed capture times are in agreement with the theoretical predictions of an ambipolar capture model. In this model, the variations of the carrier capture times are due to the quantum mechanical capture process of the electrons. The ambipolar character of the capture process was confirmed by experiments on doped samples. The dynamics of the capture process are studied by measuring the position of the quasi Fermi level as a function of time. From the dependence of the carrier capture time on the laser excess energy we find that the capture times are very sensitive to the population of the barrier subbands. Furthermore, these experiments also reveal the dominance of the LO phonon emission in the capture process.

References

1 E.M. Conwell, "High field transport in semiconductors", Solid State Physics, Suppl. 9, F. Seitz, D. Turnbull, and H. Ehrenreich eds., New York: Academic (1967).

2 D.K. Ferry, J.R. Barker, and C. Jacobani eds., "Physics of nonlinear transport in semiconductors", New York: Plenum (1979).

3 J. Shah, and R.F. Leheny, "Semiconductors probed by ultrafast laser spectroscopy", R.R. Alfano ed., New York: Academic, 45 (1984).

4 J. Shah, IEEE J. Quantum Electronics, QE-**22**, 1728 (1986).

5 K. Ploog, "Crystals: Growth, Properties and Applications", H.C. Freyhardt ed., Springer-Verlag, Berlin and New York, Vol.**3**, 75 (1980).

6 C.T. Foxon, and B.A. Joyce, Curr. Top. Mater. Sci. **7**, 1 (1981).

7 H. Mahr and M.D. Hirsch, Opt. Commun. **13**, 96 (1975).

8 D.A. Kleinmann, Laser handbook, Vol. **2**, T.E. Arechi ed., Schulz-Dubois (1972).

9 L.M. Weegels, Master thesis Eindhoven University of Technology (1988).

10 J. Shah, IEEE J. Quantum Electronics, QE-**24**, 276 (1988).

11 C.V. Shank, R.L. Fork, R.F. Leheny, and J. Shah, Phys. Rev. Lett. **42**, 112 (1979).

12 P.W.M. Blom, C. Smit, J.E.M. Haverkort, and J.H. Wolter, "Blocking of Γ→X transfer in GaAs/AlAs short period superlattices due to X-state band filling", submitted to Appl. Phys. Letters.

13 K. Kash, J. Shah, D. Block, A.C. Gossard, and W. Wiegmann, Physica **134** B, 189 (1985).

14 K. Leo, W.W. Rühle, H.J. Queisser, and K. Ploog, Appl. Phys. A **45**, 35 (1988).

15 Y. Masumoto, S. Shionoya, and H. Kawaguchi, Phys. Rev. B **29**, 2324, (1984).

16 D.A.B. Miller, D.S. Chemla, T.C. Damen, T.H. Wood, C.A. Burrus, A.C. Gossard, and W. Wiegmann,
IEEE J. Quantum Electronics QE-**21**, 1462 (1985).

17 T. Takagahara, Phys. Rev. B **31**, 6552 (1985).

18 T. Takagahara, Phys. Rev. B **32**, 7013 (1985).

19 J. Feldmann, G. Peter, E.O. Göbel, P. Dawson, K. Moore, C. Foxon, and R.J. Elliot, Phys. Rev. Lett. **59**, 2337 (1987).

20 J. Kusano, Y. Segawa, Y. Aoyagi, S. Namba, and H. Okamoto,
Phys. Rev. B **40**, 1685 (1989).

21 A. Honold, L. Schultheis, J. Kuhl, and C.W. Tu,
Phys. Rev. B **40**, 6442 (1989).

22 T.C. Damen, J. Shah, D.Y. Oberli, D.S. Chemla, J.E. Cunningham, and J.M. Kuo, Phys. Rev. B **42**, 7434 (1990).

23 M. Zachau, J.A. Kash, and W.T. Masselink, Phys. Rev. B **44**, 8403 (1991).

24 J.P. Cuypers, and W. van Haeringen,
J. Phys.: Condens. Matter **4**, 2587 (1992).

25 P.J. van Hall, P.W.M. Blom, C. Smit, L. Drost, and J.H. Wolter,
to be published.

26 P.J. Price, Ann. of Physics **133**, 217 (1981).

27 E.S. Koteles, and J.Y. Chi, Phys. Rev. B **37**, 6332 (1988).

28 S.M. Goodnick, and P. Lugli, Phys. Rev. B **37** 2578 (1989).

29 J.A. Brum, and G. Bastard, Phys. Rev. B **33**, 1420 (1986).

30 M. Babiker, and B.K. Ridley, Superlatt. and Microstruct. **2**, 287 (1986).

31 J. Feldmann, G. Peter, E.O. Göbel, K. Leo, H.-J. Polland, K. Ploog, K. Fujiwara, and T. Nakayama, Appl. Phys. Lett. **51**, 226 (1987).

32 D.J. Westland, D. Mihailovic, J.F. Ryan, and M.D. Scott,
Appl. Phys. Lett. **51**, 590 (1987).

33 B. Deveaud, F. Clerot, A. Regreny, K. Fujiwara, K. Mitsunaga and J. Ohta, Appl. Phys. Lett. **55**, 2646 (1989).

34 D. Bimberg, J. Christen, A. Steckenborn, G. Weimann, and W. Schlapp, J. Luminesc. **30**, 562 (1985).

35 B. Deveaud, J. Shah, T.C. Damen, and W.T. Tsang, Appl. Phys. Lett. **52**, 1886 (1988).

36 R. Kersting, X.Q. Zhou, K. Wolter, D. Grützmacher, and H. Kurz, Superlatt. Microstruct. **7**, 345 (1990).

37 A. Weller, P. Thomas, J. Feldmann, G. Peter, and E.O. Göbel, Appl. Physics **A48**, 509 (1989).

38 P.W.M. Blom, J.E.M. Haverkort, and J.H. Wolter, Appl. Phys. Lett. **58**, 2767 (1991).

Chapter 4

Relevance of the Carrier Capture Efficiency for Quantum Well Lasers

4.1 Introduction

Due to the modification of the density of states quantum well lasers were expected to exhibit a lower threshold current than bulk double heterostructure (DH) lasers[1]. The absence of this performance improvement in the first quantum well lasers[2] appeared to be related to the injection efficiency of the carriers in a laser structure[3], a problem which is not present in bulk lasers. It has been recently established[4-7] that the carrier capture process in a separate confinement heterostructure quantum well (SCHQW) laser adds additional damping to the relaxation oscillations which limits the modulation response of these lasers. The damping arises from well-barrier hole burning, giving rise to a carrier accumulation in the barrier layers of a quantum well laser due to a finite capture time of the carriers into the quantum well. Furthermore, the carrier accumulation in the barriers is shown to lower the differential gain leading to an increased threshold current density[8]. In the case of inefficient capture, the carriers in the structure reach a 'non-Fermi' like distribution[9] in which the barrier states are highly populated.

In the available theoretical models in literature describing the carrier capture process into a quantum well, LO phonon emission is regarded as the dominant capture mechanism[10-12] (ph-capture). Oscillations of the ph-capture time as a function of quantum well width[10] and barrier thickness[11] have been predicted and have recently been experimentally observed by us[12]. The understanding of the relevance of the carrier capture process for laser performance would allow to exploit the predicted and observed oscillations of the carrier capture time as a function of structure parameters. Specifically, the minima of these capture time oscillations predict the optimum well and barrier thickness for an optimized carrier capture efficiency and thus probably also for an optimized threshold current density[13,14] and high-speed modulation characteristics. In section 4.2 we compare our calculated electron capture times with experimental threshold currents reported by Tsang[2,3] for some GaAs/$Al_xGa_{1-x}As$ SCH-MQW laser structures. It appears that the dependence of the threshold current density on the well width, barrier width and composition of the barrier layers is correlated with the ph-capture efficiency. Such correlations between the carrier capture time and the laser characteristics are not expected immediately since it is often reasoned that the carrier capture time (1-100 ps) is negligible as compared to the radiative lifetime (1-10 ns) in a high-quality semiconductor laser.

However, with increasing bias current and carrier accumulation carrier-carrier scattering induced capture (c-c capture) is expected to enhance the capture process and thus to reduce the carrier accumulation in the barrier layers required to obtain an equilibrium thermal carrier distribution. Therefore, a detailed analysis of the relevance of the carrier capture efficiency for QW laser performance should include both the ph-capture and the c-c capture mechanisms. In section 4.3 we present a theoretical study of the probability of the c-c capture process as compared to the ph-capture. We demonstrate that the c-c capture process also oscillates as a function of well width with the maximum capture rates at the same quantum well thicknesses as the ph-capture process. As a result both the carrier capture mechanisms can be enhanced by optimizing the structure parameters resulting in an improved laser performance. Furthermore, a small phonon-induced capture rate is expected to lead to excess carrier heating due to a high carrier-carrier scattering induced capture rate.

As another mechanism for the correlation between capture efficiency and threshold current we suggest in section 4.4 that an efficient carrier capture process contributes to a uniform pumping of the different quantum wells in a MQW laser. Furthermore, it is demonstrated that an inefficient capture process gives rise to a large carrier accumulation in the barrier layers, which degrades the dynamical performance of the quantum well laser.

4.2. Comparison of Threshold Current Density and Electron Capture Time

In section 2.3 and 2.4 we demonstrated that the LO phonon induced capture time not only oscillates as a function of well width but in addition also oscillates as a function of barrier width between the wells. In the present section we compare the structure dependence of our calculated capture times with experimental threshold currents reported by Tsang[3] for some GaAs/$Al_xGa_{1-x}As$ SCH-MQW structures and by Fuji et al.[15] for some GaAs/$Al_xGa_{1-x}As$ GRINSCH-SQW laser structures. Tsang systematically investigated the influence of such structure parameters as barrier width and composition of the barrier layers on the threshold current density. In Fig. 4.1 the threshold current density and the electron capture time are plotted in the same figure as functions of the barrier thickness between the wells for a GaAs/$Al_xGa_{1-x}As$ SCH-MQW structure with 5 wells. It can be seen that the variations in the experimentally determined threshold current density and the calculated capture efficiency are in very good agreement. In particular, the minimum threshold current density matches with the maximum capture efficiency at a barrier width of 35 Å.

The dependence of the threshold current density and the electron capture time on the composition of the barrier layers between the GaAs wells in a SCH-MQW structure with 8 wells is shown in Fig. 4.2. The barrier layer thickness ranges from 47 to 60 Å and the quantum well thickness from 142 to 167 Å. Again, it can be seen that the variations of the threshold current density and the calculated electron capture time as a function of the composition are in very good agreement. The increase of the calculated capture time for aluminum fractions lower than 0.1 is caused by the fact

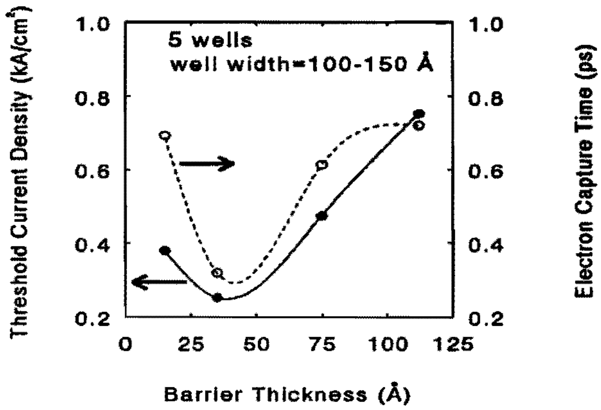

Fig. 4.1. Reported threshold current density[3] (closed circles) and electron capture time (dashed line) vs barrier width between the wells for a GaAs/Al$_x$Ga$_{1-x}$As SCH-MQW structure. The MQW structure consists of 5 wells, the well width ranges from 100 to 150 Å and the aluminum fraction x of the barrier layers amounts to 0.2.

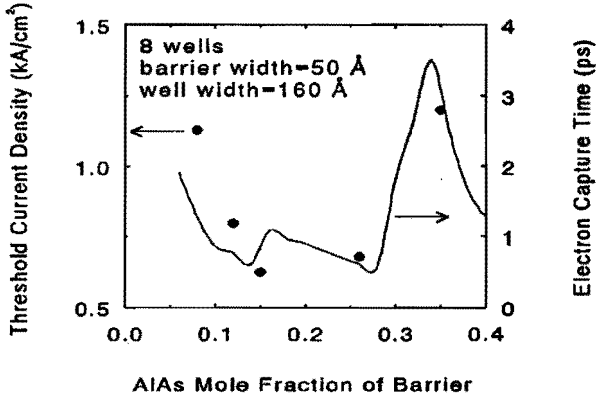

Fig. 4.2. Reported threshold current[3] (experimental points) and electron capture time (solid line) vs composition x of the barrier layers for a GaAs/Al$_x$Ga$_{1-x}$As SCH-MQW structure with 8 wells. The thickness of the barrier layers ranges from 47 to 60 Å and the quantum well thickness from 142 to 167 Å.

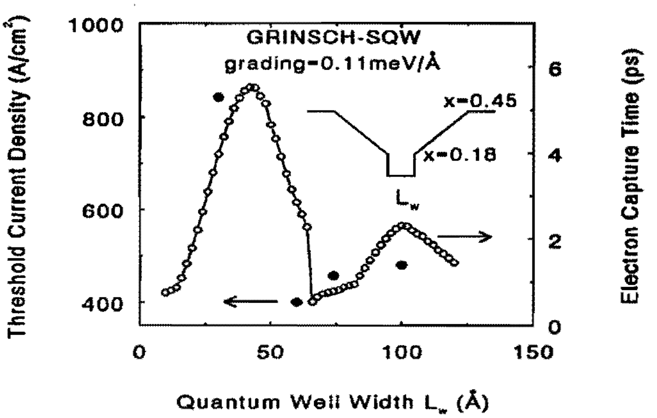

Fig. 4.3. Reported[15] threshold current density (closed circles) and calculated electron capture time (open circles) vs quantum well thickness for a $GaAs/Al_xGa_{1-x}As$ GRINSCH-SQW structure. The aluminum composition of the graded barrier layers ranges from 0.18 to 0.45 with a grading of 0.11 meV/Å. The solid line is drawn as a guide to the eye.

that for these compositions the quantum wells are almost completely filled with carriers at an injection level of 1 kA/cm^2. This band filling reduces the number of available final states for a transition from an initial barrier state to a final bound state in the well, and thus increases the capture time. Finally, in Fig. 4.3 the threshold current density of a GRINSCH-SQW, reported by Fuji et al.[15], and the electron capture time are plotted as a function of quantum well width. We find that the threshold current density is well described by the predicted oscillations of the capture time as a function of well width. Fuji et al.[15] attributed the large threshold current at small well widths to a reduced capture efficiency. A possible mechanism, however, for a possible correlation between the capture efficiency and the threshold current was not pointed out.

From theses series of experimentally obtained threshold current densities, which were the only series available to us, it appears that the dependence of the threshold current density on structure parameters and well width is statistically correlated with the LO phonon induced electron capture efficiency. However, it should be noted that a change of the structure parameters such as barrier width and composition not only changes the capture efficiency but also for example the optical confinement of the structure, which also influences the threshold current. Therefore, in order to make a valid comparison between threshold current density and capture efficiency these effects should be taken into account. Furthermore, the calculated capture times include only LO phonon emission, but for a realistic description of the carrier capture process under lasing conditions the carrier-carrier scattering induced capture process should also be included.

4.3 Carrier-Carrier Scattering in Quantum Well Laser Structures

The carrier capture process as a result of the scattering of an electron in the "continuum" state with an electron in the bottom of the quantum well is shown schematically in Fig. 4.4. It should be noted that a transfer of an electron from a continuum state to a quantum well bound state due to carrier-carrier (c-c) scattering gives rise to an increase of the energy of the electron in the quantum well as a result of energy and momentum conservation. Therefore, a capture process which is dominated by c-c scattering gives rise to an increase of the carrier temperature of the carriers in the quantum well.

Let us consider the general situation that an electron in subband i with wave vector k and a second electron in subband j with wave vector k_0 are scattered to the final states m and n respectively with wave vectors k' and k_0'. The c-c scattering rate is calculated using the Born-Approximation and is given in a quantum well structure by[16]

$$\Gamma_{i,m}(k)=\frac{4\pi e^4 m^*}{\hbar^3 A\kappa^2}\sum_{k_0,j,n} f_j(k_0)\int d\theta \frac{|F_{ijmn}(q)|^2}{(q+q_{s0})^2} , \qquad (1)$$

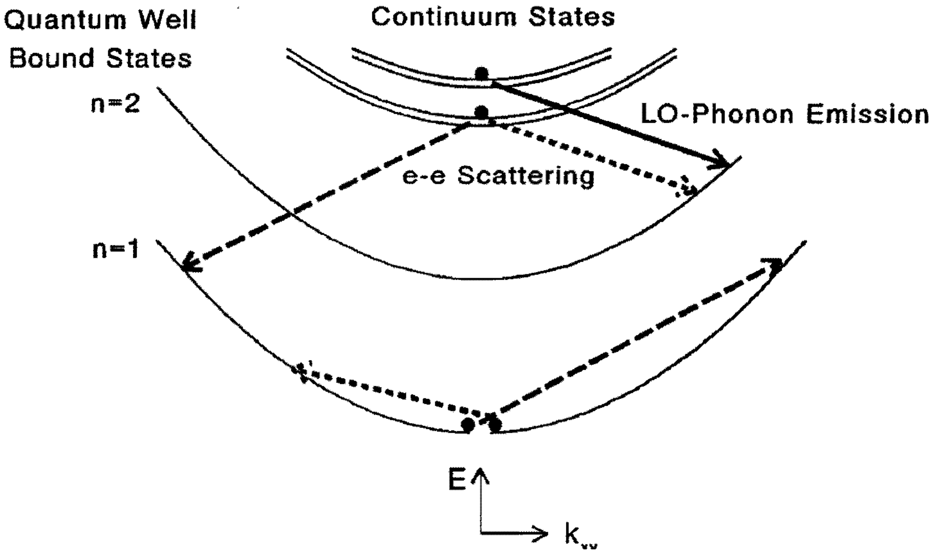

Fig. 4.4. The energy states of a single quantum well with two bound states are shown as a function of the momentum quantum number $k_{x,y}$. Also indicated are transitions into the quantum well due to LO-phonon scattering and e-e scattering.

with m* the effective mass, κ the dielectric constant, A the normalization area, $f(k_0)$ the carrier distribution function, $q = | k - k' |$, q_{s0} the inverse screening length in two dimensions, θ the angle between the relative wave vectors k_0-k and k_0'-k', and $F_{ijmn}(q)$ the form factor, which is given by

$$F_{ijmn}(q) = \int_{-\infty}^{\infty} dz \int_{-\infty}^{\infty} dz' \psi_i(z) \psi_j(z') \psi_m^*(z) \psi_n^*(z') e^{-q|z-z'|} \ . \tag{2}$$

The form factor provides information about the relative strength of the different c-c

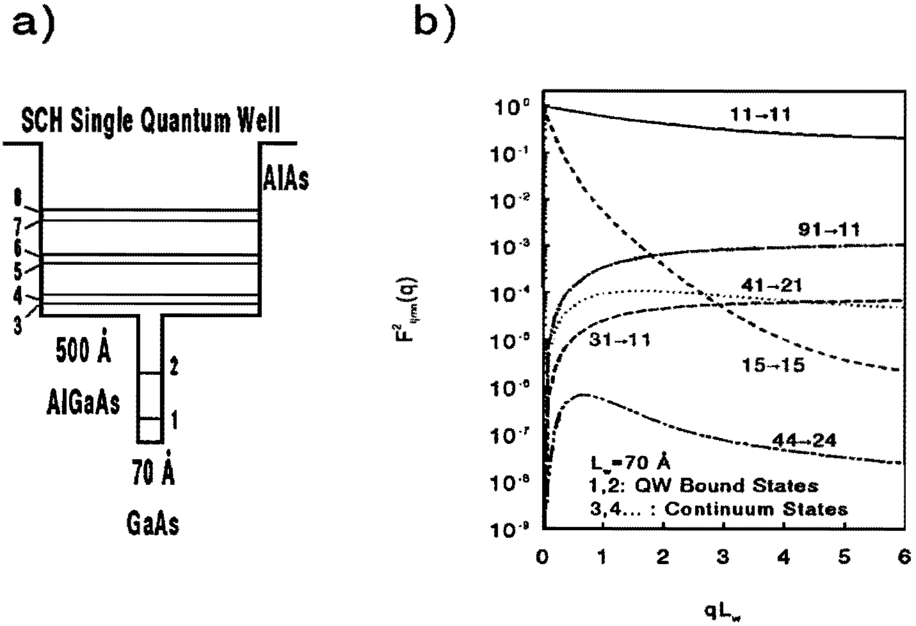

Fig. 4.5. Electron-electron scattering form factor as a function of wave vector q for a 70 Å SCH-SQW structure (Fig. 4.5b), of which the conduction band is schematically indicated in Fig. 4.5a. The energy levels labelled 1 and 2 are bound states in the QW and levels 3,..,9 are "continuum" states in the SCH-barrier. The c-c capture transitions (31→11, 91→11, and 41→21) have a three order of magnitude lower probability than the 11→11 intraband transitions.

scattering processes. We calculated the form factor for some transitions in a 70 Å GaAs/AlGaAs SCH single quantum well structure with two bound states numbered 1,2 and SCH-subbands 3,4.. in the barrier layer, as shown in Fig.4.5a. The resulting form factors are plotted in Fig. 4.5b.

It is demonstrated that the intra-subband scattering in the quantum well (11→11) is a very dominant process, as already shown by Goodnick and Lugli[16]. The form factor of the transitions labelled 31→11, 41→21, 91→11 and 44→24, in which an electron is captured by the quantum well, is at least two orders of magnitude lower than the intraband scattering and vanishes at q=0 due to the orthogonality of the wave functions. The probability of a capture process due to a scattering event between two electrons which are initially both in a continuum state (44→24) is negligibly small in comparison to the other capture processes, where one of the electrons is already in the quantum well before the capture process, even for equal carrier densities in the well and in the barrier layers. As in LO phonon emission[12], the capture probability increases with increasing subband number of the continuum state (31→11,91→11), due to the improved overlap of the corresponding wave functions. The form factor of the capture processes labelled 31→11 and 41→21, which describe transitions to the lowest and highest quantum well bound state respectively, are nearly equal. However, as can be seen in fig. 4.4, the transition in energy and momentum for a scattering event to a bound state which is close to the continuum is small in comparison with a transition to a bound state deep in the quantum well. This results in a smaller value of q and thus in an increased scattering rate since the total rate is proportional to q^{-2}.

Next, we calculate the dependence of the c-c capture rate on the quantum well width L_w. It is expected that for a quantum well width with a long ph-capture time the capture process will be dominated by c-c scattering. The dependence of the c-c and the ph-capture times on the quantum well thickness is shown in Fig. 4.6 for a carrier density of 1.10^{11} cm^{-2}. First it can be seen that the c-c capture time also oscillates as a function of well width with approximately the same minima in the capture time as the ph-capture time. These oscillations of both processes are due to an oscillating wave function overlap between the continuum states and the bound states in the quantum well[12], which for c-c scattering gives rise to an oscillation in the form factor. Furthermore, for the considered electron density we find that the transition probabilities of both capture processes are of the same order of magnitude.

For laser operation, c-c capture is fundamentally different from ph-capture since the excess energy of the carrier before the scattering event is not transferred to the phonon bath, but this excess energy is fed into the carrier plasma inside the quantum well. The energy exchange in a scattering event between a barrier state and a bound

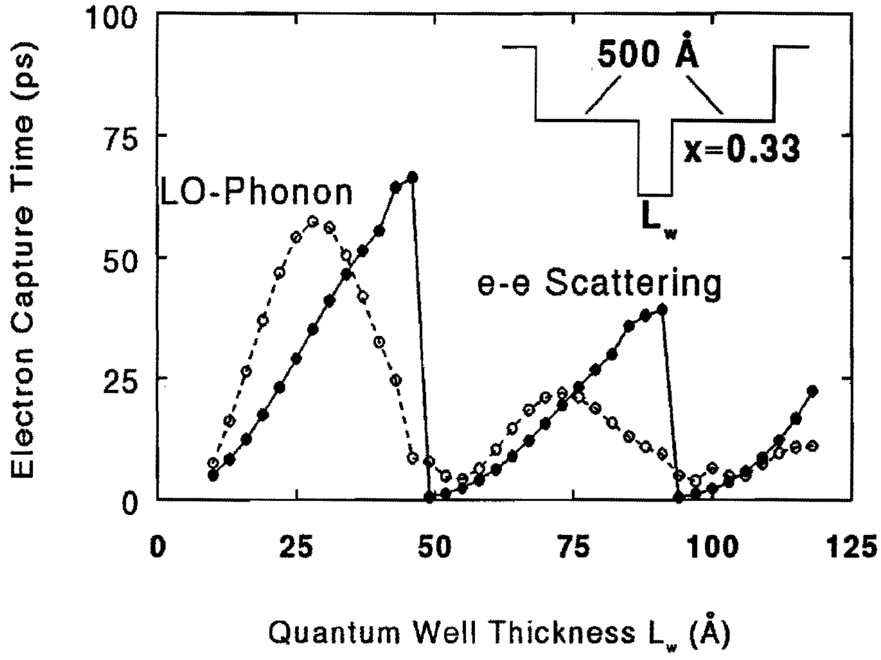

Fig. 4.6. Average LO phonon (open circles) and e-e scattering induced capture rates (closed circles) as a function of the quantum well width in a $GaAs/Al_xGa_{1-x}As$ SCH-SQW. The thickness and composition of the barrier layers was 500 Å and 0.33 respectively. For the calculation of the e-e capture rate we assumed a carrier density of 1.10^{11} cm^{-2} in the quantum well. The abrupt drops in the curves occur whenever a new bound state is coupled into the quantum well.

state close to the barrier continuum, where the capture rate is large, is smaller than the energy exchange with a bound state deep in the quantum well. As a result the energy exchange in a c-c capture event is dependent on the quantum well width, in contrast to ph-capture where the carriers transfer 36.8 meV to the phonon bath. The

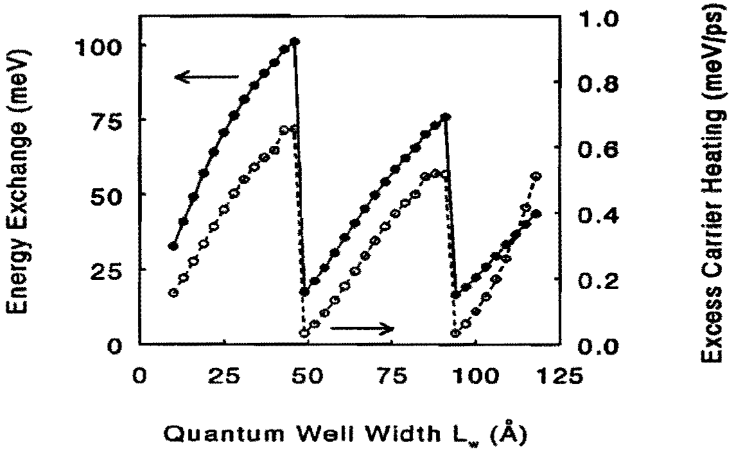

Fig. 4.7. Excess energy exchange (closed circles) and excess carrier heating (open circles) for a single e-e scattering induced capture process as a function of the quantum well width in a GaAs/Al$_x$Ga$_{1-x}$As SCH-SQW with a carrier density of 1.10^{11} cm^{-2} in the quantum well. The thickness and composition of the barrier layers was 500 Å and 0.33 respectively.

energy exchange per c-c capture event as well as the product of capture rate and energy exchange are shown in Fig. 4.7. For quantum well lasers with a well thickness below 40 Å, the c-c capture rate is large as compared to the ph-capture rate (Fig. 4.6) and the energy exchange per c-c scattering event is also large (up to 100 meV), leading to excess carrier heating.

In Fig. 4.8 the dependence of the c-c capture time on the carrier density in the quantum well is shown for quantum well widths of 30 Å and 55 Å, which correspond to maximum and minimum LO phonon induced capture times (see Fig. 4.6). For both well widths the ratio between the ph- and the c-c capture times is nearly equal, varying from a factor of 1.5 for a carrier density of 1.10^{11} cm^{-2} to a factor 8 for a carrier density of 1.10^{12} cm^{-2} in the quantum well. Thus for both well widths the relative contribution of the c-c scattering process to the total capture process is equal.

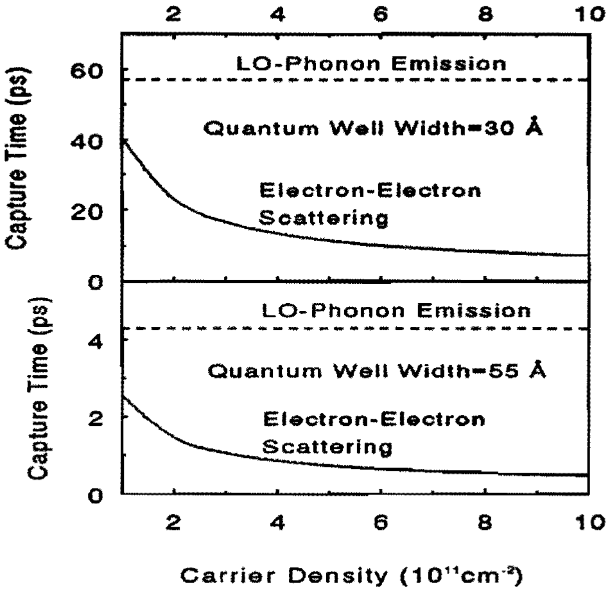

Fig. 4.8. Average LO phonon (dashed line) and e-e scattering induced capture times (solid line) as a function of the carrier density in the quantum well for an electron making a transition from a continuum state to a quantum well bound state. The quantum well thickness was chosen to be 30 or 55 Å, which correspond to maximum and minimum LO phonon capture times respectively. The temperature was assumed to be 300 K.

However, as shown in Fig. 4.7, the exchange of energy for the 55 Å quantum well is smaller than the energy exchange for the 30 Å well. Thus the increase of carrier temperature is indeed larger for the 30 Å quantum well.

So far, we have demonstrated that both the LO phonon induced and the c-c scattering induced carrier capture times depend on the structure parameters of a SCHQW laser structure. The excess carrier heating is determined by the ratio between the ph- and c-c capture times and also by the average energy transition in a c-c scattering event. Hence, the cooling of the carriers down to the bottom of the quantum well, after injection from the cladding layers, can be strongly enhanced by choosing an optimum quantum well width. From the strong dependence of the optical gain on the carrier temperature around threshold[17], it is well-known that a small increase of the carrier temperature gives rise to an increase of the threshold current density. Thus a low capture efficiency, giving rise to a large population of the barrier states, affects the threshold current density not only by additional recombination losses in the barrier layers but also by excess carrier heating in the quantum well. The LO phonon induced capture process is expected to be particularly relevant for laser structures in which the carrier accumulation in the quantum wells is relatively small, i.e. MQW lasers or lasers with HR-coated facets. When carrier accumulation in the quantum wells is important, i.e. in SQW lasers, the relative probability for c-c capture will become high since this process is proportional to the product of the barrier and well carrier densities.

4.4 Carrier Accumulation in the Barriers of a Quantum Well Laser

It should be noted that an oscillating phonon and carrier-carrier induced capture time is only expected for lasers in which the coherence length of the carriers exceeds the SCH-barrier width, i.e. for lasers with thin (<1000 Å) SCH layers such as GRINSCH-SQW lasers. For lasers with very thick barriers (>2000 Å), the capture process is the sum of a classical transport time in the SCH-barriers and a small local capture time. In the latter type of lasers, radiative and non-radiative recombination in the SCH-barriers will also be important, introducing a loss mechanism in the barriers which makes it obvious that the threshold current density should correlate[18] with the capture efficiency in these type of lasers. In order to obtain an estimate of the local capture time used in a classical description we compare our quantum mechanical model with the classical diffusion model. In the quantum mechanical model the temporal dependence of the carrier density in the barrier layers, after excitation with a short laser pulse, is given by

$$n_b(t) = n_b(0) \exp(-t / \tau_a) , \tag{3}$$

with τ_a the ambipolar overall capture time. In the classical model this carrier density is described, neglecting recombination losses in the barrier layers, by a one-dimensional rate equation,

$$\frac{\delta\, n_b(z,t)}{\delta\, t} = D \cdot \frac{\delta^2\, n_b(z,t)}{\delta\, z^2} - \frac{n_b(z,t)}{\tau_{loc}} \cdot W \tag{4}$$

with z the direction perpendicular to the quantum well layer. In this equation D is the ambipolar diffusion constant, W is unity in the well and zero elsewhere, and τ_{loc} is the local capture time. This local capture time can be used as a fit parameter in order to equate the total carrier density in the barrier, resulting from Eq. 4, to the density, as given by Eq. 3, for a certain overall capture time as a function of time. By equating the quantum mechanical capture rate to the classical capture rate, we are able to transfer the overall capture time (Fig. 3.16) into a local capture time and a diffusion constant. The observed resonances of the overall capture time of 3-20 ps as a function of well width give rise to oscillations in the local capture time of 0.1-1.8 ps for a diffusion constant of 25 cm^2/s, as is shown in Fig. 4.9. The increase of the amplitude of the oscillations with increasing well width is due to the fact that in the classical model the carrier capture rate is proportional to the well width. As a result, for a large well width a relatively slow capture time is sufficient to obtain a large flow of carriers into the quantum well. Therefore, the well width dependence of the carrier capture rate is obtained by normalizing the local carrier capture times to the quantum well width. In our opinion a local capture time, which is dependent on well width, gives a more realistic description of the capture process in large QW laser structures than the bulk GaAs LO phonon scattering time of 0.1 ps. We demonstrated that a relatively

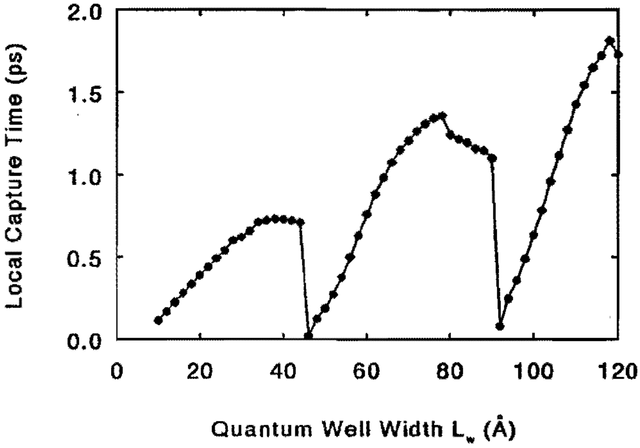

Fig. 4.9. Classically defined local capture time deduced from experiment as a function of quantum well thickness for a SCH single QW structure. The ambipolar diffusion constant was taken to be 25 cm²/s, a value which is common for $Al_xGa_{1-x}As$.

small local capture time (0.1-1.8 ps) as well as its oscillations are not insignificant for device performance. Although it may appear that such a small local capture time can easily be neglected, it corresponds to quite large oscillations of the overall capture time (3-20 ps).

An intermediate case between the quantum mechanical and classical description is the SCH-MQW laser with a total structure width of about 1500 Å as is schematically illustrated in Fig. 4.10. We first discuss a simple model in which we assume a constant carrier distribution in the barrier layers. The time dependence of the carrier concentration is then given by

$$\frac{dn_b}{dt} = \frac{J}{eL} - \frac{n_b}{\tau_b} - \frac{n_b}{\tau_{LO}} - \frac{n_b}{\tau_{e-e}} , \tag{5}$$

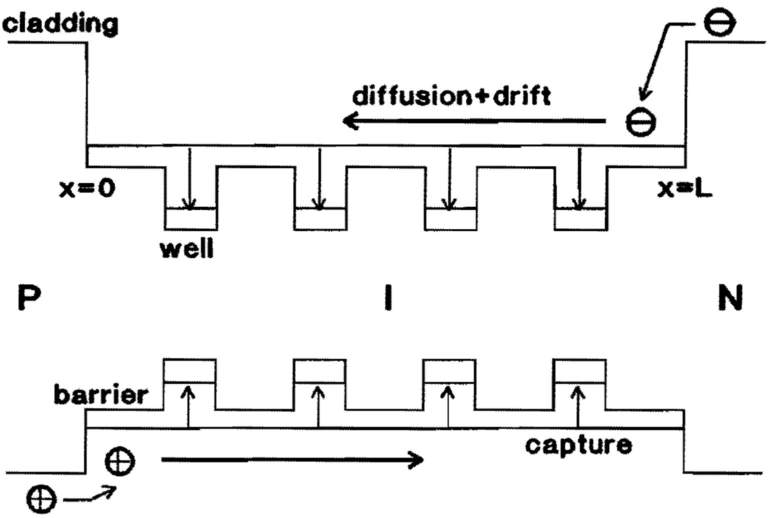

Fig. 4.10. Schematic representation of a SCH-MQW laser structure with a p-doped cladding layer on the left (x=0) and a n-doped cladding layer on the right (x=L) of the active region. The overall capture time defines a mean free path for transport over the barrier states.

with J the injected current density, L the thickness of the active region, τ_{LO} the LO phonon induced overall capture time, $\tau_{e\text{-}e}$ the carrier-carrier scattering induced capture time, τ_b^{-1} the sum of the radiative and non-radiative recombination rate of the carriers in the barrier layers. The net capture time τ_c is then given by

$$\tau_c = \frac{\tau_{LO} \cdot \tau_{e-e}}{\tau_{LO} + \tau_{e-e}} . \qquad (6)$$

The losses in the barrier layer n_b/τ_b can safely be neglected, because the lifetime of the carriers is in the order of nanoseconds while the capture time is in the picosecond regime. As stated above, an inefficient capture process only gives rise to significant additional losses in QW structures with very thick barrier layers of several thousands of angstroms, since for these structures the capture time is of the same order of magnitude as the lifetime of the carriers in the barrier layers. Neglecting barrier losses, a steady state solution yields

$$n_b = \tau_c \frac{J}{eL} , \tag{7}$$

which means that the *accumulation* of carriers in the barrier layers is proportional to the capture time τ_c for a certain injection current. In the case of inefficient capture, the carriers in the structure can reach a "non-Fermi" like distribution[9] in which the barrier states are highly populated.

As indicated in Fig. 4.10 electrons are injected into the barrier layers from the n-cladding layer whereas holes are injected from the p-cladding layer, which gives rise to large drift fields and concentration gradients. So the assumption of a uniform carrier distribution as presented in the simple model above is not correct. The carrier distribution in a SCHQW laser can be calculated[13] by regarding the laser with undoped active layers as a p-i-n diode. After injection, the electrons in the barrier states drift towards the p-contact (x=0) and the holes towards the n-contact (x=L). The number of electrons and holes which reaches the p- and n-contact respectively is dependent on the electron and hole mobilities and on the carrier capture efficiency at a certain bias current. So the capture time defines a mean free path length for carrier transport in the barrier states. Since the holes combine a large capture efficiency with a low mobility and the electrons have a high mobility combined with a low capture efficiency, we expect that the accumulation of carriers at the p-contact is larger than at the n-contact. If, however, the electron capture efficiency is increased, more electrons will be captured directly after injection by the quantum wells located near the injecting n-contact. These electrons will also attract more holes to the n-contact as a result of the strong internal electric fields which tend to maintain charge neutrality in the structure. Therefore, an improved electron capture efficiency is expected to give rise to a more uniform distribution of the carriers in the active region of SCH-MQW laser structures and thus to a more uniform pumping of the quantum wells.

The transport of the carriers in the barrier states of a SCH-MQW structure, which is dominated by drift and diffusion, is characterized by the current-flow equations

$$J_n = e\mu_n n(x)E(x) + eV_T\mu_n\frac{dn}{dx} , \tag{8}$$

$$J_p = e\mu_p p(x)E(x) - eV_T\mu_p\frac{dp}{dx} , \tag{9}$$

with e the electronic charge, E(x) the electric field and V_T the thermal voltage kT/e. Assuming ambipolar conditions, the carrier transport can further be described by the master equation[19]

$$-\frac{\epsilon}{e}\frac{d}{dx}\left(E(x)\frac{dE(x)}{dx}\right) + (n_{b0}-p_{p0})\frac{dE(x)}{dx} + 2V_T\frac{d^2n_b(x)}{dx^2} = \frac{(\mu_n/\mu_p+1)(n_b(x)-n_{b0})}{\mu_n\tau_c} , \tag{10}$$

which can be derived from the particle conservation equations and the Poisson equation with n_{bo} and p_{bo} the thermal equilibrium density of electrons and holes in the barrier, n_b the total free carrier density in the barrier and τ_c the carrier capture time. The carrier transport is further characterized by the boundary conditions

$$n_b(0) = \frac{JL_a}{2e\mu_p V_T} , \tag{11}$$

$$n_b(L) = \frac{JL_a}{2e\mu_n V_T} , \tag{12}$$

$$L_a = \sqrt{\frac{2V_T\ \mu_n \tau_c}{\mu_n\ /\mu_p + 1}} , \tag{13}$$

which are directly obtained from the conditions $J_n(0)=0$ and $J_p(L)=0$, and with the drift term in Eqs. 8 and 9 neglected in the vicinity of the cladding layers. Within one ambipolar diffusion length L_a from the cladding layers the transport of the carriers is diffusion dominated, because the flow of electrons and holes is blocked at the p- and n-cladding layer respectively, which gives rise to a large accumulation of carriers and small electric fields at the cladding layers. Therefore, the equations can be solved by using the Regional Approximation Method by Lampert and Schilling[19], in which the transport of carriers in the barrier layers is dominated by diffusion within one ambipolar diffusion length of the cladding layers and by drift in the barrier layers located in the middle of the structure. In Fig. 4.11 the calculated carrier distribution in the continuum states is shown for capture times of 0.1 and 1.0 ps respectively in a SCH-MQW structure with a width of 1500 Å.

We find that for a multiple quantum well laser the uniformity of the pumping of the quantum wells in the middle of the structure is improved. For example, the carrier concentration reduces from x=250 Å to x=1250 Å by a factor 3 for a capture time of 0.1 ps and by a factor 5.5 for a capture time of 1.0 ps. In a MQW with nonuniform pumping the spontaneous emission losses in the quantum wells which not yet have reached lasing threshold should be compensated for by the gain of the lasing quantum wells, which leads to a degradation of the threshold current. From a model of current injection in MQW lasers it was already proposed by Dutta[20] that a uniform pumping of the quantum wells can be achieved by increasing the well-to-barrier ratio. This condition is met in our model, in which an increase of the well-to-barrier ratio gives rise to an increase of the carrier capture efficiency and thus to more uniform

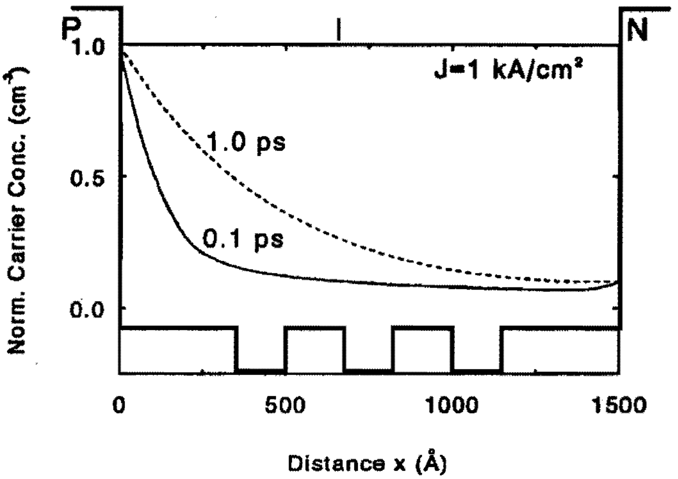

Fig. 4.11. Carrier distribution in a SCH-MQW laser structure for capture times of 0.1 ps and 1.0 ps at an injection current of 1 kA/cm². The total width of the active layer is assumed to be 1500 Å.

pumping conditions.

As stated above, a slow capture process leads to carrier accumulation in the barrier layers until a steady state is obtained in which the flow of carriers into the quantum wells equals the injection current. We emphasize that in a steady state the number of carriers making a transition to the quantum well per unit time (n_b/τ_c) only depends on the injection level and not on the carrier capture time. The carrier capture time determines the carrier accumulation in the barrier layers and the carrier distribution in the quantum well. After a disturbance of the steady state, by for example a sudden increase of the injection current, a new steady state will be reached when the injection current will have added extra carriers to the barrier layers, in order to obtain a larger flow of carriers into the quantum wells.

In a quantum well laser with an efficient capture process and thus a small amount of carriers in the barrier layers, only a small absolute change of the carrier

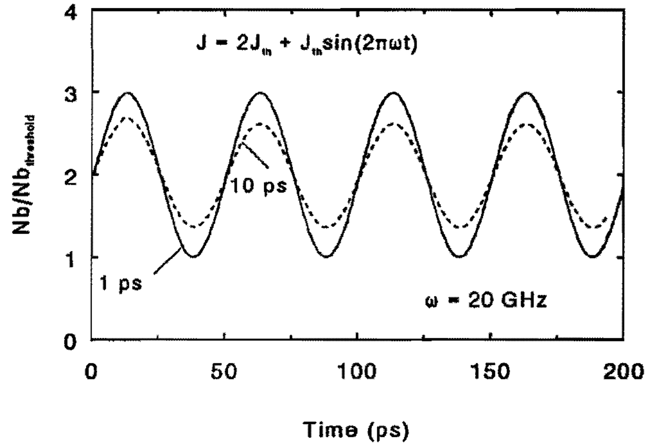

Fig. 4.12. Variations of the total carrier concentration in the continuum states of a SCHQW laser as a result of a modulated injection current for capture times of 1 ps (solid line) and 10 ps (dashed line). The modulation frequency in the calculation is 20 GHz.

concentration is needed to obtain a new equilibrium. As a result, a large capture efficiency enables a quantum well laser to follow very rapid external current modulations. In Fig. 4.12 the temporal variation of the total carrier concentration in the barrier layers is shown for capture times of 1 and 10 ps as a result of a modulated injection current. It can be seen that a laser with a capture time of 1 ps is able to follow the 20 GHz current modulation exactly, while a capture time of 10 ps reduces the modulation response by a factor of 2. We thus conclude that the carrier capture also limits the maximum attainable modulation frequency of a quantum well laser. Since the carrier capture rate linearly increases[11] with the number of wells, a MQW structure is expected to exhibit a larger modulation frequency than a SQW structure. A more precise relation between the carrier capture time and the maximum attainable modulation frequency of a QW laser has been recently established. It has been shown that the capture time adds an additional damping of the relaxation oscillations which also limits the modulation response of a SCHQW laser[4-7] to an upper modulation bandwidth of $f_{mod}=0.22/\{\tau_{cap}\eta_{eq}^2\}$, with η_{eq} the equilibrium barrier to well density[4]. The advantage of adding more quantum wells can now be simply understood in terms of the carrier capture efficiency which enhances η_{eq} as well as τ_{cap}.

In conclusion, we have demonstrated that the carrier capture efficiency is a very important parameter with respect to the performance of a quantum well laser. As a mechanism for the correlation between the carrier capture efficiency and the threshold current density we suggest that, apart from recombination losses in the barrier layers, the carrier temperature in the quantum well depends on the carrier capture process. By optimizing the structure parameters in a quantum well laser, the cooling of the carriers in the quantum well can be enhanced, giving rise to low threshold current. Furthermore, for SCH-MQW lasers a low capture efficiency tends to pile up all carriers in the quantum well nearest to the p-doped side, resulting in unequal pumping of the different quantum wells. The dynamical behaviour of a quantum well laser, in particular the modulation response and the maximum attainable modulation frequency, is also improved by an efficient capture process, which reduces the accumulation of carriers in the barrier layers.

References

1 N. Holonyak, Jr., R.M. Kolbas, R.D. Dupuis, and P.D. Dapkus, IEEE J. Quantum Electron. **QE-16**, 170 (1980).

2 W.T. Tsang, Appl. Phys. Lett. **39**, 204 (1980).

3 W.T. Tsang, Appl. Phys. Lett. **39**, 786 (1981).

4 W. Rideout, W.F. Sharfin, E.S. Koteles, M.O. Vassell, and B. Elman, IEEE Photon. Technol. Lett. **3**, 784 (1991).

5 R. Nagarajan, T. Fukushima, S.W. Corzine, and J.E. Bowers, Appl. Phys. Lett. **59**, 1835 (1991).

6 W.F. Sharfin, J. Schlafer, W. Rideout, B. Elman, R.B. Lauer, J. LaCourse, and F.D. Crawford, IEEE Photon. Technol. Lett. **3**, 193 (1991).

7 R. Nagarajan, T. Fukushima, M. Ishikawa, J.E. Bowers, R.S. Geels, and L.A. Coldren, IEEE Photon. Lett. **4**, 121 (1992).

8 B. Zhao, T.R. Chen, and A. Yariv, Appl. Phys. Lett. **60**, 1930 (1992).

9 N. Tessler, R. Nagar, D. Abraham, G. Eisenstein, U. Koren, and G. Raybon, Appl. Phys. Lett. **60**, 665 (1992).

10 J.A. Brum, and G. Bastard, Phys. Rev. **B33**, 1420 (1986).

11 P.W.M. Blom, J.E.M. Haverkort, and J.H. Wolter, Appl. Phys. Lett. **58**, 2767 (1991).

12 P.W.M. Blom, C. Smit, J.E.M. Haverkort, and J.H. Wolter, accepted for publication in Phys. Rev. B.

13 P.W.M. Blom, J.E.M. Haverkort, and J.H. Wolter, Proceedings of the international meeting on the optics of excitons in confined systems, edited by A. D'Andrea, R. Del Sole, R. Girlanda, A. Quattropani, Institute of physics, 301 (1992).

14 P.W.M. Blom, P.J. van Hall, J.E.M. Haverkort, and J.H. Wolter, SPIE Proceedings Vol. **1677**: Ultrafast Laser Probe Phenomena in Semiconductors and Superconductors, edited by R.R. Alfano, to be published.

15 T. Fuji, S. Yamakoshi, K. Nanbu, O. Wada, and S. Hiyamizu,
J. Vac. Sci. Technol. **B2**, 259 (1984).

16 S.M. Goodnick, and P. Lugli, Phys. Rev. B37, 2578 (1989).

17 N.K. Dutta, J. Appl. Phys. **53**, 7211 (1982).

18 J. Nagle, S. Hersee, M. Krakowski, T. Weil, and C. Weisbuch,
Appl. Phys. Lett. **49**, 1325, 1986.

19 M.A. Lampert, and R.B. Schilling, "Current injection in solids: The regional approximation method," Semiconductors and semimetals, vol. **6**, chp. 1, New York: Academic Press, edited by R.K. Willardson and A.C. Beer (1970).

20 N.K. Dutta, J. Quantum Electron. **QE-19**, 794 (1983)

Summary

This thesis deals with the capture of injected or photoexcited carriers into a semiconductor quantum well, a process which is expected to be relevant for the performance of quantum well lasers. Specifically, the carrier capture efficiency influences both the quantum efficiency and the dynamic performance. However, there seemed to be a fundamental problem in the understanding of the carrier capture process by a quantum well according to the large differences between observed and predicted capture times in literature. In a quantum mechanical model, in which the carrier capture process is governed by the emission of optical phonons, strong resonances (30 ps-1 ns) of the capture time as a function of quantum well thickness were predicted by Brum and Bastard. The experimental capture times ranged from 0.3-3 ps and no dependence on well width was observed. The question whether the capture process is dominated by classical diffusion and drift (no oscillations expected) or by quantum mechanical capture (oscillations expected) is relevant for the optimization of the capture efficiency in quantum well laser structures.

In chapter 2 we present the results of a theoretical study on the carrier capture process in separate confinement heterostructure quantum well (SCHQW) structures. The capture model of Brum and Bastard is extended to multiple quantum well (MQW) structures and it is demonstrated that the predicted capture times for large MQW structures are very short ($<$ 1 ps), in agreement with the reported experimental results for precisely these structures. Furthermore, we present an ambipolar capture model in which the different capture times of electrons and holes as well as the their dependence on the barrier subband population are taken into account.

The results of our experimental study of the carrier capture process in SCHQW structures by sub-picosecond rise time measurements of the quantum well

luminescence as well as by pump-probe correlation measurements of the population decay in the barrier layer are shown in chapter 3. We for the first time observed an oscillating carrier capture time between 3 and 20 ps as a function of quantum well thickness, in excellent agreement with the theoretical predictions of chapter 2. In a classical picture, our results correspond to a local capture time oscillating between 0.1 and 1.8 ps. Furthermore, the dependence of the capture time on the excitation energy is analyzed and the time-dependent position of the quasi Fermi level in the barrier layer is tracked experimentally. We find that the carrier capture time is very sensitive to the detailed structure parameters as well as to the carrier distribution in the barrier. Carrier capture is found to be an ambipolar process in which the oscillations of the observed capture times are due to the quantum mechanical oscillation of the electron wave function overlap above the well. At low carrier densities the electron capture is demonstrated to be dominated by LO phonon emission.

In chapter 4 we discuss the relevance of the carrier capture process for the device characteristics of a quantum well laser. The dependence of the threshold current density on the structure parameters of the layers in the active region seems to be correlated with the electron capture efficiency. Under lasing conditions our calculations reveal that the carrier capture into a quantum well can be due to either optical phonon emission or carrier-carrier scattering. Both capture mechanisms have been calculated and show oscillations as a function of the quantum well thickness. The predicted structure parameters for an optimum capture efficiency are equivalent for these scattering processes, since in both capture mechanisms these oscillations arise from oscillations in the wave function overlap. A small phonon-induced capture rate is expected to lead to excess carrier heating due to a high carrier-carrier scattering induced capture rate. Furthermore, in MQW lasers a large capture efficiency contributes to uniform pumping of the quantum wells. By maximizing the carrier capture efficiency in laser structures we are able to predict the structure parameters of the layers in the active region for an optimum laser performance.

Samenvatting

Dit proefschrift is gewijd aan een onderzoek naar de invangst van optisch of elektrisch geïnjecteerde ladingsdragers in GaAs/$Al_xGa_{1-x}As$ quantumput structuren. De invangsttijd van ladingsdragers in een Separate Confinement Heterostructure Quantum Well (SCHQW) laser is mede bepalend voor de efficiëntie en maximale modulatiefrequentie van de laser. Tot nu toe bestond er echter een ernstige discrepantie tussen de theoretisch berekende en de experimenteel bepaalde waarden voor deze invangsttijd. In een quantum mechanisch model van Brum en Bastard (1986), waarin de ladingsdragersinvangst wordt gedomineerd door emissie van optische fononen, werden sterke resonanties (30 ps-1 ns) voorspeld in de invangsttijd als funktie van de breedte van de quantumput. De in de literatuur gerapporteerde experimentele invangsttijden variëerden daarentegen van 0.3-3 ps en er werd geen afhankelijkheid van de quantumputbreedte waargenomen. De vraag of de ladingsdragersinvangst in een quantumput al dan niet gedomineerd wordt door een klassiek diffusieproces (geen afhankelijkheid van de putbreedte verwacht) of door een quantum mechanisch invangstproces (resonanties in de invangsttijd verwacht) is relevant voor de optimalisatie van de ladingsdragersinvangst in quantumput lasers.

In hoofdstuk 2 worden de resultaten van een theoretische studie naar de invangst van ladingsdragers in SCHQW structuren gepresenteerd. Door het theoretische model van Brum en Bastard toe te passen op meervoudige quantumput (MQW) structuren, is er aangetoond dat de voorspelde invangstijden voor deze structuren zeer snel zijn (< 1 ps), hetgeen in overeenstemming is met de experimenteel gerapporteerde waarden in de literatuuur voor deze MQW structuren. Het theoretische model is vervolgens verder uitgebreid tot een ambipolair invangstmodel, waarin rekening wordt gehouden met de verschillende invangsttijden van gaten en elektronen als ook hun afhankelijkheid van de bezetting van de energieniveaus in de barrière.

De resultaten van onze experimentele studie naar de invangst van ladingsdragers in SCHQW structuren zijn weergegeven in hoofdstuk 3. De invangsttijden zijn bepaald door middel van subpicoseconde stijgtijdmetingen van de luminescenctie uit de quantumput als ook door z.g. twee-puls correlatie metingen, waarin de afname van de ladingsdragersdichtheid in de barrièrelagen ten gevolge van het invangstproces wordt gemeten. Met deze beide experimentele technieken hebben wij waargenomen dat de invangsttijd oscilleert tussen 3 en 20 ps als functie van de breedte van de quantumput, hetgeen goed overeenstemt met de theoretische voorspellingen uit hoofdstuk 2. Verder is er waargenomen dat de invangstijd sterk afhangt van de ladingsdragersverdeling in de barrière. Voor lage ladingsdragersconcentraties hebben wij aangetoond dat het invangstproces, zoals reeds in het theoretisch model verondersteld, wordt gedomineerd door emissie van optische fononen.

In hoofdstuk 4 wordt de relevantie van de invangst van ladingsdragers in quantumput lasers behandeld. Gezien de hoge ladingsdragersconcentratie onder laserwerking moet het bestaande invangstmodel, waarin de emissie van optische fononen als het dominante proces werd verondersteld, worden uitgebreid met de onderlinge verstrooiing van ladingsdragers. Uit onze berekeningen blijkt dat beide invangstmechanismes aanleiding geven tot oscillaties in de invangsttijd met dezelfde optimale quantumputbreedtes, omdat in beiden de oscillaties voortkomen uit resonanties in de overlap tussen de golffuncties in de barrière en in de quantum put. Indien het invangstproces wordt gedomineerd door de onderlinge verstrooiing van ladingsdragers, wordt er een toename van de ladingsdragerstemperatuur in de quantumput verwacht, hetgeen de werking van een quantumputlaser nadelig beïnvloedt. In MQW lasers draagt een optimaal invangstproces bovendien bij tot een uniforme verdeling van de geïnjecteerde ladingsdragers over de verschillende quantumputten. Door de efficiëntie van de ladingsdragersinvangst in quantumputlasers te maximalizeren zijn we in staat de optimale laagdiktes in het actieve gebied van een quantumputlaser te voorspellen.

List of Publications

1. P.M. Koenraad, F.A.P. Blom, P.W.M. Blom, C.T. Foxon, E.N.M. Frijns, J.J. Harris, G. Weimann, and J.H. Wolter, "Dependence of spin-asymmetry in the Shubnikov-De Haas resistance on back-gating, illumination and uniaxial stress", Superlatt. and Microstruct. 5, p. 519 (1989).
2. P.W.M. Blom, P.M. Koenraad, F.A.P. Blom, and J.H. Wolter, "Analysis of the shallow and deep center occupancies in Si-doped $Al_xGa_{1-x}As$ using a multilevel donor model", *J. Appl. Phys.* 66, p. 4269 (1989).
3. P.W.M. Blom, R.F. Mols, J.E.M. Haverkort, M.R. Leys, and J.H. Wolter, "Picosecond carrier capture by a separate confinement laser structure", *Proceedings of the 16th European Conference on Optical Communications*, Amsterdam 1990, Vol. 1, p. 59 (1990)
4. P.W.M. Blom, R.F. Mols, J.E.M. Haverkort, M.R. Leys, and J.H. Wolter, "Measurement of the ambipolar capture time in a $GaAs/Al_xGa_{1-x}As$ separate confinement heterostructure quantum well", *Superlatt. and Microstruct. 7,* p. 319 (1990)
5. P.W.M. Blom, J.E.M. Haverkort, and J.H. Wolter, "Optimization of barrier thickness for efficient carrier capture in graded-index and separate-confinement multiple quantum well lasers", *Appl. Phys. Lett.* 58, p. 2767 (1991)
6. P.W.M. Blom, J.E.M. Haverkort, and J.H. Wolter, "Low threshold current of multiple quantum well lasers by optimization of carrier capture efficiency", *Inst. Phys. Conf. Ser. 123*: Proceedings of the International Meeting on Optics of Excitons in Confined Systems, p. 301 (1991)
7. P.W.M. Blom, P.J. van Hall, J.E.M. Haverkort, and J.H. Wolter, "Reduction of the threshold current in quantum well lasers by optimization of

the carrier capture efficiency", *SPIE Proceedings Vol. 1677*: Ultrafast Laser Probe Phenomena in Semiconductors and Superconductors, edited by R.R. Alfano, accepted for publication.

8. P.W.M. Blom, C.Smit, J.E.M. Haverkort, and J.H. Wolter, "Carrier capture into a semiconductor quantum well", accepted for publication in Phys. Rev. B.
9. P.W.M. Blom, J.E.M. Haverkort, P.J. van Hall, and J.H. Wolter, "Carrier-carrier scattering induced capture in quantum well lasers", submitted to Appl. Phys. Lett.
10. P.W.M. Blom, C. Smit, J.E.M. Haverkort, and J.H. Wolter, "Blocking of Γ→X transfer in GaAs/AlAs short period superlattices due to X-state band filling", submitted to Appl. Phys. Lett.
11. P.W.M. Blom, P.J. van Hall, C. Smit, J.P. Cuypers, J.E.M. Haverkort, and J.H. Wolter, "Selective exciton formation in thin GaAs/AlGaAs quantum wells", submitted to Phys. Rev. Let.

12 P.J. van Hall, and P.W.M. Blom, "Exchange effects in carrier-carrier scattering", submitted to Superlatt. and Microstruct.

13. P.J. van Hall, P.W.M. Blom, C. Smit, L. Drost, and J.H. Wolter, "Monte-Carlo Simulations of New resonances in the relaxation of hot carriers in GaAs quantum wells", submitted to the 8th Vilnius Symposium on Ultrafast Phenomena in Semiconductors, Vilnius 1992, Litouwen.
14. P.J. van Hall, and P.W.M. Blom, "Exchange effects in carrier-carrier scattering", submitted to the 8th Vilnius Symposium on Ultrafast Phenomena in Semiconductors, Vilnius 1992, Litouwen.

Curriculum Vitae

Paul Blom werd geboren op 14 januari 1965 te Maastricht. Van 1977-1983 doorliep hij het VWO aan de Scholengemeenschap "Sophianum" te Gulpen. In 1983 begon hij de studie Technische Natuurkunde aan de Technische Universiteit Eindhoven. In augustus 1988 studeerde hij af in de groep halfgeleider fysica onder leiding van Prof. dr. J.H. Wolter met als onderwerp: "Uniaxiale druk op een GaAs/AlGaAs heterostructuur: de rol van het diepe donor niveau". Vanaf oktober 1988 startte hij aan de TUE in de vakgroep Vaste Stof als medewerker van de stichting FOM zijn promotieonderzoek onder leiding van Prof. dr. J.H. Wolter met als titel: "Carrier capture in III-V semiconductor quantum wells". In de afgelopen 4 jaar heeft hij zowel theoretisch als experimenteel onderzoek verricht aan de ladingsdragersdynamica in quantumput structuren op picoseconde tijdschaal.

Stellingen

behorende bij het proefschrift van

Paul W.M. Blom

Carrier capture in III-V semiconductor quantum wells

1. Ten onrechte veronderstellen Damen et al. dat excitonen, die door middel van fononemissie gevormd worden, een grote impuls bezitten.
   T.C. Damen et al., Phys. Rev. B 42, p. 7434 (1990).

2. In tegenstelling tot eerder gepubliceerde resultaten vertoont de invangsttijd van ladingsdragers in een quantumput een sterke afhankelijkheid van de putbreedte.
   B. Deveaud et al. , Appl. Phys. Lett. 52, p. 1886 (1988).
   Dit proefschrift

3. In een meervoudige quantumputstructuur kan de invangst van ladingsdragers aanzienlijk versneld worden door een geschikte keuze van de barrièredikte.
   Dit proefschrift

4. De verandering van de elektronendichtheid in een 2-dimensionaal elektronengas ten gevolge van hydrostatische druk wordt goed beschreven door een model met gekoppelde donorniveaus.

5. De "momentum conservation approximation", zoals beschreven door Ridley et al., wordt soms ten onrechte gebruikt bij het berekenen van de kans op intersubbandverstrooiing geïnduceerd door optische fononen.
   B.K. Ridley, J. Phys. C: Solid State Phys. 15, p. 5899 (1982).
   T. Kuhn and G. Mahler, Physica Scripta. 38, p. 216 (1988).

6. Fletcher et al. rapporteren ten onrechte dat de insnoeringen in de Shubnikov-de Haas oscillaties van een 2-dimensionaal elektronengas met meerdere subbanden aan fononverstrooiing kunnen worden toegeschreven.
R. Fletcher et al., J. Phys.: Condens. Matter 3, p. 3479 (1991)

7. De luminescenctie van een type-II superrooster kan een volledig type-I karakter hebben.

8. Farouki et al. veronderstellen dat het elektrische veld in de grenslaag van een RF-plasma constant is, hetgeen leidt tot een onjuiste ionen energieverdeling.
R.T. Farouki et al., Phys. Rev. A 45, p. 5913 (1992)

9. Indien de dimensionering van een numeriek probleem aangepast wordt aan de beschikbare werktijd, is de rekentijd onafhankelijk van de gebruikte computer.

10. Als maatstaf voor het verschil tussen pingpongen en tafeltennissen kan de maximaal bereikbare frequentie waarmee de bal de tafel raakt genomen worden.